Design & generation of an efficient *E. coli* cell-factory for the overproduction of the compatible solutes ectoine & hydroxyectoine

Dissertation

zur

Erlangung des Doktorgrades (Dr. rer. nat.)

der

Mathematisch-Naturwissenschaftlichen Fakultät

der

Rheinischen Friedrich-Wilhelms-Universität Bonn

vorgelegt von

Lukas Bethlehem

aus

Düren

Bonn, im Dezember 2019

Angefertigt mit Genehmigung der Mathematisch-Naturwissenschaftlichen Fakultät der

Rheinischen Friedrich-Wilhelms-Universität Bonn.

1. Gutachter: Prof. Dr. Erwin A. Galinski

2. Gutachter: Prof. Dr. Uwe Deppenmeier

Tag der Promotion: 19.03.2020

Erscheinungsjahr: 2020

Content

Figures

Tables

Abbreviations

Genes are given in small italic letters, while proteins are given in standard font and with a capital first letter.

αKG	alpha-ketoglutaric acid
ADABA	N-γ-acetyl-L-2,4-diaminobutyric acid
ADAM	1-aminoadamantane
ADP	adenosine diphosphate
AHT	anhydrotetracycline
AmpR	ampicillin resistance (conferred by β-lactamase)
AP	alkaline phosphatase
APS	ammonium persulfate
Ask	L-aspartate kinase
AspAT	L-aspartate amino transferase
AspDH	L-aspartate β-semialdehyde dehydrogenase
ATP	adenosine triphosphate
BCA	bicinchoninic acid
bp	base-pair(s)
BSA	bovine serum albumin
cDNA	complementary DNA
CFU	colony forming unit
CmR	chloramphenicol resistance (conferred by Cm-acetylase)
CoA	Coenzyme-A
DABA	L-2,4-diaminobutyric acid
dcw	dry cell-weight
DMSO	dimethyl sulfoxide
DNA	deoxyribonucleic acid
DNase	deoxyribonuclease
dNTP	deoxyribonucleoside triphosphate
DSM	German collection of microorganisms
DTT	dithiothreitol
EctA	L-2,4-diaminobutyric acid acetyltransferase

EctB	L-2,4-diaminobutyric acid transaminase
EctC	ectoine synthase
EctD	ectoine hydroxylase
ectoine	(4S)-2-methyl-3,4,5,6-tetrahydropyrimidine-4-carboxylic acid
EDTA	ethylenediaminetetraacetic acid
et al.	*et alii* (and others)
FMOC	9-fluorenylmethyloxycarbonyl
g	gravitational force
Glu	glutamate
GTP	guanosine triphosphate
H_2O_{demin}	demineralized water
H_2O_{pure}	ultrapure water
HPLC	high performance liquid chromatography
hydroxyectoine	(4S,5S)-5-Hydroxy-2-methyl-1,4,5,6-tetrahydropyrimidine-4-carboxylic acid
IPTG	isopropyl β-D-thiogalactopyranoside
kb	kilobases
kDa	kilodalton
LacI	repressor of the lac-operon
lac-promotor	promotor of the lac-operon
LB	lysogenic broth
ln OD_{600}	natural logarithm of the optical density at 600 nanometers
LysC	L-aspartate kinase (from *C. glutamicum*)
MM63	minimal medium 63
mRNA	messenger RNA
rRNA	ribosomal RNA
NAD	nicotinamide adenine dinucleotide
NADP	nicotinamide adenine dinucleotide phosphate
NMR	nuclear magnetic resonance
OD_{600}	optical density at a wavelength of 600 nanometers
PAGE	polyacrylamide gel electrophoresis

PCR	polymerase chain reaction
PEP	phosphoenolpyruvate
pH	*potential hydrogenii*
pI	isoelectric point
ppm	parts per million
RBS	ribosomal binding site
RI	refractive index
RNA	ribonucleic acid
RNase	ribonuclease
rpm	revolutions per minute
RSB	reducing sample buffer
RT	room temperature
qPCR	quantitative PCR
SDS	sodium dodecyl sulfate
tac-promotor	hybrid promotor of *trp*- and *lac*-promotor
TCA	tricarboxylic acid cycle
TEMED	N,N,N′,N′-Tetramethylethane-1,2-diamine
tet-promotor	promotor of the gene for tetracycline resistance
TetR	tetracycline operator repressor
T_m	melting temperature (of double stranded DNA)
TMSP	trimethylsilyl propanoic acid
TRIS	2-Amino-2-(hydroxymethyl)propane-1,3-diol
U	unit
UDP	uridine diphosphate
UV	ultraviolet
≥, ≤	larger than or equal, smaller than or equal
% (w/v)	percentage of mass per volume
% (v/v)	percentage of volume per volume

Summary

The compatible solutes ectoine and hydroxyectoine are produced by halophilic or halotolerant bacteria in order to balance and adapt to osmotic alterations in their habitat. Besides this, the potent ability of these compounds to stabilize protein and cellular structures has led to significant interest in the scientific and industrial community over the last two decades. Successful marketing of especially ectoine in various skin-care and medical products has been achieved and the field of application is further growing through new implementations in critical medical fields like inflammatory bowel disease (IBD) or Alzheimer's disease.

The industrial production of these compatible solutes, however, remains inefficient and costly, due to the limitations of the natural producer strain *Halomonas elongata*. The world-wide effort to develop an industrially relevant and cost-effective heterologous overproduction strain, has been moderately successful so far. The low productivities of these strains could be related to a poor activity of the employed halophilic enzymes to produce ectoine and hydroxyectoine in their non-halophilic heterologous host systems.

To overcome these obstacles, I transferred the hydroxyectoine gene cluster from the non-halophilic *Acidiphilium cryptum* into *Escherichia coli*. The design of an optimized expression plasmid led to very high product titers and exceptional productivities in shake flask experiments. Overproduction could be performed at low salt conditions (0% NaCl) leading to the natural excretion of > 99% of the produced ectoines into the culture medium. The scale-up of the production in bioreactor experiments, however, revealed an insuperable halt in production after only 10 hours, hence limiting ectoine titers. By qPCR and mass-spectrometry analysis we observed a rapid loss of ectoine biosynthesis enzymes over time, caused by plasmid instability in combination with the high productivity of the heterologous strain. We were able to solve this issue by the addition of a β-lactam inhibitor into the culture medium, ultimately resulting in high product titers (10 g/L) and the most effective heterologous ectoine overproduction process described in literature to date (3 $g_{ectoine}/g_{dcw}$). The low salt conditions of this cell factory facilitate downstream processes and reduce the costs of waste-water treatment and equipment maintenance. By performing detailed ^{13}C-flux analysis of the strain's metabolic activity we further identified potential bottle-necks of the here established protocol, eventually allowing for additional metabolic engineering processes that could even enhance strain productivity and efficiency.

1. Introduction

1.1. Extremophilic Microorganisms

Organisms that thrive under extreme environmental conditions are termed extremophiles. Due to their definite adaptations these organisms are restrained to very unique and harsh environments, while extremotolerant organisms are less specialized and able to grow under alternating conditions. In contrast to Extremophiles however, extremotolerant organisms only withstand moderate levels of stress factors (MacElroy, 1974). Regular or non-extreme conditions are universally defined as temperatures between 20 °C and 40 °C, pressure of 0.1 MPA, a pH around neutral, and moderate levels of nutrients and salts (Satyanarayana *et al.*, 2005). In comparison, extreme conditions are for example found within natural hot springs, hyperthermal vents and the arctic deep-sea, or within manmade environments like salterns and industry facilities. Most of extremophilic organisms are actually polyextremophiles, meaning they tolerate a combination of extraordinary physical or geochemical factors, including temperature, pressure, radiation, salinity and pH (Rothschild and Mancinelli, 2001). Since extreme conditions, such as high temperatures or extreme pH, were found to be economically favorable for various bioprocesses there is a growing interest in understanding extremophiles and utilizing them for the development of new profitable applications (Zeikus *et al.*, 1998). Examples include the use of specialized enzymes, like the thermostable *Taq*-DNA polymerase derived from *Thermus aquaticus* enabling the modern polymerase chain reaction (PCR). Furthermore extremophilic organisms or communities are used for applications like bio-remediation of toxic soil and water (Chien *et al.*, 1976; Nichols *et al.*, 1999).

1.2. Halophiles

Halophiles are a group of extremophilic microorganisms that inhabit aquatic environments with extremely high salinities. They can be categorized according their salt tolerance into slight (0.3-0.8 M, seawater), moderate (0.8-3.4 M) or extreme halophilic (3.4-5.1 M) (Ollivier *et al.*, 1994).Water with high salinity contains a high ionic strength due to the dissolved ionic compounds (osmolytes).These compounds decrease the chemical potential of water which strives for an equilibrium. Since microorganisms ensure the controlled exchange of particles with the

surrounding milieu by a semipermeable membrane, a difference in chemical potential can occur for inside and outside the cell. If not balanced otherwise this leads to the outflow of water towards the lower chemical potential (Guell and Brenner, 1996). For non-halophilic microorganisms the loss in turgor pressure under high salinity causes a fatal collapse of scaffold and a failure in the microbial metabolism (Brown, 1976).

Halophilic and halotolerant bacteria have developed two main strategies to cope with high salinity: The salt-in strategy (I) or the production of organic osmolytes (II). Both strategies aim to equilibrate the cytoplasm to the exterior ionic strength, so that no water loss occurs over the semipermeable membrane. The salt-in strategy relies on the influx of inorganic counterions, mostly K^+ and Cl^-. This represents a very quick response, which however requires the adaptation of the entire proteome to the elevated salt concentrations to prevent enzymes from degradation. Organisms following this strategy alone are restraint to higher salt concentrations and cannot effectively adopt to lower salt concentrations. Accordingly only specialized bacteria and archea (extreme halophiles) rely on this strategy (Galinski and Trüper, 1994). A more flexible mechanism of halophilic adaptation is the accumulation or production of organic osmolytes. These small organic compounds are amino acids, sugars, polyols, betains or derivatives of these compounds, with high water solubility (Galinski, 1995). In contrast to the salt-in strategy, the organic osmolytes do not impair the cell metabolism and are therefore called compatible solutes. Their *de novo* synthesis however, demands a significant redirection of resources for the organism, which is why the transport from the exterior milieu is privileged (Kempf and Bremer, 1998; Oren, 1999). The controlled uptake and efflux by specific transporters allows for a dynamic adaptation. Furthermore, some microorganisms have developed specialized degradation pathways for compatible solutes, enabling the recovery of resources.

1.3. The Compatible Solutes Ectoine & Hydroxyectoine

The zwitterionic amino acid derivative ectoine is one of the most thoroughly studied compatible solute, not only due to its prevalence among salt adopted organisms, but also due to its remarkable properties for the biotech-industry (Pastor *et al.*, 2010). Since its initial discovery in *Halorhodospira halochloris* by Galinski in 1985, ectoine has been implemented into a variety of

commercial products. Its main feature is a protein- and cell-structure stabilizing effect, which is explained by the phenomenon of preferential exclusion (Arakawa and Timasheff, 1985; Zaccai *et al.*, 2016). All biomolecules are stabilized in their natural conformation by water, due to hydration forces stabilizing and packing the protein structure (Levy & Onuchic 2004). Ectoine is a kosmotropic agent, meaning it contributes to this effect by enhancing the order of water molecules. This leads to preserving effects on cells and proteins under desiccation, heat-, cold- and oxidation-stress (Lippert and Galinski, 1992; Louis, Trüper and Galinski, 1994; Goeller & Galinski, 1999; Borges *et al.* 2002).

Useful applications of ectoine as a stabilizer in molecular biology have been demonstrated, for example during protein expression or storage, as well as functioning as a PCR-enhancer by increasing the stability of DNA polymerase at high temperatures (Inbar and Lapidot, 1988). The most extensive use of ectoine, however, is recorded in dermatological applications, where the compound is used to stabilize and protect epithelia and mucosa from dehydration. By the preferential exclusion of ectoine from the hydration monolayer of proteins an enhanced organization of lipid-headgroups and thus a protective function for membranes could be demonstrated (Harishchandra *et al.*, 2010). Furthermore, an absorbing effect for UVA-radiation energy has been observed, adding to the dermatological potential of ectoine (Botta *et al.*, 2008). More recently, beneficial, often anti-inflammatory functions of ectoine have been described in upper airway inflammatory diseases, colitis, Alzheimer's disease and for the treatment of radiation-induced side effects of cancer therapy (Abdel-Aziz *et al.*, 2015; Casale *et al.*, 2019; Castro *et al.*, 2019; Rieckmann *et al.*, 2019; Tran *et al.*, 2019). If ectoine becomes approved as a drug in treating these diseases, an improved industrial production is inevitable. Notably, the potential of the ectoine derivative hydroxyectoine has so far been impaired entirely by ineffective industrial production processes, even though its protective features might be even greater than those of ectoine due to its increased glass-forming properties (Inbar and Lapidot, 1988; Tanne *et al.*, 2014). With a high glass transition temperature of 87 °C it exhibits increased desiccation protection compared to ectoine (47 °C) (Manzanera *et al.*, 2004). This feature is attributed to the enforced intermolecular hydrogen bonds, generated by the hydroxyl group of the ectoine derivative. Consequently, its production is commonly observed in cells entering the stationary phase or upon increasing temperatures.

The biosynthetic pathway of ectoine and hydroxyectoine branches from the tricarboxylic acid cycle (TCA) into the family of the aspartate amino acids, beginning with the addition of an amino group from glutamate to oxaloacetate by the aspartate aminotransferase (**Figure 1**). In the following, L-aspartate is phosphorylated by the aspartate kinase, consuming one ATP. This step can be critical for the precursor supply of ectoine biosynthesis due to feedback inhibition by the products of the aspartate amino acid family (threonine, methionine and lysine) (Bestvater, Louis and Galinski, 2008). The L-aspartate β-semialdehyde dehydrogenase generates the central precursor for the ectoine biosynthesis and the aspartate amino acid family, L-aspartate-β-semialdehyde. The subsequent transamination via EctB forms L-2,4-diaminobutyric acid (DABA). After the acetylation to Nγ-acetyl-L-2,4-diaminobutyric acid (ADABA) by the acetyltransferase EctA, consuming acetyl-CoA, ectoine is cyclized in a dehydration reaction by the ectoine synthase EctC. For the conversion to hydroxyectoine, the ectoine ring is hydroxylated by the ectoine hydroxylase EctD, which needs α-ketoglutarate and molecular oxygen for the dioxygenase reaction. Furthermore, both EctC and EctD are dependent on Fe^{2+} as a cofactor and show highest activity at elevated to neutral pH (Bursy *et al.*, 2007; Widderich *et al.*, 2014).

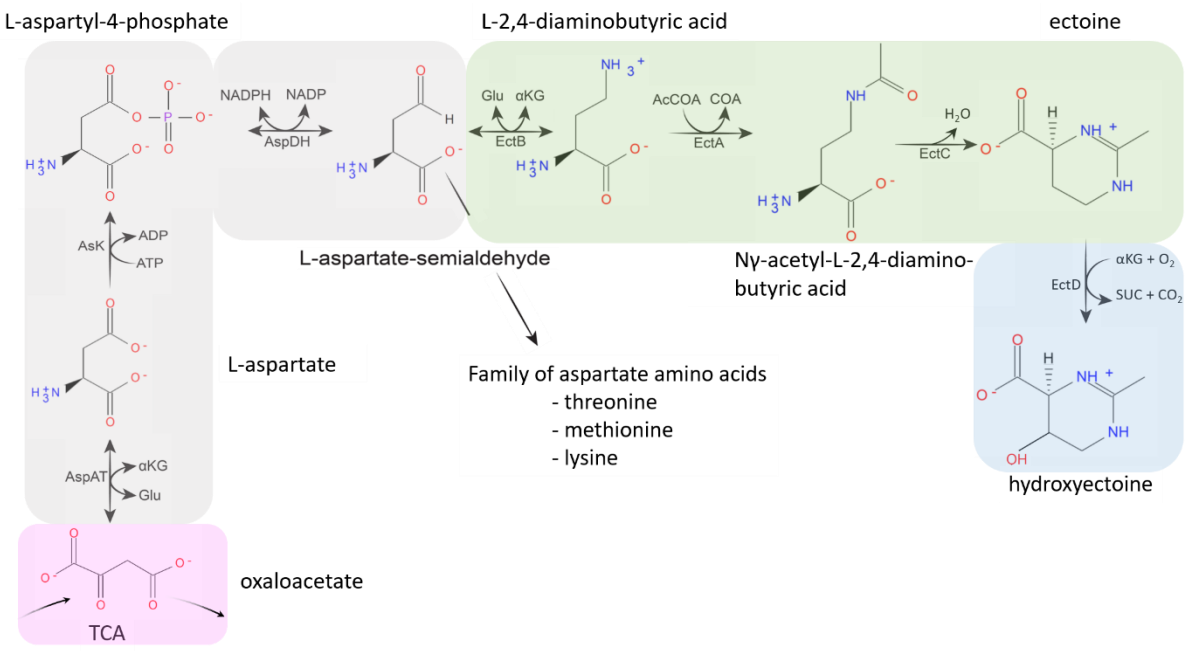

Figure 1 Ectoine (green) and hydroxyectoine (blue) biosynthesis, branching from the pathway of aspartate amino acids (grey), which originates from the TCA (pink). TCA: tricarboxylic acid cycle; AspAT: L-aspartate aminotransferase, αKG: α-ketoglutarate, Glu: glutamate, Ask: L-aspartate kinase, AspDH: L-aspartate β-semialdehyde dehydrogenase, EctB: L-2,4-diaminobutyric acid aminotransferase, EctA: Nγ-acetyl-L-2,4-diaminobutyric acid acetyltransferase, EctC: L-ectoine synthase, EctD: L-ectoine hydroxylase, SUC: succinate

1.3.1. The Hydroxyectoine Biosynthesis Gene Cluster of *Acidiphilium cryptum*

The gram-negative α-proteobacterium *Acidiphilium cryptum* can be found in acidic mine drainage, soils and sewage (Harrison *et al.*, 1980). Thriving in a pH range between 2.0-5.2, it is classified as an acidophile. Furthermore, it is a facultative anaerobic microorganism, utilizing Fe^{3+} as a terminal electron acceptor for anaerobic respiration. With a high abundance of guanine and cytosine in the genome (up to 70%), it exhibits an elevated GC-content compared to other microorganisms. Also, the organism exhibits effective mechanisms for detoxification in metal rich environments, by the reduction of Cr^{6+} to Cr^{3+} and an increased aluminum tolerance (Fischer *et al.*, 2002; Cummings *et al.*, 2007). Growth of *A. cryptum* is inhibited by sodium-acetate (0.01%) and other organic substrates already at low concentrations (Kishimoto and Tano, 1987).

As a non-halophilic organism, it is unusual that *A. cryptum* exhibits an aluminum and salt inducible hydroxyectoine biosynthesis gene cluster. The capability of producing this compatible solute is most likely connected to a not yet characterized resistance mechanism against elevated metal-ion concentrations (Moritz *et al.*, 2015). The hydroxyectoine biosynthesis gene cluster in *A. cryptum* comprises the genes for hydroxyectoine biosynthesis (*ectABCD*) including an additional L-aspartate kinase (*ask*) overlapping with *ectD* (**Figure 2**). Similarly, *ectA* and *ectB* exhibit an overlapping sequence. The GC-content of the gene cluster is elevated (65-71%) compared to the average GC-content of *E. coli* K-12 MG1655 (50.8%) (Kent *et al.*, 2002).

Figure 2 Hydroxyectoine gene cluster of *A. cryptum* including ***ectA*** (Nγ-acetyl-L-2,4-diaminobutyric acid acetyltransferase, 71% GC), ***ectB*** (L-2,4-diaminobutyric acid aminotransferase, 70% GC), ***ectC*** (L-ectoine-synthase, 65% GC), ***ectD*** (L-ectoine hydroxylase, 66% GC) and ***ask*** (L-aspartate kinase, 70% GC). *ectA* and *ectB* as well as *ectD* and *ask* share overlapping genomic sequences.

In contrast to their halophilic counterparts, the ectoine synthase and ectoine hydroxylase of *A. cryptum* show a maximal activity without NaCl and drop in activity with increasing salt concentration (Widderich *et al.*, 2014; Moritz *et al.*, 2015). This particular difference to halophilic enzymes points to a high potential for the implementation of these enzymes for heterologous ectoine/hydroxyectoine overproduction at low-salt conditions in *E. coli*.

1.3.2. Industrial Production of Ectoine & Hydroxyectoine

The industrial production of ectoine is performed in the natural producer *Halomonas elongata*, which produces ectoine intracellularly upon osmotic stress. In order to extract the product most efficiently from the wildtype strain, the method of bacterial milking was developed by Sauer and Galinski in 1998. In this process, the organism produces ectoine intracellularly upon fermentation at high salinities (10-15% NaCl). The organism is subsequently separated from the medium and exposed to a hypoosmotic shock (2 – 3% NaCl), which leads to the efflux of the compatible solute to evade cell rupture by water influx. Ectoine can then be purified from the medium by microfiltration of the biomass, desalting of the medium, chromatographic capturing of the product and crystallization (**Figure 3**). In this procedure the product yield is restraint by the intracellular accumulation of ectoine and the loss of product during the elaborate down-stream processes.

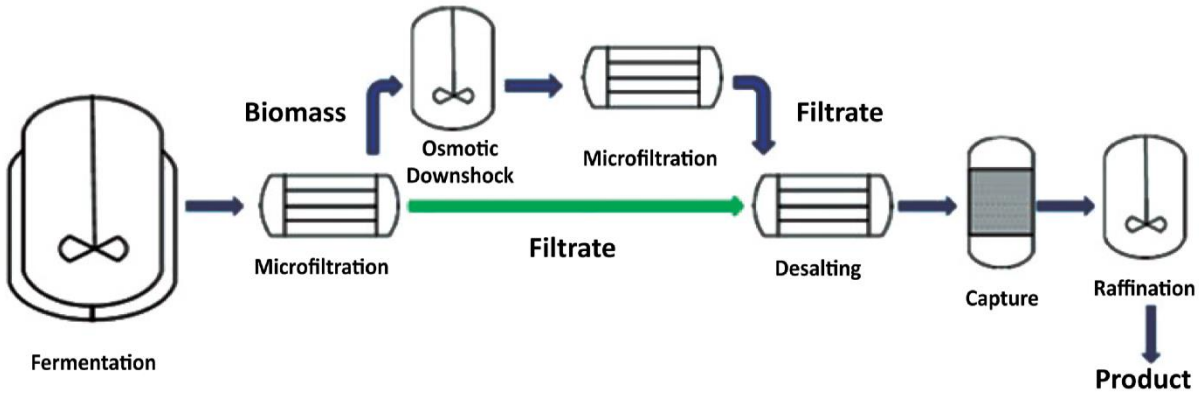

Figure 3 Overview of the industrial production processes generating ectoine with *H. elongata*. In a fermentation process the organism produces ectoine intracellularly, when cultivated in high salt conditions. After microfiltration, the cells are exposed to an osmotic down-shock, upon which they release the product into the medium (bacterial-milking). The medium gets separated from the biomass for further purification of ectoine, via electrodialysis (desalting), chromatography (capture) and crystallization (raffination). The biomass can afterwards be reused in another fermentation. By employing leaky-mutants of *H. elongata* ectoine is directly secreted into the medium, which makes the bacterial milking process obsolete (green arrow).
Adapted from Kunte, Lentzen and Galinski (2014).

Until now, the production of ectoine has been optimized by the design of so-called leaky mutants. Through the deletion of ectoine uptake and degradation systems in *H. elongata* the product is continuously secreted into the medium by the producer strain (Grammann *et al.*, 2002; Kunte, Lentzen and Galinski, 2014). This simplifies the production process and makes the bacterial-milking procedure obsolete. Since the product titer is no longer depending on intracellular

accumulation, the NaCl content can be decreased. However, still a high concentration of salt is necessary to induce ectoine production within this strain, making the down-stream process costly and inefficient. No further optimization processes were successful in increasing overall ectoine yield within the natural producer strain. Alternatively, ectoine can be produced via chemical synthesis, but this process is economically inferior to the biological production, due to high costs of the precursor DABA. Notably, the production of the ectoine derivative hydroxyectoine is even more inefficient in *H. elongata.* Hydroxyectoine can only be generated in a 50% mixture with its precursor ectoine at > 10% NaCl, making any purification extremely elaborate. Consequently, industrial hydroxyectoine production is not economically feasible, limiting its application so far.

1.3.3. Heterologous Production of Ectoine

Until the discovery of *Corynebacterium glutamicum* in 1956, it was a common misconception that the accumulation of amino acids in bacteria was impossible (Tryfona and Bustard, 2005). Since then, an increasing variety of microbial fermentation processes have been developed to produce amino acids or derivatives, mainly employing *C. glutamicum* and *E. coli*. To overcome the limitations of ectoine production within the natural producer strain *H. elongata*, numerous heterologous production strains have been designed with moderate success. For ectoine overproduction at low salinities generally halophilic or halotolerant sets of genes were employed (Schubert *et al.*, 2007; Becker *et al.*, 2013; He *et al.*, 2015; Czech *et al.*, 2016; Pérez-García *et al.*, 2017). The first competitive *E. coli* overproduction strain was generated by Ning *et al.* (2016), through elaborate metabolic engineering of *E. coli* W33110. Utilizing the biosynthesis gene cluster of *H. elongata* they were able to produce the industrially reasonable titer of 25.1 g/L. More recently, a breakthrough in ectoine production with *C. glutamicum* was achieved by Gießelmann *et al.* (2019). By optimizing the heterologous expression balance of each ectoine biosynthesis gene, originating from the halotolerant *Pseudomonas stutzeri*, a remarkable product titer of 65 g/L could be generated. Despite proving both organisms valuable for ectoine overproduction, they exhibit a critically low specific production ($g_{product}/g_{dry\ cell\ weight\ (dcw)}$), leaving room for further optimization.

Astonishingly, there have been only few reported attempts to generate a heterologous hydroxyectoine overproduction strain (Seip, Galinski and Kurz, 2011; Eilert *et al.*, 2013; Czech *et al.*, 2018). These, however, have reported only poor results by exhibiting either low product titers or a high precursor accumulation.

1.4. *E. coli* Strain Design & Development

The γ-proteobacterium and common inhabitant of human intestines *E. coli* is one of the most thoroughly studied and employed microorganisms in research and industrial applications. It grants various benefits, like its well-characterized genetics and fast growth to high cell densities in inexpensive media (Huang *et al.*, 2012). Due to its frequent utilization for more than a century, many different variants have been generated with almost all laboratory strains originating from non-pathogenic K-12 or B strains (Daegelen *et al.*, 2009). While the K-12 strains were widely used in research, developing most of the recombinant DNA techniques we use today, the B strains were more frequently used for physiological studies, due to their faster growth and susceptibility to external stress factors. *E. coli* B did also serve as the host for the T1-T7 bacteriophage studies by Delbruck (1946), culminating in the construction of the prominent *E. coli* BL21(DE3) strain by Studier and Moffatt in 1986. The unique features of this strain led to a wide usage for recombinant protein expression in academia and industry. As a member of the E. *coli* B family, BL21(DE3) displays a higher membrane permeability, mediated by expression of the large porin protein OmpF (Herrera *et al.*, 2002). Also, the strain is deficient for the major protease Lon and the outer membrane protease OmpT (Marisch *et al.*, 2013). Both features stabilize and facilitate recombinant protein formation and secretion. Additionally, an increased growth of *E. coli* B on minimal medium and a low acetate production under high cell density conditions proved beneficial for industrial applications (Phue *et al.*, 2005).

Besides increasing system-wide knowledge about specific strains, the decision on which base strain to choose for a strain development approach is still hard to answer on a rational basis alone and has to be determined empirically. The keys for heterologous production and strain optimization are high productivity and stability of the foreign process. Traditionally, hyperproducer strains have been developed by numerous rounds of random mutagenesis, being a

time-consuming and labor-intensive process. Also, this often led to unwanted alterations in the genome of the modified producer strain and the adjustments are restricted to the capacity of the host genome itself. Understanding system-wide biology including the interplay of genomics, transcriptomics, proteomics and metabolomics, paved the way for genetically defined hyperproducer strains. Since these new developments, numerous successful integrations have already proven the power of rational metabolic engineering (Lee *et al.*, 2007; Becker *et al.*, 2011; Ning *et al.*, 2016). The classical path for this strategy can be summarized in the so-called five-word strategy: Enter, flow, moderate, block, exit (Li *et al.*, 2017) (**Figure 4**). At first the uptake speed of the carbon source and the catabolic reactions are enhanced (**enter**). In the next step, the **flow** towards the desired product is reinforced, by releasing feedback-inhibition or overexpressing expedient pathways. By the **moderation** of competing pathways, the byproduct formation is decreased and the flux is condensed into the product. In the last two steps, pathways degrading the product are cut-off (**block**) and the efflux of product is facilitated (**exit**). The definite route of these steps is, however, unique to any given metabolic engineering approach. Hence each metabolic engineering strategy differs with each target application, but generally can use the five-word strategy as a road-map during strain optimization.

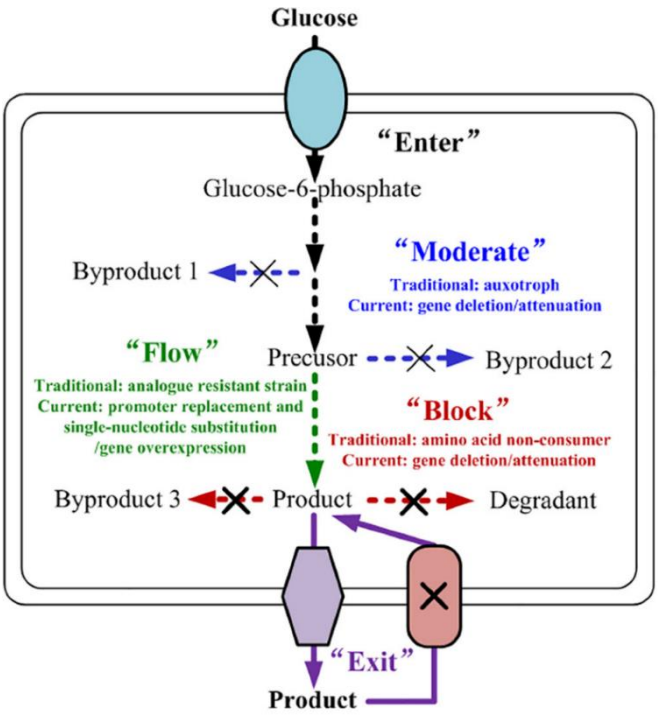

Figure 4 The "five-word breeding strategy" for strain development by metabolic engineering. The strategies are defined as enter, flow, moderate, block and exit. These steps of the process optimization can be achieved by traditional or current techniques of molecular biology. Adapted from Li *et al.* (2017).

Besides base-strain design and engineering, the choice and architecture of the plasmid for heterologous protein production is of utmost importance for productivity and stability of the process. Through the arrangement of vector elements (promotor, ribosomal binding site (RBS), bicistronic-elements, terminators and origin of replication) the expression strength can be adjusted, determining the foundation of success for an overproduction strain (Gießelmann *et al.*, 2019). The stability of a plasmid-based expression system, on the other hand, is greatly defined by the selective pressure employed by the plasmid-addiction system. Sieben *et al.* (2016) showed that over 60% of plasmids can be lost in the first 24 h of a biotechnological cultivation with *E. coli*. Plasmid loss depends on the effectiveness and stability of the plasmid addiction system as well as on the metabolic burden generated by the heterologous construct. Plasmid-free cells tend to grow faster than plasmid bearing cells, establishing the emergence of a faster growing plasmid-free cell-population (Bentley and Kompala, 1990). In consequence, only bacterial biomass will be produced instead of the intended product. The growth rate difference of the two competing populations determines the degree of imbalance (de Taxis du Poët *et al.*, 1987). This problem of population heterogeneity in biotechnological processes can be assessed by using biosensors, which enable to distinguish producing from non-producing cells. Spatial resolution can be achieved by live-cell microscopy, determining the amount of cells containing the plasmid (= contributing to product formation) and thus ultimately monitoring the change in a cell population over time (Mahr *et al.*, 2014).

To overcome plasmid instability in such cell populations, cells are commonly selected for antibiotic resistance provided by the plasmid. Despite the wide utilization and easy implementation of antibiotic selection the system carries the risk of selective pressure release, due to the degradation of the antibiotic. Furthermore, implementation of antibiotics in an industrial process is usually avoided, since thorough product and waste-water purification to remove the antibiotics is compulsory, decreasing product yield and inflating process costs (Friehs, 2004). Alternative selection strategies are auxotrophy complementation, toxin/antitoxin selection or RNA based selectable markers (Fedorec *et al.*, 2019).

1.5. Systems Biology: Metabolic Flux Analysis

The relatively new discipline of systems biology allows for a precise description and analysis of an organism as a whole, and therefore has many advantages to classical approaches describing isolated cellular phenomena (Palsson, 2004). Systems biology is based on several recent advances in the field of 'omics' technologies including genomics, transcriptomics, proteomics, metabolomics and fluxomics. All these techniques rely on computational assisted analyses, which drive powerful genome-scale reconstructions and enable *in-silico* simulations to predict genotypic alterations. The most effective perturbations determined *in-silico* can subsequently be transferred into strain optimization processes, preserving time and enabling new solutions. Such an *in-silico*-driven genome-scale network reconstruction (GENRE) approach, relies on accurately curated primary biological information extracted from different omics datasets, deposited in a bio-chemically, genetically and genomically (BiGG) structured data-base (Joyce and Palsson, 2006).

For *E. coli*, more and more complex GENREs have been developed covering over 50% of the annotated functional open reading frames (ORFs) (Orth *et al.*, 2011). The development of correct and effective application and integration of these rich data is, however, an iterative process. The most successful systems biology application in biotechnology so far is the genome-scale metabolic flux analysis (MFA). This technique allows for the description of metabolite consumption and production rates upon comparison of experimentally determined isotope (^{13}C) distributions to a defined network of reactions. The underlying networks can be scaled to fit the process and the calculation usually relies on stoichiometric modeling and optimum-based flux analysis techniques (**Figure 5A**). To perform these mathematical operations, the reactions are constituted in a matrix, wherein rows represent the compounds and columns represent the chemical transformations (**Figure 5B**) (Kim *et al.*, 2008).

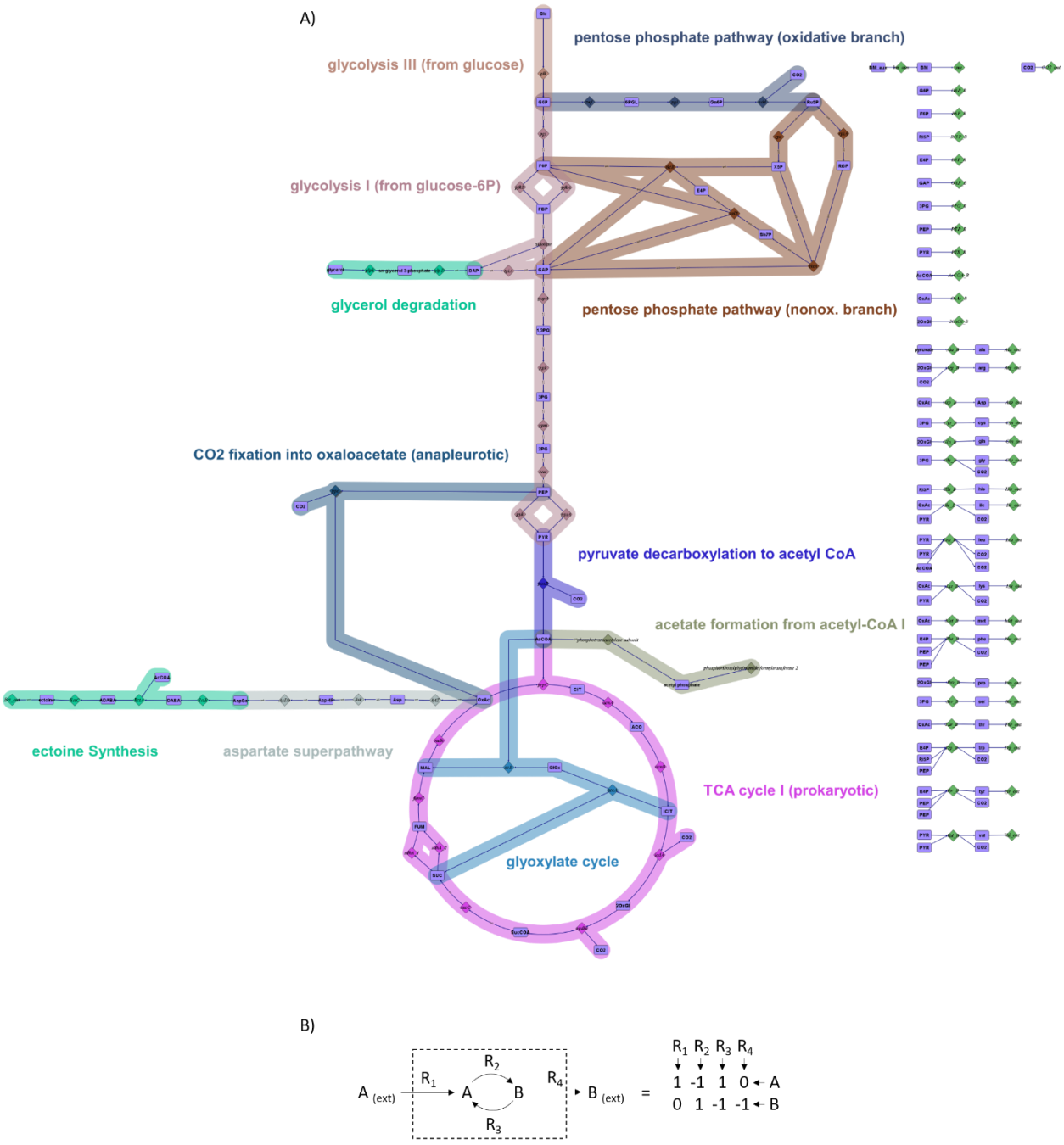

Figure 5 Metabolic network, generated in this study, showing ectoine formation including the main metabolic routes from glucose and glycerol, as well as the generation and efflux of relevant amino acids (A). The model was generated using the Omix Visualization software (Lennestadt, Germany). With the help of metabolic models, simulations can be performed elucidating possible genotypic alterations for e.g. flux optimization. Mathematically, the stoichiometry of reactions is often described in a matrix (B). The example describes a simple reaction between A and B, where A is generated in reaction 1 (R_1) and R_3, whereas B is formed by R_2 and withdrawn by R_4.

After the network design and mathematical modeling of such a metabolic flux, the real fluxes are experimentally determined by feeding stable isotope variants of carbohydrates into the system. With the known composition of introduced isotopes and the pattern of their distribution in the metabolic building-blocks, the flux can be calculated. To trace the path of the isotopes in these networks, information on the underlying carbon transitions need to be available (**Figure 6**).

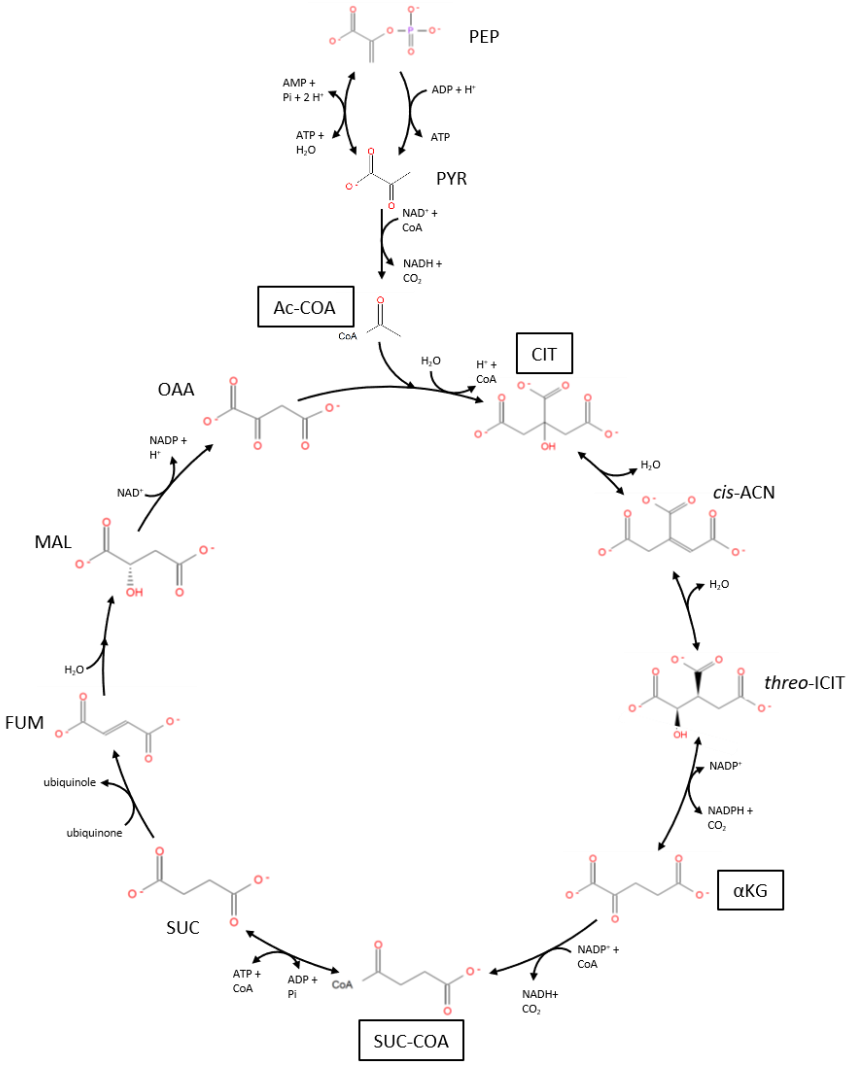

Figure 6 Overview of the tricarboxylic acid cycle beginning with phosphoenolpyruvate, including compound structures and side-reactions. Reaction steps with a change in carbon atom arrangement are encircled. These reactions are crucial to analyze ^{13}C-labelling experiments. PEP = phosphoenolpyruvate, PYR = pyruvate, Ac-COA = acetyl-CoA, CIT = citrate, *cis*-ACN = *cis*-aconitate, *threo*-ICIT = *threo*-isocitrate, αKG = α-ketoglutarate, SUC-COA = succinyl-CoA, SUC = succinate, FUM = fumarate, MAL = malate, OAA = oxaloacetate

Based on the known chemical reactions of, for example, the ectoine biosynthesis pathway a theoretic labelling network can be designed, which is able to follow the introduced carbon isotopes through the pathways until no change in ^{13}C distribution occurs (**Figure 7**). The displayed network includes only the reactions of the TCA which are relevant for carbon atom rearrangement (cf. Figure 6). The final ectoine ^{13}C labelling pattern is constituted of the pattern present in oxaloacetate and acetyl-CoA. This is a helpful model to predict and mimic ectoine biosynthesis *in silico* and to subsequently improve the employed production strain to generate the highest possible yield. Furthermore, the network is helpful in designing the labelling experiment itself, by finding the composition of isotope variants resulting in the richest information output. By comparing the real measurements to the model's assumptions, its accuracy can be validated and it can be employed to perform various optimizations *in-silico*.

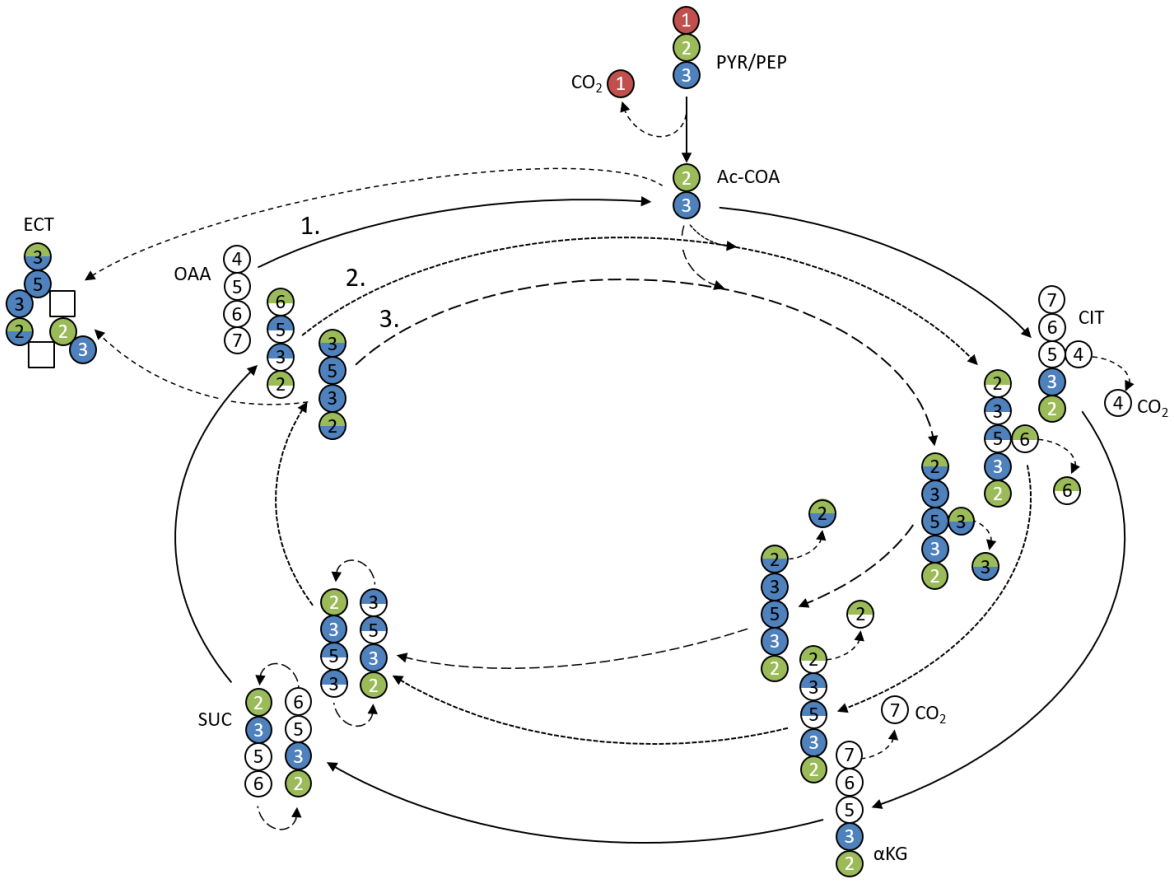

Figure 7 Theoretical labelling pattern for different ^{13}C-isotopes in positions 1 (red), 2 (green) and 3 (blue) of pyruvate passing the standard TCA cycle until no alteration in labelling distribution occurs. After repeated cycles the labelling distribution is equilibrated as shown for the ectoine molecule. Circles represent carbon atoms, rectangles nitrogen atoms. White circles are not labeled (^{12}C) and white numbers are newly introduced ^{13}C-isotopes. Displayed are only reactions relevant for carbon transition or ectoine formation. Since succinate is a symmetrical molecule the isotope pattern is randomized (50/50). PYR/PEP = pyruvate/phosphoenolpyruvate, Ac-COA = acetyl-CoA, CIT = citrate, αKG = α-ketoglutarate, SUC = succinate, OAA = oxaloacetate, ECT = ectoine

1.6. Aim of the thesis

There is an increasing demand for an efficient production process of the compatible solutes ectoine and hydroxyectoine in the biotechnology industry. This demand is prompted by new medical applications for these compounds in the treatment of widespread diseases, such as Alzheimer's, inflammatory bowel disease or respiratory inflammation. The stagnating improvements of ectoine or hydroxyectoine production by standard fermentation processes employing the natural producer strain *H. elongata* are not sufficient to meet this demand.

Besides many inefficient attempts for heterologous ectoine and hydroxyectoine overproduction at low salinity, a few industrially relevant strains have been developed. These strains, however, collectively exhibit a low specific production. This might be explained by the low activities of the mostly halophilic enzymes at the low salt conditions employed. In 2015, Moritz *et al.* described an exceptionally high activity of the ectoine synthase from the non-halophilic *A. cryptum* at low NaCl concentrations. Based on these observations, the ectoine biosynthesis gene cluster of *A. cryptum* was implemented into *E. coli*, resulting in the excretion of ectoine even at low salinities with a remarkably high specific production (Bethlehem, 2015). In a first attempt the process could be optimized marginally, by changing the carbon source and decreasing the NaCl content (Moritz, 2018). The implementation in bioreactor processes, however, could not successfully be established. A halt in product formation and an increase in precursor generation could not be overcome, ultimately creating low product titers and preventing industrial application.

In this thesis I aimed to identify the reason for the limitation in heterologous ectoine production and optimize the ectoine overproduction in *E. coli* with the ectoine biosynthesis gene cluster from the non-halophilic *A. cryptum*. This way, an efficient ectoine biosynthesis production system should be realized that works at low salt concentrations. Finding a valid base strain and optimizing the expression vector for ectoine overproduction is a critical step in this process. Subsequently, I intend to characterize the base-process by ^{13}C-flux analysis to elucidate the pathway of product formation in the new host system and to reveal potential bottlenecks. In the following, the eminent problem of process instability should be questioned and clarified by protein and transcript studies of the heterologous proteins during advanced fermentation. Finally, the stop in product formation should be eliminated, thus granting an industrially competitive overproduction process for ectoines, with a high specific production.

2. Material & Methods

If not stated otherwise all enzymes and kits were utilized and prepared according to manufacturer's instructions (cf. 2.5. Chemicals, Enzymes and Kits).

2.1. Bacterial Strains and Plasmids

Table 1 Employed bacterial strains in this study.

Strain	Genotype	Reference
Acidiphilium cryptum DSM2389^T	wildtype	(Harrison, 1980)
Escherichia coli DH5α	F^-, *supE44*, *recA1*, *endA1*, *relA1*, *hsdR17* (rk, mk^-), *gyrA96*, λ^-, *thi*-1, Δ*lac*U169 (ϕ80*lacZ*αM15)	(Hanahan, 1983)
Escherichia coli BL21	F^-, *ompT*, *gal*, *dcm, lon*, $hsdS_B(r_B^- m_B^-)$, $[malB^+]_{K\text{-}12}(\lambda^S)$	(Studier and Moffatt, 1986)
Escherichia coli K12 DSM498^T	wildtype	DSMZ (498)
Escherichia coli W3110	F^-, λ^-, rph^{-1}, INV (rrnD, rrnE)	(Hill and Harnish, 1981)
Escherichia coli MG1655	K-12, F^-, λ^-, ilvG$^-$, rfb-50, rph-1	(Guyer *et al.*, 1981)
Corynebacterium glutamicum DSM20300^T	wildtype	DSMZ (20300)

Table 2 Employed plasmids in this study.

Plasmid	Features	Reference
pASK-IBA3	*tet*-Promotor, *tet*-Repressor, Strep-Tag, AmpR, ColE1-Ori	IBA-Lifesciences (Göttingen, Germany)
pASK_ectABCD$_{mut}$	pASK-IBA3 + *ectABCD* from *A. cryptum*, mutation T353C in *ectD*	(Bethlehem, 2015)
pASK_ectABCDask	pASK-IBA3 + *ectABCDask* from *A. cryptum*	(Bethlehem, 2015)
pASK_ectABC	pASK-IBA3 + *ectABC* from *A. cryptum*	This study[2]
pASK2C_ectABC	pASK-IBA2C[1] + *ectABC* from *A. cryptum*, CmR	This study[3]
pBBR1_pyc	*tet*-Promotor, CmR, pBBR1-OriV + *pyc* from *C. glutamicum*	This study[2]
pAKect1	*tac*-Promotor + *ectABC* from *Marinococcus halophilus* with promotor *promA*, *lysC* from *C. glutamicum,* CmR	(Bestvater, Louis and Galinski, 2008)

[1] plasmid identical to pASK-IBA3, besides the antibiotic resistance
[2] cloning schemes in Suppl. Figure 1 & Suppl. Figure 2
[3] cloning scheme redundant to pASK_ectABC

2.2. Cloning

2.2.1. DNA and Plasmid Isolation

DNA isolation was performed for insert amplification via PCR. For this purpose, 8 mL of overnight culture, grown in appropriate medium, were centrifuged (10,000 x *g*, 3 min), the pellet washed in 1 mL TES buffer, centrifuged and resuspended in 1 mL of TES-buffer. By the addition of 20 µL SDS (20%, w/v) for 30 min at room temperature (RT) cells were lysed. For DNA separation, 0.3 mL phenol/chloroform/isopentyl with a ratio of 25:24:1 was mixed thoroughly with the cell suspension and phase separation was enforced by centrifugation (14,500 x *g*, 10 min). The upper aqueous phase was transferred into a new sample-tube and the extraction was repeated until no interphase (containing contaminating proteins) was detectable. For DNA precipitation, 3 M Na-acetate solution (1/10 sample volume) and ice-cold isopropyl (1 sample volume) were added and the DNA incubated for 30 min at -20 °C. Then samples were centrifuged at 4 °C for 5 min at 14,500 x *g*. The pellet was washed with 0.5 mL ice-cold ethanol (70%, v/v), recentrifuged under same conditions, the supernatant discarded and the DNA-pellet dried at 60 °C for at least 10 min. For storage at -20 °C, the DNA was resuspended in 50 µL sterile H_2O.

If plasmids were used for insert amplification or sequencing, isolation was performed by Zyppy plasmid-miniprep kit according to manufacturer's instructions (Zymo Research, Irvine, USA). If plasmids were isolated for control restriction after cloning, isolation was performed by no-column (NC) procedure. For the latter, cells were grown in LB-medium overnight, 1.5 mL centrifuged (10,000 x *g*, 1 min), culture supernatant discarded and the pellet resuspended in 250 µL NC-buffer 1. By mixing with 250 µL NC-buffer 2 for 2 min, alkaline cell lyses was performed and stopped by adding 250 µL NC-buffer 3. To remove cell debris, samples were centrifuged (14,500 x *g*, 3 min) and the supernatant mixed with 500 µL chloroform and centrifuged (14,500 x *g*, 3 min). For DNA precipitation, the aqueous phase was transferred into 500 µL ice-cold isopropyl and centrifuged (14,500 x *g*, 3 min). The supernatant was discarded and the pellet was washed in ice-cold ethanol (70%, v/v). After repeating the centrifugation step and discarding the supernatant, the pellet was dried for 30 min at 60 °C, and then resuspended in 50 µL pure water and stored at – 20 °C.

2.2.2. Polymerase Chain Reaction (PCR)

Amplification of genetic sequences for cloning purposes was performed with the *Pfu* DNA polymerase. Amplicons longer than 2kb were amplified using the *Phusion* DNA polymerase (Thermo Fischer Scientific, Waltham, USA). Both polymerases exhibit a 3'-5' exonuclease activity, reducing the rate of errors during PCR. The *Phusion* DNA polymerase is a derivative of the *Pyrococcus furiosus* enzyme, but contains highly increased fidelity. The enzymes were used according to manufacturer's instructions (**Table 3, Table 4**). When using the *Phusion* DNA polymerase for amplification, the annealing step was obsolete and therefore omitted, if the melting temperature (T_m) was higher than 68 °C.

Table 3 PCR formulation and amplification protocol for *Pfu* DNA polymerase.

Formulation		**Amplification**				
Component	**Volume [µL]**	**Step**		**Temperature [°C]**		**Time**
Pfu-buffer (10x) + $MgSO_4$	5	1.	denaturation	95	1x	2 min
dNTPs (10 mM)	1	2.	denaturation	95		30 sec
primer (5' + 3', 10 µM)	2.5-5		annealing	T_m - 5	30x	30 sec
DNA (10-500 ng/µL)	1		elongation	72		2 min/kb
glycine-betaine (5 M)[1]	0-10	3.	final elongation	72	1x	10 min
Pfu (2.5 U/µL)	0.5	4.	hold	4		∞
H_2O_{pure}	ad 50					

[1] added when insert exhibited high GC-content

Table 4 PCR formulation and amplification protocol for *Phusion* DNA polymerase.

Formulation		**Amplification**				
Component	**Volume [µL]**	**Step**		**Temperature [°C]**		**Time**
HF-buffer (5x)	10	1.	denaturation	98	1x	30 sec
dNTPs (10 mM)	1	2.	denaturation	98		10 sec
primer (5' + 3', 10 µM)	2.5-5		annealing	T_m + 3	30x	20 sec
DNA (10-500 ng/µL)	1		elongation	72		15-30 sec/kb
glycine-betaine (5 M)[1]	0-10	3.	final elongation	72	1x	10 min
Phusion (2 U/µL)	0.5	4.	hold	4		∞
H_2O_{pure}	ad 50					

[1] added when insert exhibited high GC-content

Primer for insert amplification and sequencing were designed using SnapGene software (GSL Biotech, Chicago, USA) and ordered from Eurofins Genomics as lyophilized oligos (**Table 5**). Sequencing was performed with the Mix2seq kit according to manufacturer's instructions (Eurofins Genomics, Ebersberg, Germany). Primers were dissolved in ultrapure water at a concentration of 50 µM and stored at -20 °C.

Table 5 Primers used for cloning and sequencing. RS = restriction site

Name	Sequence (5'-3')	RS	Reference
f_acry_Xba	ATT TCT AGA CGG TGG CGC TGC GTC	XbaI	(Bethlehem, 2015)
Rev_ectABC_HindIII	AAT AAG CTT CGT CAG GCC GCC TCG CCG A	HindIII	This study
Pyc_SacI_fwd	ATT GAG CTC TAG TGT CGA CTC ACA C	SacI	"
Pyc_HindIII_rev	ATT AAG CTT GGT TTA GGA AAC GAC	HindIII	"
Pyc_tet_HindIII_fwd	ATT AAG CTT TCA CAT GAC CCG ACA	HindIII	"
Pyc_HindIII_rev	ATT AAG CTT GGT TTA GGA AAC GAC	HindIII	"
pASK_Seq_fwd	GAGTTATTTTACCACTCCCT	Seq.	AG Deppenmeier
Acry2 (f)	CTACTGCACCGCGATCC	Seq.	(Moritz, 2012)
Acry3 (f)	CCATTTCTGGAGCGATGA	Seq.	"

2.2.3. Agarose Gel Electrophoresis

To analyze, purify and quantify amplicons, as well as to asses restriction digests agarose gel electrophoresis (1%, w/v) was performed. For this, DNA fragments were separated in an electrical field (60-100 V). Agarose was heated in 1x TAE-buffer until completely dissolved. After pouring the gel, the electrophoresis chambers were filled with 1x TAE-buffer. For loading, samples and ladder (1 kb/100 bp GeneRuler, Thermo Scintific) were prepared in 1x loading-dye. DNA fragments were stained with GelRed (Biotium, Fremont, USA) for 5-20 minutes at RT and visualized in a Gel-Imager (Intas, Göttingen, Germany). For cloning, fragments were gel-extracted and purified using the peqGOLD gel extraction kit (Peqlab, Erlangen, Germany) according to manufacturer's instructions. The purification is based on resuspension of gel-bound DNA, which then binds to a silica membrane and becomes eluted in a small volume of elution-buffer or water (30-50 µL).

2.2.4. Restriction Digest

For cloning, insert- and vector-DNA were hydrolyzed for 2.5 hours (h) by restriction enzymes (Thermo Fisher Scientific, Waltham, USA) according to the manufacturer's instructions (**Table 6**). To prevent religation of the plasmid, DNA was then incubated with 1 U FastAP (alkaline phosphatase, Thermo Fisher Scientific) for 30 min. The hydrolysis and dephosphorylation were stopped by heating to 75 °C for 10 minutes. Subsequently, the DNA fragments were cleaned from enzymes using the peqGOLD column purification kit (Peqlab, Erlangen, Germany).

Table 6 Formulation for restriction enzyme hydrolysis of DNA.

Component	**Ligation [µL]**	**Clone-screening [µL]**
DNA	15	2
buffer (10 x)	4	1.5
restriction enzymes (10 U/µL)	1-2	0.5-1
H_2O_{pure}	ad 40	ad 15

2.2.5. Quantification of DNA

DNA for ligation was quantified by agarose gel electrophoresis or measured photometrically using a BioSpectrometer (Eppendorf, Hamburg, Germany). Gel electrophoresis allowed for semiquantitative results, by comparing the fluorescence intensity of the fragment to a standard of known concentration. The molar concentration was determined utilizing the following equation:

$$DNA\left[\frac{mol}{\mu L}\right] = \frac{DNA\ concentration\left[\frac{g}{\mu L}\right]}{660\frac{g}{mol} * basepairs\ of\ fragment}$$

Advantages of this method are that DNA contamination or an incomplete DNA digest may be visualized. The photometrical quantification at 260 nm is more precise, but does not distinguish between DNA contamination or the desired product. Absorption at 280 nm, however, can indicate protein contamination. A DNA sample with a (260/280) ratio ≥ 1.8 was generally accepted as pure.

2.2.6. Ligation

Digested insert and vector were ligated using T4-DNA ligase (Thermo Fisher Scientific, Waltham, USA), which conjoins 3'-hydroxyl and 5'-phosphate strands. The success of ligation is highly dependent on plasmid:insert ratio and overall concentration. In general, at least 20 ng vector were mixed with the insert in a 1:1-1:3 molar ratio (**Table 7**). To resolve secondary structures vector and insert were first heated at 60 °C for 10 minutes in water, before adding ligation reagents. Ligation was performed at 16 °C for 11 h, with subsequent inactivation at 65 °C for 10 minutes. The ligation was stored at -20 °C or directly used for transformation.

Table 7 Formulation for ligation of DNA fragments.

Component	**Amount**
plasmid DNA	≥ 20 ng
insert DNA	1:1-1:3 molar ratio
buffer (10 x)	3 µL
ATP (10 mM)	3 µL
T4-DNA ligase (5 U/µL)	1 µL
H_2O_{pure}	ad 30 µL

2.2.7. Transformation

To facilitate the inefficient uptake of DNA by *E. coli* chemically competent *E. coli* cells were generated using the TSS protocol (Chung *et al.*, 1989). According to the protocol, cells were grown (1%, v/v) in 50 mL LB medium at 37 °C until reaching an OD_{600} of 0.3-0.4. The cells were centrifuged under sterile conditions at 4 °C (5,000 x *g*, 5 min) and resuspended in 5 mL TSS-buffer. For storage, the cells were frozen in 200 µL aliquots at -70 °C.

For the transformation of plasmids into *E. coli*, competent cells were thawed on ice, mixed with the ligation reaction or 1-2 µL of plasmid DNA and incubated for 20 minutes on ice. The uptake of DNA was facilitated by a heat-shock for 1.5 minutes at 42 °C, followed by 2 minutes of incubation on ice. After cell regeneration in 2xYT medium at 37 °C for 1.5 h, the cell mixture was plated in appropriate dilutions (1:10-1:100) on selective agar plates and incubated at 37 °C overnight. The next morning, single colony forming units (CFU) were transferred into 5 mL LB medium containing selective antibiotics and cultured at 37 °C overnight, generating biomass for plasmid preparation. Plasmids were isolated and successful plasmid integration was screened by restriction digest and subsequent agarose gel electrophoresis. Positive clones were additionally verified by sequencing, and clones were then stored at -70 °C in glycerol solution.

2.3. Cultivation

2.3.1. Media

All liquid media were prepared in demineralized water (H_2O_{demin}). For agar plates, additionally 2% (w/v) agar was added to the liquid medium. All media were then sterilized by autoclaving and liquid media stored at RT for no longer then one month. After cooling, but before hardening agar plates were supplemented with antibiotics. Antibiotics were prepared as stock solutions and stored at -20 °C. Agar-plates were stored at 4 °C. LB medium agar plates (Bertani, 1951) were used for strain preservation and non-ectoine overproduction experiments (**Table 8**). Strains were transferred onto fresh plates if stored longer than two weeks.

Table 8 Formulation of LB medium.

Component	Amount [g/L]
casein-peptone	10
yeast-extract	5
NaCl	5
pH 7.2	

When preparing competent cells and for transformation, 2xYT medium (Sambrook, 1989) was used to provide best conditions for cell regeneration.

Table 9 Formulation of 2xYT medium.

Component	Amount [g/L]
casein-peptone	16
yeast-extract	10
NaCl	5
pH 7.2	

Performing experiments for the overproduction of ectoines under low salt conditions, the synthetic medium MM63 (Larsen *et al.*, 1987) was utilized (**Table 10**). If the basic medium was modified it is stated in the experiment. The pH was adjusted before adding NaCl. $FeSO_4$ was freshly prepared in a stock solution of 0.0011 g/mL, sterile filtrated and added after autoclaving the basic medium. The carbon source was prepared separately in 50 mL, autoclaved and added to the sterile medium after cooling.

Table 10 Formulation of MM63.

	Component	Amount [g/L]
1.	KH_2PO_4	13.61
	KOH	4.21
	$(NH_4)_2SO_4$	1.98
	$MgSO_4$ * 7 H_2O	0.25
	NaCl	0-1% (w/v)
	H_2O	ad 950 mL
	pH 7.2	
2.	$FeSO_4$ * 7 H_2O	0.0011
3.	Carbon source	4.6 (glycerol) 5 (glucose) 5.5 (pyruvate)
	H_2O	ad 50 mL

When cultivating the thiamine auxotrophic strain *E. coli* DH5α in minimal medium, 1 mL/L vitamin solution (VA) (Imhoff and Trüper, 1977) was added. The solution was prepared in a stock solution and stored at 4 °C under light exclusion.

Table 11 Formulation of vitamin solution.

Component	Amount [mg/L]
biotin	100
nicotinamide	350
thiamine hydrochloride	300
p-aminobenzoic acid	200
pyridoxal hydrochloride	100
potassium pantothenate	100
cyanocobalamin	50

For cultivating strains in bioreactors 1 mL/L trace element solution (TES) (Rippka *et al.*, 1979) was added to facilitate high cell density formation (**Table 12**). TES was prepared in a stock solution and stored at 4 °C under light exclusion.

Table 12 Formulation of trace element solution.

Component	Amount [g/L]
H_3BO_3	2.86
$MnCl_2 * 4 H_2O$	1.81
$ZnSO_4 * 7 H_2O$	0.222
$Na_2MoO_4 * 2 H_2O$	0.39
$CuSO_4 * 5 H_2O$	0.079
$Co(NO_3)_2 * 6 H_2O$	0.049

2.3.2. Shake Flask Experiments

Before starting experiments, bacterial strains were transferred from cryo-culture to fresh LB plates, containing antibiotics in case of plasmid bearing strains and incubated over night at 30 °C. Biomass was transferred onto another fresh plate and now incubated at 37 °C, to ensure strain fitness. Subsequently, strains were stored at 4 °C for up to two weeks.

Before starting shake flask experiments, a liquid pre-culture was performed. Therefore, cell material was transferred from the agar plate in 10-50 mL of the respective main culture medium plus antibiotics and incubated over night at 37 °C and 180 rpm. For inoculation of the main-culture, the pre-culture was centrifuged under sterile conditions (4,000 x *g*, 5 min) and the pellet resuspended in fresh medium. Shake flask experiments were carried out using OD-flasks (250 mL), allowing for a direct, undiluted measurement of the optical density (OD), which was sufficient for the experiments. A linear relation between the OD-reading and cell growth was assumed for $OD_{600} \leq 0.4$. To determine growth rates the OD values were displayed as their natural logarithm plotted against time and the highest slope during exponential growth-phase calculated.

Inoculation to OD_{600} 0.1 in 50 mL of the respective main culture medium plus antibiotics and supplements was carried out with the freshly resuspended pre-culture biomass. For the overproduction of ectoines MM63 with 0-0.5% NaCl was used. Deviations are given in the experiment. Cells were grown at 37 °C and 180 rpm until reaching an OD_{600} of 0.3-0.4 and induced with 0.2 mg/L AHT, in case of pASK-IBA plasmids, and with 120 mg/L IPTG, in case of pAKect1. During the subsequent product formation, OD was determined and sampling was performed (1-10 mL) for HPLC and protein analysis. Sampling occurred in appropriate reaction tubes and supernatant was separately stored from biomass at -20 °C after centrifugation (10,000 x *g*, 2 min). In some shake flask experiments a feed with carbon source was executed to prevent starvation of the cells over night. Therefore, the same amount of carbon source, e.g. 4.6 g glycerol in 50 mL, was prepared and added to the main culture under sterile conditions. In these cases, the amount of ammonium sulfate was doubled at the beginning of the experiment, to prevent N-limitation. After reaching the stationary phase, culture harvest was performed by centrifugation (11,000 x *g*, 20 minutes) at RT or 4 °C if necessary (protein analysis, qPCR). The supernatant was separated from the biomass and stored at -20 °C. The biomass was freeze-dried for weight determination or stored at -20 °C until protein purification.

In case of the isotope labelling experiments, the main culture was performed as described, but 20% of the carbon source was substituted with a derivative carrying the respective ^{13}C-isotope. Furthermore, isotope experiments with glycerol were performed with reduced buffer concentrations to facilitate the enrichment of ectoine from the supernatant. Therefore, only a quarter of KH_2PO_4 (3.4 g/L) and KOH (1.1 g/L) were added during these experiments. For isotope

experiments with pyruvate the buffer was substituted by TRIS/HCl-buffer (50 mM, pH 7) to prevent alkalization of the medium.

2.3.3. Bioreactor experiments

To execute the overproduction of ectoines in higher cell densities and under stable conditions, bioreactor experiments were performed. Adjusting the process demands, different fermentation set-ups were employed, described in more detail later. During all bioreactor processes the pH was controlled via probes and regulated by automated peristaltic pumps (5M KOH). The O_2 supply was provided by compressed air introduced through a sterile filter. Foaming of cells was prevented or counteracted by the addition of antifoam (Dehysan Z 2111, Cognis, Düsseldorf, Germany). Sampling was executed through silicon ports, the culture material centrifuged at RT (10,000 x *g*, 2 min) and biomass and supernatant stored separately at -20 °C. Determination of growth was performed photometrically at OD_{600} in cuvettes, representing the real OD. This allowed for the translation of OD_{600} of 1 into a cell dry weight of 0.515 g/L (Myers *et al.* , 2013). The medium used in all fermentations is the basic MM63 medium with 100 mg/L carbenicillin and 1 mL/L TES. Modifications are given in the experiment. Before filling with medium components under sterile conditions, the bioreactors were filled with H_2O_{demin} and autoclaved for sterilization.

The **1 L-DasGip** (Jülich, Germany) fermentation system does provide a heating jacket to control the temperature efficiently above RT, by automated adjustment through a feedback probe. Stirring of cell culture was achieved with a magnetic stirrer bar, which was regulated manually. In combination with the provision of compressed air through a sparger-block, O_2 supply could be regulated to some degree. The process was operated as a fed-batch, pumping feed-solution via manually operated peristaltic pumps. The culture medium was MM63 with reduced ammonium sulfate (1 g/L) and glycerol (2.8 g/L) amounts, sufficient to reach the fed-batch phase. The feeding occurred at a flowrate of 1.5 mL/h, resulting in the addition of 0.45 g/h glycerol and 0.2 g/h ammonium sulfate, as well as 1.75 mg/h carbenicillin (**Table 13**).

Table 13 Fed-batch feeding solution.

Component	Amount [g/L]
glycerol	300
$(NH_4)_2SO_4$	132
carbenicillin	1.2
H_2O_{demin}	Ad 1 L

For inoculation to an OD_{600} of 0.15, cell material from fresh agar-plates was used and precultures were prepared as described for shake flask experiments. 2 mL samples were extracted frequently for HPLC and OD determination. Induction was performed by the addition of 0.2 mg/L AHT at an OD_{600} of 0.3-0.4, as well as after 13 h.

The fermentation in the **5 L-Bioengineering** (Wald, Switzerland) fermenter was performed to increase the soluble O_2 provided during fermentation. Therefore, the incorporated bladed stirrer was adjusted manually to ensure an O_2 saturation above 20% throughout the process, by increasing stirrer speed. Additionally, compressed air supply through a tubing with thin openings facilitated a more even distribution of air in the fermenter. To track O_2 saturation, an additional O_2-probe was implemented into the reactor. The temperature was controlled by heated water circulation in the double-walled tank. The process was operated in a discontinuous fed batch mode, adding 9.2 g/L glycerol and 6 g/L ammonium sulfate in a sterile stock solution after 14 h. The cultivation medium was basic MM63 with 9.2 g/L glycerol and 6 g/L ammonium sulfate, plus 100 mg/L carbenicillin and 1 mL/L TES. Sampling and induction were performed as described before.

For fermentation at 28 °C a 0.2 L **small-scale bioreactor setup** from DasGip (Jülich, Germany) was utilized. The bioreactors were mounted in a Perspex rack, with silicon sealings and the temperature was regulated by a water cooler. Oxygen supply was regulated as described for the 1 L DasGip system and monitored as described for the 5 L Bioengineering fermenter. The basic MM63 medium contained 9.2 g/L glycerol and 3.4 g/L ammonium chloride, which were added again in 10 mL stock solutions after 14, 21 and 34 h. Ammonium sulfate was substituted for ammonium chloride to achieve better solubility of components in the medium. The inoculation was performed as described before, starting with a higher OD_{600} of 1. Induction was performed by adding 0.2 mg/L AHT at OD_{600} 1.5-2 and after 21 h.

Sampling for HPLC and OD determination was conducted as described before. Additionally, 10 mL samples were extracted for the analysis of proteins via mass-spectrometry and transcripts via qPCR. These samples were centrifuged directly at 4 °C (10,000 x *g*, 2 min), biomass was separated from supernatant and stored at -20 °C. For the fermentation with β-lactamase inhibitor, 10 mg/L clavulanic acid was added at the beginning of the fermentation and supplemented again after 21 and 34 h.

2.4. Analytics

2.4.1. High Performance Liquid Chromatography (HPLC)

For the identification and quantification of liquid dissolved compounds in the supernatant of ectoine overproduction experiments high performance liquid chromatography (HPLC) was employed. Therefore, samples are diluted in an adequate degassed mobile phase and pumped with high pressure on a column (stationary phase) for separation. The separation occurs due to the physical and chemical properties of the dissolved compounds interacting with the properties of the stationary phase. With different combinations of mobile and stationary phase, as well as with different conditions like temperature and pH, various separation patterns can be achieved. In comparison to MS and NMR the method does not detect all compounds in a sample. An unknown signal is identified and quantified by the comparison of the specific retention time and the characteristic readout-pattern (e.g. UV/RI) of the compound with a standard of known concentration.

Substances exhibiting no net-polarity at neutral pH (**ectoine, hydroxyectoine**) were separated on a reversed-phase silica column, with polar amino groups attached to hydroxyl groups via hydrophobic propyl chains (LiChospher 100 NH_2, 5 µm, Merck, Darmstadt, Germany). Samples were diluted 5-10 times in the mobile phase (80% acetonitrile, v/v) at physiological pH, centrifuged (10,000 x *g*, 5 min) and checked for phase separation. If no separation was visible, the diluted samples were pumped at a flowrate of 1 mL/min at RT and captured by refractive-index (RI, Shodex RI-71, Showa Denko K.K., Tokyo, Japan) and UV-detection (SpectraSystem UV1000, 210 nm, Thermo Fisher Scientific). This method was used for the detection of ectoines and ADABA, as well as for the carbon source glycerol. For the analysis of the fermentation

samples a different HPLC was utilized (Azura, Knauer, Berlin, Germany) including a RI (RID 2.1) and UV (UVD 2.1 190-500 nm) detector utilizing the same column as before (NH_2) and a buffered mobile phase (3 parts 100% acetonitrile, 1-part KH_2PO_4 buffer, v/v), ensuring more equal results.

For the quantification of **organic acids and sugars** in fermentation supernatants, the polymer based Aminex HPX-87H (Bio-Rad, Hercules, USA) was utilized. Samples were diluted 2-10 times in the mobile phase (0.02 N H_2SO_4), centrifuged (10,000 x *g*, 5 min) and pumped at a flow rate of 0.6 mL/min. The compounds were analyzed by UV (Accela PDA detector, Thermo Scientific) and RI with refractoMonitor IV (Milton Roy, Ivyland, USA). Mainly the fermentation side products acetate and formate were analyzed by this method.

Substances of low abundance, exhibiting **reactive primary or secondary amino groups** were quantified by the sensitive FMOC-ADAM HPLC. Therefore, the solutes were derivatized with 9-fluorenylmethyloxycarbonyl (FMOC), which can be detected by a fluorescence-detector (SpectraSystem FL3000, 254nm (ex.), 316nm (em.), Thermo Fisher Scientific). To prevent over-detection, free FMOC was captured by 1-aminoadamantane (ADAM). This method was mainly used to detect the precursor molecule ADABA at low concentrations. A reversed-phase silica column was used as stationary phase. The mobile phase A (20% acetonitrile, 80% Na-acetate buffer, 0.5% THF (v/v)) was gradually mixed with mobile phase B (80% acetonitrile, 20% Na-acetate buffer (v/v)) (**Figure 8**).

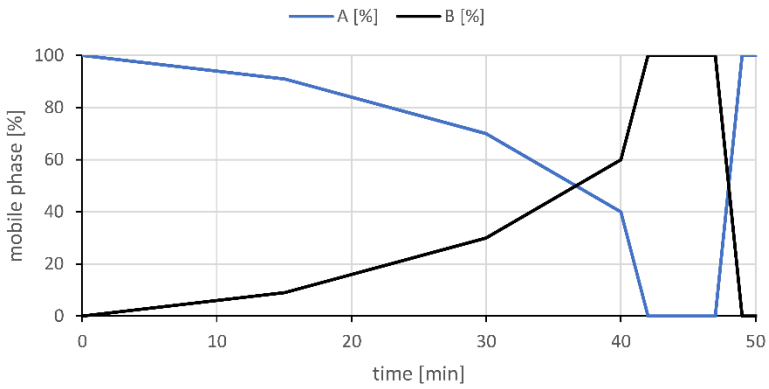

Figure 8 Gradient of the mobile phases A and B during FMOC-ADAM HPLC.

Samples were 20-50 times diluted in pure water and centrifuged (10,000 x *g*, 5 min). Then, 40 µL of the sample was mixed with the same volume borate buffer (0.5 M boric acid, pH 7.7), which included 25 µM taurine as an internal standard. The derivatization with 80 µL FMOC buffer (1 mM FMOC in acetone) was performed for 45 seconds on a shaker at RT and was stopped by the addition of 100 µL ADAM buffer (40 mM ADAM in borate buffer, 1:1 mixed in acetone) for 45 seconds. At last, 140 µL of the mobile phase A was added and mixed. The sample was pumped at a flowrate of 1.25 mL/min and separation occurred at a temperature of 45 °C.

2.4.2. Protein Extraction

The expression of the heterologous proteins EctABC from *A. cryptum* in *E. coli* K12 DSM498 was analyzed using SDS-PAGE, as well as mass-spectrometry. The host strain was cultivated in the small-scale bioreactor system with MM63, 0% NaCl and no clavulanic acid (cf. 2.3.3. Bioreactor experiments). The cells were inoculated to an OD_{600} of 1 and cultivated until reaching an OD of 1.5-2 for induction with 0.2 mg/L AHT. Sampling of biomass for protein analysis was executed before induction, as well as 5, 17 and 30 h post induction, by sampling 10 mL of culture volume and centrifugation at 4 °C (10,000 x *g*, 2 min). Cell pellets were subsequently stored at -20 °C until further processing.

For the extraction of soluble cell protein, the pellets were thawed on ice and resuspended in 200 µL resuspension-buffer. After mixing thoroughly with 2 µL Lysozyme solution (10%, w/v), the cells were incubated for 30 minutes on ice, followed by the addition of 10 µL SDS solution (10%, w/v) and another 30 minutes incubation on ice. By the addition of 2 µL DNaseI (1%, w/v) and 1 µL $MgCl_2$ solution (50 mM) the DNA was hydrolyzed for 1-2 h on ice. Subsequently, the samples were frozen for 30 minutes at -20 °C. Through ultra-sonification for 45 minutes on ice cell disruption was completed and cell debris were separated from the soluble protein containing supernatant by centrifugation at 4 °C (16,000 x *g*, 30 min). In the following, the supernatant was transferred into a fresh tube and stored at –20 °C. For the extraction of insoluble proteins, the cell-pellet was washed two-times with 500 µL resuspension-buffer and centrifuged (14,500 x *g*, 5 min) to remove remaining soluble protein. By the addition of 1 mL SDS solution (1%, w/v) and heating at 80 °C and 700 rpm for 2 h, the insoluble fraction was extracted.

2.4.3. Protein quantification

To determine the protein concentration for SDS-PAGE, mass-spectrometry and for biomass determination during cultivation, a colorimetric assay after Smith *et al.* (1985) was performed. In the assay Cu^{2+} is reduced to Cu^{+} by reacting with peptide bonds in alkaline solution, which leads to the formation of a photometrically detectable violet complex with bicinchoninic acid (BCA). The protocol was executed according to the manufacturer's instructions (BCA Protein Assay Kit, VWR, Darmstadt, Germany). The soluble proteins were diluted 1:20-1:50 in H_2O_{pure} and the insoluble proteins 1:10-1:20. The quantification was executed by comparing the absorbance at 550 nm to known concentrations of bovine serum albumin (BSA) protein (50-500 µg/mL).

2.4.4. SDS-Polyacrylamide Gel Electrophoresis (SDS-PAGE)

By performing SDS-PAGE analysis after Laemmli (1970), the expression of the heterologous proteins EctABC were visualized for various time-points in the cultivation process. Through the addition of dithiothreitol (DTT) and SDS, the tertiary structure and charge of the proteins were equalized to allow for a separation according to protein size in the polyacrylamide gel. The proteins, now exhibiting a negative net charge, were focused in the concentrating-gel (pH 6.8) and subsequently separated according to their size in a gel exhibiting a pH of 8.8 and a lower pore size (separating-gel).

Table 14 Formulation of the discontinuous SDS-PAGE gels. For polymerization 50 µL APS (10%, w/v) and 10 µL TEMED were added to the mixed solutions.

Formulation [mL]			
concentrating-gel		**separating-gel**	
buffer	1.25	buffer	2.5
acrylamide-mix	1	acrylamide-mix	6.5
SDS (10%, w/v)	0.05	SDS (10%, w/v)	0.1
H_2O_{demin}	ad 5	H_2O_{demin}	ad 10

Protein samples were incubated with loading dye (4x RSB) at 70 °C for 10 minutes to ensure complete denaturation and reduction of proteins. Subsequently, 20 µg of protein were transferred into each lane of the SDS-PAGE gel. For size discrimination a protein ladder was loaded into one

lane (PageRuler prestained, Thermo Fisher Scientific). The proteins were focused in the discontinuous SDS-PAGE applying 60 V and separated in the second part of the gel at 100 V. After the electrophoresis, the separation gel was washed with H_2O_{demin} and incubated in Quick Coomassie staining solution (Serva, Heidelberg, Germany) for 1 hour. Subsequently, the background-staining was removed by washing with H_2O_{demin} several times.

2.4.5. Mass Spectrometry

For the abundance determination of the heterologous proteins EctABC from *A. cryptum* the proteins were purified and quantified as described earlier (cf. 2.4.2. Protein Extraction, 2.4.3. Protein quantification) and handed in for analysis to the mass-spectrometry core-facility (Dr. Marc Sylvester, Institute of Biochemistry and Molecular Biology, Bonn, Germany). The proteins were subjected to in-solution preparation of peptides, vacuum concentrated, dissolved in 20 mM triethyl ammonium bicarbonate buffer (TEAB) and labelled with isobaric TM10plex reagents (Thermo Fisher Scientific, Darmstadt, Germany). For LC-MS, peptide separation was performed on a Dionex Ultimate 3000 RSLC nano HPLC system (Dionex GmbH, Idstein, Germany) with a C18 analytical column made in-house (200 mm length, 75 µm inner diameter, ReproSil-Pur 120 C18-AQ, 1.9 µm). Labelled peptides were resuspended in 0.1% formic acid (FA) (solvent A) and separated in a linear gradient (1 – 35%) with solvent B (90% acetonitrile, 0.1% FA) within 180 min at 300 nL/min. The nanoHPLC was coupled online to an Orbitrap Fusion Lumos mass spectrometer (Thermo Fisher Scientific, Bremen, Germany). Raw data processing was performed with Proteome Discoverer software 2.3.0.523 (Thermo Fisher Scientific). MS data were searched against the *E. coli* K12 reference proteome sequences from Uniprot (2019/05), relevant ectoine synthesis enzymes, and contaminants (cRAP). The abundances are given as the median of a biological triplicate, including the standard deviation.

2.4.6. Nuclear Magnetic Resonance Spectroscopy (NMR)

To analyze the incorporation of the ^{13}C-isotope into ectoine, inverse-gated ^{13}C-NMR was performed by the "Institute of Pharmaceutical Biology" (Dr. Stefan Kehraus, Bonn, Germany). ^{13}C-NMR is used to resolve and quantify organic compounds, by stimulating the nuclear spin with radio waves into nuclear magnetic resonance. The change in the magnetic field can be detected and is dependent on the chemical surrounding of the atom. This allows for the determination of the functional groups of the substance. Resonance frequencies are given as a deviation in respect to a standard compound in parts per million (ppm). To account for disproportionality of the signals, inverse gated NMR was performed, allowing for more quantitative results.

A negative aspect of NMR-spectroscopy is the demand for relatively high concentrations of analyte (≥ 5 mg/mL). To generate respective concentrations of ectoine from the medium of shake-flask cultivations (cf. 2.3.2. Shake Flask Experiments), the medium was evaporated in a vacuum concentrator (SpeedVac Savant ISS110, Thermo Fisher Scientific). The concentrated medium components were resuspended in low volumes of D_2O (≤ 2 mL). In case of labelling experiments with ^{13}C-glycerol, the reduction of buffer components allowed for a direct concentration of ectoine from the medium. During the cultivation with ^{13}C-pyruvate, however, it was not possible to reduce buffer components (50 mM TRIS/HCl), making a desalting with ion-exchange chromatography necessary. Therefore, the cultivation medium was acidified to pH 1.8 with HCl (6 M) and 50 mL were pumped over 25 g of an ion-exchange resin with sulfonic-acid functional groups (Dowex 50wx8, Merck, Darmstadt, Germany). Before application, the resin was flushed with 150 mL KCl (2 M) and subsequently washed with H_2O_{demin}. The elution was initiated by the addition of 0.5 M NH_3-solution. Detection of solutes was performed with refractive index (RI) and $UV_{220\ nm}$, while auto-sampling occurred in volumes of 4.5 mL into falcon-tubes at a flow rate of 1.5 mL/min. After chromatography, the NH_3-solution was vaporized at RT under a fume-hood and the concentration of ectoine was determined through HPLC-analysis, after titrating the samples to pH 7 with HCl. Samples containing high concentrations of ectoine were vaporized by vacuum concentration and dissolved in D_2O, as described before. As a standard 1,2-^{13}C-acetate in the same molar concentration as ectoine, as well as 5 mg Na-trimethyl-propionate (TMSP) were added. The acquisition was executed with Avance 300DPX spectrometer (Bruker, Billerica, USA) at a frequency of 300 MHz. Integrals of the signals were obtained with MestReNova 8.0.1 and

normalized to the natural abundancy of ^{13}C-isotopes by subtracting a control measurement without added isotopes.

The *in-silico* analysis of ^{13}C-NMR results was performed using a software developed in cooperation with Moritz L. Sümmermann (Institute for mathematical didactics, University Cologne). The software utilizes experimentally determined labelling patterns to calculate probabilities of the fluxes in a given network closest to the measured distribution. The model describes the synthesis of oxaloacetate as a reflection of the ectoine labelling in carbon C1-C4 (**Figure 9**). The network begins with phosphoenolpyruvate/pyruvate, where β is the probability that pyruvate is introduced into the TCA via acetyl-CoA and 1-β gives the probability for phosphoenolpyruvate being directly converted to oxaloacetate. The likelihood of a flux into the glyoxylate-shunt, splitting isocitrate into succinate and glyoxylate, which is condensed to malate by the addition of acetyl-CoA, is reflected by α. The conventional path of the TCA from isocitrate into succinate is given by β-α. The possibility that the labelling pattern is flipped by the symmetry in succinate/fumarate is described by γ. This could happen by equilibria reactions in the TCA or by aspartate lyases.

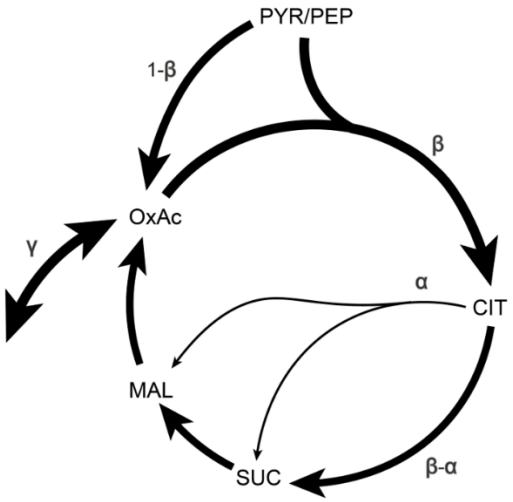

Figure 9 Representation of the network for *in-silico* flux analysis. Fluxes are determined in dependence of each other starting with pyruvate (PYR) and phosphoenolpyruvate (PEP) (β), followed by the glyoxylate-shunt (α). The only further alteration in labelling distribution appears due to the symmetry (γ) of the molecules succinate (SUC) and fumarate. The labelling pattern in ectoine can be directly derived from the distribution in oxaloacetate (OxAc) and acetyl-CoA.
CIT = citrate, MAL = malate

The program finds the best fit for flux ratios in minimizing the difference between experimentally obtained and computed labeling percentages solving a linear equation system, constrained by a set of quadratic equations. The computation of such an optimal solution consists of two steps. First the quantities of all molecules in the system are computed relative to the substrate. These quantities are defined only by the reactions chosen to be part of the pathway and not by the measurements made. These quantities, parametrized by the flux ratio values, are then used to define a stochastic matrix, which is then used to establish the linear equation system (Sümmermann, Bethlehem and Galinski, unpublished).

2.4.7. Quantitative-PCR (qPCR)

For the analysis of transcripts during the ectoine overproduction in the small-scale bioreactors using MM63 with 0% NaCl and without clavulanic-acid (cf. 2.3.3. Bioreactor experiments), qPCR was executed. All RNA-protocols were executed utilizing sterile and RNase-free material at a dedicated RNA-workbench treated with RNase-Away (Carl Roth, Karlsruhe, Germany). 2 mL samples were extracted directly from the bioreactor, centrifuged at 4 °C (10,000 x *g*, 2 min) and the pellet stored at -20 °C. The extraction of RNA from an appropriate cell-number ($\leq 10^8$) was executed according to the manufacturer's instructions using *Quick*-RNA miniprep kit (Zymo Research, Irvine, USA). The Isolation is based upon a cell-lysis buffer system in combination with a column purification. The included on-column DNaseI treatment was supplemented by a separate DNA hydrolysis after the purification, to ensure a complete digestion of genomic- and plasmid-DNA. The reaction was performed for 1 hour at 37 °C in DNaseI reaction-buffer (100 mM TRIS/HCl, pH 7.5, 25 mM $MgCl_2$, 1 mM $CaCl_2$) and incubation stopped with 5 mM EDTA at 75 °C for 10 minutes (**Table 15**).

Table 15 Formulation of DNaseI reaction after RNA purification.

Component	Amount
RNA	10 µg
reaction-buffer (10x)	10 µL
DNaseI (RNase-free)	1 µL (2 units)
H_2O_{pure} (RNase-free)	Ad 100 L

The purified RNA was directly used for qPCR with the CAPITAL qRT-PCR probe mix (4x) (biotechrabbit, Berlin, Germany). The formulation was executed on ice and pipetted into the CFX-qualification plates before starting the analysis in the CFX Connect Real-Time PCR Detection System (Bio-Rad, Hercules, USA) (**Table 16**). As a housekeeper gene *hcaT* was used, expressing the 3-phenylpropionic transporter (Zhou *et al.*, 2011). Analysis was performed with the CFX Manager software (version 3.1.1517.0823), evaluating the melting curves and normalizing the relative expression for the housekeeper. Measurements were executed in three technical replicates.

Table 16 qPCR formulation and amplification protocol.

Formulation		**Amplification**				
Component	**Amount**	**Step**		**Temperature [°C]**		**Time**
one-step mix (2x)	25 µL	1.	cDNA synthesis	45-55	1x	10-20 min
RT-mix (20x)	2.5 µL	2.	initial activation	95	1x	2 min
primer (10 µM)	2 µL	3.	denaturation	95		10 sec
RNA	0.1-1 µg		annealing	T_m - 5	35-40 x	10 sec
H_2O_{pure} (RNase-free)	Ad 50 µL		elongation	72		30-60 sec/kb
		4.	final elongation	72	1x	5 min
		5.	storage	4	1x	∞

Primer were designed with Primer3 using default settings (Rozen and Skaletsky, 2000) (**Table 17**).

Table 17 Primers used for qPCR.

Name	**Sequence (5'-3')**
EctA_RTQPCR-front_fwd	TCC GGC GGT GAC CGC
EctA_RTQPCR-front_rev	AGC ACG CAG GTT TCG G
RTqPCR_EctA # 1_fwd	CTG TTC GAA AGC CTT GCC C
RTqPCR_EctA # 1_rev	AGA TGT CCT TTC GTG CTG GT
RTqPCR_EctA # 2_fwd	AGA CCT CTC GCG CAT CTT C
RTqPCR_EctA # 2_rev	CTT TCG AAC AGC CGC CAC
RTqPCR_EctB_fwd	AAT CAT CCG GTG CTG AAA CG
RTqPCR_EctB_rev	GCT TCA GGA TCA CGG TTT CC
RTqPCR_EctC_fwd	GCT TCT CGT TCC ACA TCA CC
RTqPCR_EctC_rev	GTT GAG CAC ATA GAG CAC GC

2.5. Chemicals, Enzymes and Kits

Chemicals	Manufacturer
acetonitrile (≥ 99%)	Merck, Darmstadt, Germany
Nγ-acetyl-L-2,4-diaminobutyric acid, ADABA	Isolated from *H. elongata* WUB01
acrylamide (30%)	Carl Roth, Karlsruhe, Germany
adenosine triphosphate disodium salt	Sigma-Aldrich, Steinheim, Germany
agar-agar Kobe I	Carl Roth
agarose	Carl Roth
1-aminoadamantan hydrochloride, ADAM (≥ 99%)	Sigma-Aldrich
ammonia solution, NH_3 (25%)	Merck
ammonium chloride, NH_4Cl (≥ 99%)	Carl Roth
ammonium persulfate, APS (≥ 98%)	Bio-Rad, Hercules, USA
ammonium sulfate, $(NH_4)_2SO_4$ (≥ 99.5%)	Carl Roth
anhydrotetracylcine hydrochloride	IBA, Göttingen, Germany
biotin (≥ 99%)	Sigma-Aldrich
boric acid, H_3BO_3 (≥ 99%)	Fluka, Buchs, Switzerland
bovine serum albumin, BSA	Sigma-Aldrich
bromophenol blue	Merck
calcium chloride dehydrate, $CaCl_2$ x 2 H_2O (≥ 99.5%)	Merck
carbenicillin disodium salt (≥ 88%)	Carl Roth
casamino acids	Becton Dickinson, Franklin Lakes, USA
casein peptone (NZamin)	Carl Roth
chloramphenicol	Carl Roth
chloroform (≥ 99.8%)	Merck
cobalt (II)-nitrate, $Co(NO_3)_2$ x 6 H_2O (≥ 99%)	Merck
deoxyribonucleoside triphosphate mix, dNTPs (10 mM)	Thermo Fisher Scientific, Waltham, USA
deuterium oxide (≥ 99%)	Merck
potassium dihydrogen phosphate, KH_2PO_4 (≥ 99%)	Carl Roth
dimethyl sulfoxide, DMSO (≥ 99.5%)	Carl Roth

dithiothreitol, DTT (≥ 99%)	Carl Roth
ectoine	behawe Naturprodukte, Rietberg, Germany
iron(II)-sulfate heptahydrate, $FeSO_4$ x 7 H_2O (≥ 99%)	Sigma-Aldrich
acetic acid (100%)	Merck
ethanol (≥ 99.8%)	Carl Roth
ethylenediaminetetraacetic acid, EDTA (≥ 99%)	Carl Roth
9-fluorenylmethyloxycarbonyl, FMOC (≥ 97%)	Sigma-Aldrich
formaldehyde (≥ 37%)	Carl Roth
GelRed	Biotium, Fremont, USA
GeneRuler DNA ladder	Thermo Fisher Scientific
D-glucose monohydrate (≥ 99%)	VWR, Darmstadt, Germany
glycerol (≥ 99.5%)	Carl Roth
1,3- & 2-^{13}C glycerol (≥ 99%)	Cambridge Isotope Laboratories, Tewksbury, USA
yeast extract	Carl Roth
hydroxyectoine (≥ 95%)	Sigma-Aldrich
isopropanol (≥ 99.8%)	Carl Roth
isopropyl-β-D-thiogalactopyranoside, IPTG (≥ 99%)	Carl Roth
potassium chloride, KCl (≥ 99.5%)	Carl Roth
potassium hydroxide, KOH (≥ 85%)	Carl Roth
copper sulfate pentahydrate, $CuSO_4$ x 5 H_2O (≥ 99%)	Carl Roth
Laemmli-buffer (SDS-PAGE, 10 x)	Serva, Heidelberg, Germany
magnesium chloride heptahydrate, $MgCl_2$ x 7 H_2O (≥ 99%)	Carl Roth
magnesium sulfate heptahydrate, $MgSO_4$ x 7 H_2O (≥ 99.5%)	Merck
manganese(II)-chloride tetrahydrate, $MnCl_2$ x 4 H_2O (≥ 99%)	Merck
methanol (≥ 99.9%)	Carl Roth
N,N'-methyl bis-acrylamide (2%)	Merck
Na-acetate trihydrate (≥ 99.5%)	Sigma-Aldrich
Na-carbonate, Na_2CO_3 (≥ 99.5%)	Merck

Na-chloride, NaCl (≥ 99.5%)	Carl Roth
Na-dodecyl sulfate, SDS (≥ 99%)	Serva
Na-hydroxide, NaOH (≥ 99%)	Merck
Na-molybdic dihydrate, Na_2MoO_4 x 2 H_2O (≥ 98%)	Merck
Na-trimethylsilyl propanoic acid, TMSP (≥ 98%)	Merck
nicotinamide (≥ 99.5%)	Fluka
PageRuler prestained protein ladder	Thermo Fisher Scientific
pyridoxal hydrochloride (≥ 99.5%)	Merck
pyruvate sodium salt (≥ 99%)	Carl Roth
1-, 2-, 3-^{13}C pyruvate sodium salt (≥ 99%)	Cambridge Isotope Laboratories
Ouick Coomassie stain	Generon, Slough, UK
hydrochloric acid, HCl (37%)	Carl Roth
sulfuric acid, H_2SO_4 (95-97%)	Merck
N,N,N',N'-tetramethyl ethylene diamine, TEMED (≥ 99%)	Carl Roth
thiamine hydrochloride (≥ 99%)	Fluka
2-Amino-2-(hydroxymethyl) propane-1,3-diol, TRIS (≥ 99.9%)	Carl Roth
Triton X-100	Fluka
zinc sulfate heptahydrate, $ZnSO_4$ x 7 H_2O (≥ 99.9%)	

Enzymes	**Manufacturer**
deoxyribonuclease I, DNase I	Sigma-Aldrich
DNase I RNase-free (1 U/µL)	Zymo Research, Irvine, USA
lysozyme	Carl Roth
Pfu-DNA-polymerase (2.5 U/µL)	Thermo Fisher Scientific
Phusion high fidelity DNA-polymerase (2 U/µL)	Thermo Fisher Scientific
restriction endonucleases	Thermo Fisher Scientific
Ribonuclease A, RNase A	Carl Roth
Taq-DNA-polymerase (5 U/µL)	Thermo Fisher Scientific
alkaline phosphatase, FastAP (1 U/µL)	Thermo Fisher Scientific

T4-DNA-ligase (5 Weiss U/µL)	Thermo Fisher Scientific

Kits	**Manufacturer**
BCA protein assay kit	VWR
CAPITAL qRT-PCR probe mix (4x)	biotechrabbit, Berlin, Germany
peqGOLD gel extraction kit	New England Biolabs, Ipswich, USA
Quick-RNA miniprep kit	Zymo Research
Zyppy plasmid miniprep kit	Zymo Research

2.6. Solvents and Buffer

Isolation of DNA	
TES-buffer	5 mM TRIS/HCl pH8, 5 mM NaCl, 5 mM EDTA
Na-acetate solution	3 M Na-acetate pH 4.8
Isolation of plasmids	
NC-buffer 1	50 mM TRIS/HCl pH 8, 10 mM EDTA, RNaseA (10%, w/v), stored at 4 °C
NC-buffer 2	200 mM NaOH pH 12.5, SDS (1%, w/v)
NC-buffer 3	3 M potassium acetate pH 5.5, stored at 4 °C
Gel electrophoresis	
TAE-buffer (50x)	2 M TRIS/HCl pH 8, 0.5 M EDTA, glacial acetic acid (3%, v/v)
loading dye (6x)	10 mM TRIS/HCl pH 7.6, 60 mM EDTA, bromophenol blue (0.03%, w/v), glycerol (60%, v/v), stored at 4 °C
Generation of competent cells	
TSS	PEG 3350 (10%, w/v), DMSO (5%, v/v), 50 mM $MgSO_4$, resuspended in LB medium pH 6.5 (sterile filtered)
Protein extraction	
Resuspension buffer	20 mM TRIS/HCl pH 8, o.5 M NaCl
SDS-PAGE	
concentrating gel buffer	0.5 M TRIS/HCl pH 6.8
separating gel buffer	1.5 M TRIS/HCl pH 8

acrylamide mix	32.7 mL acrylamide (30%), 10 mL bisacrylamide (2%), ad 50 mL (H_2O_{demin})
reducing sample buffer (4x)	4.5 mL conc. Gel-buffer, 5 mL glycerol, SDS (5%, w/v), DTT (3.68%, w/v), bromophenol blue (tip of a spatula), ad 10 mL (H_2O_{demin}), stored at -20 °C

2.7. Software

Program	Reference
ChromQuest (version 5.0)	Thermo Scientific, Wlatham, USA
EcoCyc (*E. coli* Database Collection)	SRI International, Menlo Park, USA
KEGG (Kyoto Encyclopedia of Genes and Genomes)	Kanehisa Laboratories, Kyoto, Japan
MestReNova (version 8.0.1)	Mestrelab Research, Santiago de Compostela, Spain
NCBI (National Center for Biotechnology Information)	U.S. National Library of Medicine, Bethesda, USA
Omix Visualization (version 1.9)	Omix Visualization GmbH & Co. KG, Lennestadt, Germany
Primer3 (version 0.4.0)	Whitehead Institute for Biomedical Research, Cambridge, USA
RBS Calculator (version 2.0)	Salis Lab, Penn State University, USA
SnapGene (version 5.0.1)	GSL Biotech, Chicago, USA
CFX Manager software (version 3.1.1517.0823)	Bio-Rad Laboratories, Hercules, USA

2.8. Laboratory Equipment

Eqipment	Manufacturer
agarose gel electrophoresis chamber Biometra Horizon 58	Analytik Jena, Jena, Germany
Alpha I-6 freeze dryer	Martin Christ, Osterode, Germany
bioreactor 0.2 & 1 L	DASGIP, Jülich, Germany
bioreactor 5 L	Bioengineering, Wald, Switzerland
BioSpectrometer (DNA quantification)	Epp Eppendorf, Hamburg, Germany
centrifuge J2-HS, rotor JA-14	Beckman Coulter, Brea, USA

centrifuge tabletop 5418	Eppendorf
centrifuge Avanti J-20, rotor JA-10	Beckmann Coulter
centrifuge Megafuge 1.0, rotor BS4402	Haereus Instruments, Hanau, Germany, Thermo Fisher Scientific, Waltham, USA
CFX Connect Real-Time PCR Detection System	Bio-Rad, Hercules, USA
Gel-Imager	Intas, Göttingen, Germany
HPLC-degasser SDM1000 (SpectraSystem)	Thermo Fisher Scientific
HPLC Azura	Knauer, Berlin, Germany
HPLC-pump P100, P1000, P2000 (SpectraSystem)	Thermo Fisher Scientific
HPLC-fluorescence detector (FMOC-ADAM) FL3000 (SpectraSystem)	Thermo Fisher Scientific
HPLC-RI detector (NH_2) Shodex RI-71	Showa Denko K.K., Tokio, Japan
HPLC-RI detector (Aminex) refractoMonitor IV	Milton Roy, Warminster, USA
HPLC-RI detector (Azura) RID 2.1	Knauer
HPLC-UV detector (NH_2) Accela PDA detector	Thermo Fisher Scientific
HPLC-UV detector (Azura) UVD 2.1	Knauer
Novaspec II photometer	Pharmacia, Uppsala, Sweden
PCR-thermocycler MyCycler	Bio-Rad
pH-, pO_2-probes	Mettler Toledo, Gießen, Germany
pH meter	Knick, Berlin, Germany
plate incubator B 6420	Heraeus Instruments
Plate reader Infinite M200	Tecan, Crailsheim, Germany
rotation shaker IKA-Vibrax-VXR	Janke & Kunkel, Staufen, Germany

SDS-PAGE chamber Mini-PROTEAN	Bio-Rad
SpeedVac Savant ISS110	Thermo Fisher Scientific
thermo incubator AI 70	Infors AG, Bottmingen, Switzerland
Thermomixer	Eppendorf
ultrasonic bath Sonorex TK 52	Bandelin, Berlin, Germany

3. Results

3.1. Design of the Ectoine Overproduction Strain

The ability of the hydroxyectoine biosynthesis gene cluster of *A. cryptum* to produce the compatible solute hydroxyectoine upon salt induction has been shown by Moritz *et al.* (2015). The subsequent successful implementation into *E. coli* demonstrated its potential for heterologous production of the compatible solutes ectoine and hydroxyectoine in gram-negative bacteria at low salt concentration (Bethlehem, 2015). Upon induction with anhydrotetracycline (AHT) a production of 6 mM ectoine (0.9 g/L) was achieved using the pASK_ectABCD$_{mut}$ plasmid in *E. coli* DH5α. Similarly, a production of 8 mM (1.3g/L) hydroxyectoine was achieved using the pASK_ectABCDask plasmid. This corresponds to a specific production of 0.9 g_{solute}/g_{dcw} ectoine and 1.2 g_{solute}/g_{dcw} hydroxyectoine. These results were achieved with glucose as carbon source and 1% NaCl in shaking flask experiments. Under these conditions the compatible solutes were excreted naturally into the cultivation medium. By changing the carbon source to glycerol and performing experiments in presence of 0.5% NaCl Moritz (2018) could increase the production of ectoine to 1.7 g/L and of hydroxyectoine to 1.6 g/L, with an elevated specific production of 2.9 g_{solute}/g_{dcw} and 2.2 g_{solute}/g_{dcw}, respectively. Other attempts to optimize production efficiency or product titer, however, remained unsuccessful.

3.1.1. Testing Base Strains

To begin the strain optimization process for *E. coli* DH5α pASK_ectABCD$_{mut}$ a base strain was chosen, which was supposed to fit the process profile while being free of unknown or unwanted mutations impairing performance (cf. 1.4. *E. coli* Strain Design & Development). The UV-perturbated genome of *E. coli* DH5α naturally harbors random mutations (Casali, 2003), such as an auxotrophy for thiamine. Therefore this strain serves as a poor basis for further optimizations of the production process. In science and industry, a wide range of *E. coli* strains are employed, most of them belonging to either the *E. coli* K- or B-family. Due to its superior properties for industrial processes described in literature, *E. coli* BL21 was chosen as the designated base strain (Yoon *et al.*, 2009). Additionally, the strain K12 DSM498 was tested as an *E. coli* wildtype

K-strain. The original plasmid for ectoine production (pASK_ectABCD$_{mut}$) was generated by Bethlehem (2015) and further described by Moritz (2018). It carries a critical point mutation in *ectD*, which is why *E. coli* DH5α pASK_ectABCD$_{mut}$ produces only ectoine (Moritz, 2018). The pASK_ectABCD$_{mut}$ plasmid was transformed into competent *E. coli* BL21 and K12 cells and production efficiency for both strains was subsequently compared to the original *E. coli* DH5α strain. The overproduction was performed in shake flasks with 0.1 L MM63 medium containing 0.5% NaCl and either 5 g/L glucose (25 mM) or 4.6 g/L glycerol (50 mM). To enable growth of DH5α cultures in minimal medium, vitamin solution was added. A salt concentration of 0.5% corresponded to the optimum ectoine production conditions for the DH5α strain. Production cultures were inoculated with an OD of 0.1 and production was induced by addition of 0.2 mg/L AHT at OD 0.3-0.4. The cultures were harvested in stationary growth phase, after approximately 24 h.

When using glucose as carbon source both new strains exhibited accelerated growth characteristics, compared to the original *E. coli* DH5α (**Figure 10A**). The final OD was highest for the BL21 strain (OD 1.3), but to a similar extent lower in the K12 and the original DH5α strain (OD 1.1). Also, when using glycerol as carbon source BL21 and K12 initially grew slightly faster than DH5α (**Figure 10B**). The BL21 strain reached a very similar final OD as on glucose (OD 1.3) and the K12 and DH5α strains showed again a significantly lower final OD of 0.9.

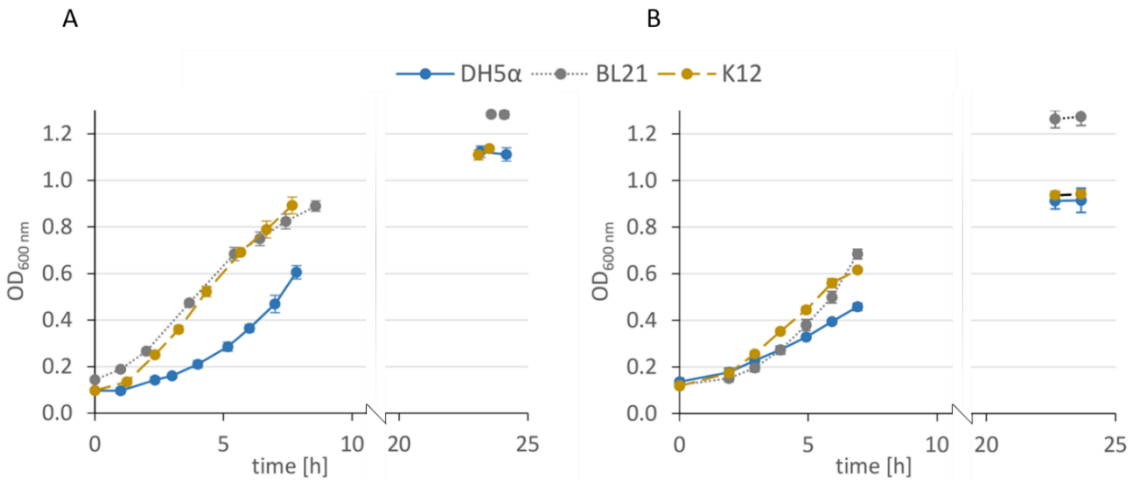

Figure 10 Growth data (OD$_{600\ nm}$) of *E. coli* DH5α, BL21 and K12 with the ectoine production plasmid pASK_ectABCD$_{mut}$ in MM63 medium with 0.5% NaCl and either 5 g/L glucose (**A**) or 4.6 g/L glycerol (**B**) as carbon source. All cultures were supplemented with 100 mg/L carbenicillin and in case of DH5α additionally with 1 mL/L VA solution. Induction occurred at an OD between 0.3-0.4 adding 0.2 mg/L AHT. Growth was recorded by direct OD measurement.

Determination of the ectoine concentration in the culture supernatant was carried out for the final timepoint of cultivation and compared among the different strains and carbon sources along with their highest growth rate (**Figure 11**). Ectoine production with glucose as a carbon source led to a final product concentration of 6 mM ectoine for the DH5α strain (at the lowest growth rate of 0.26 h^{-1}), 3.6 mM ectoine for the K12 strain (at a growth rate of 0.4 h^{-1}) and only 1 mM ectoine for the BL21 strain (at a growth rate of 0.35 h^{-1}). When supplementing glycerol as carbon source all strains produced more ectoine, while growing slower. Under these conditions the K12 strain produced the same amount of ectoine as the DH5α strain (7.9 mM), while showing a substantially elevated growth rate of 0.35 h^{-1}compared to DH5α (0.22 h^{-1}). The BL21 strain again produced only low ectoine concentrations of 1.2 mM at a growth rate of 0.3 h^{-1}.

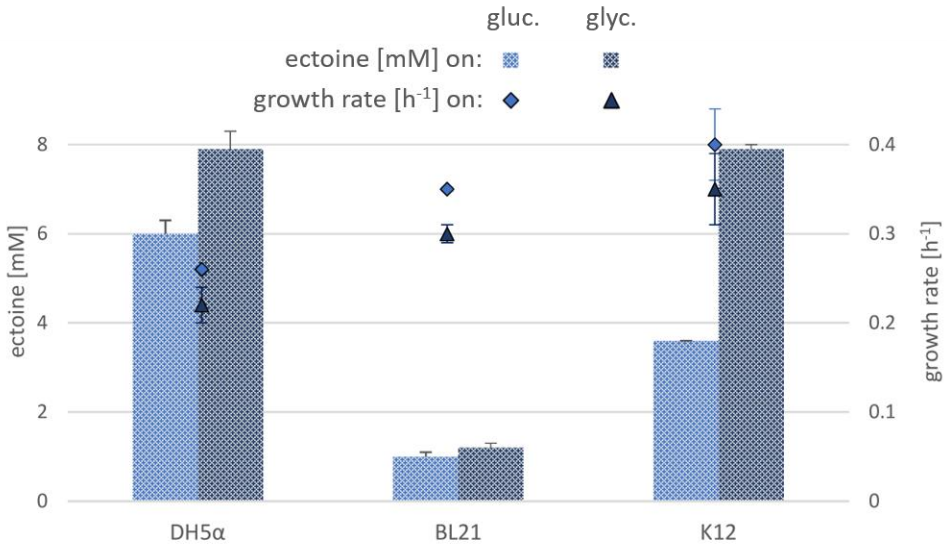

Figure 11 Ectoine production (mM) and growth rate (h^{-1}) of the original *E. coli* DH5α strain compared to the new base strain candidates BL21 and K12 carrying the ectoine production plasmid pASK_ectABCD$_{mut}$. Production culture was performed in shake flasks with 0.1 L MM63, 0.5% NaCl and either 5 g/L glucose (light blue) or 4.6 g/L glycerol (dark blue) as carbon source.

Since the *E. coli* K12 DSM498 is a wildtype strain, but uncommon in industry or research, two more common strains of the K-family were tested (MG1655 and W33110). The tested strains were cultured in comparable shake flask experiments for ectoine production utilizing glycerol as carbon source. Both strains, MG1655 and W33110, exhibited ectoine concentrations below 3 mM at similar growth rates as K12 DSM498 (data not shown) and were therefore not considered as candidates. K12 DSM498 was hereupon used as the base strain for further experiments and is subsequently referred to as K12.

3.1.2. Improving the Plasmid and Culture Conditions

To further improve ectoine production, a new plasmid was generated, encoding for the ectoine biosynthesis gene cluster *ectABC*, but lacking the mutated and unfunctional *ectD* of the previously used production plasmid pASK_ectABCD$_{mut}$. The newly generated vector will from now on be referred to as pASK_ectABC. To do so, the heterologous genes for ectoine production (*ectABC*) were amplified by PCR and cloned into pASK-IBA3 by restriction cloning, utilizing the same restriction sites on the plasmid as for pASK_ectABCD$_{mut}$ (Suppl. Figure 1). As a next step, the medium composition and culturing conditions for ectoine production were modified, to improve the ectoine production performance. Since ectoine production was higher when using glycerol, this carbon source was used for further experiments. In previous experiments it was observed that glycerol levels were exhausted after approximately 16 h of cultivation, when ectoine production was reaching its peak. Therefore, additional 4.6 g/L glycerol were fed at that time point, to increase the downstream ectoine production. In accordance, the amount of the nitrogen source was doubled (3.96 g/L $(NH_4)_2SO_4$) from the beginning of the experiments. At last the NaCl concentration was reduced to 0% to facilitate ectoine excretion and downstream processes, such as ectoine purification.

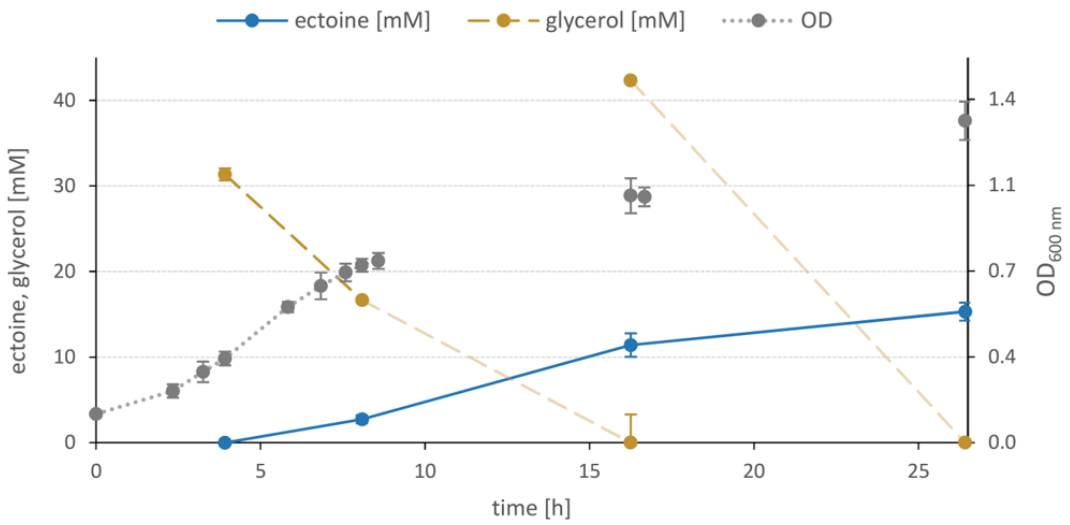

Figure 12 Ectoine production under optimized conditions, utilizing *E. coli* K12 pASK_ectABC in MM63 with 0% NaCl. The carbon source glycerol (4.6 g/L) was fed again after depletion (16 h). The transparent lines for the glycerol concentration indicate that the full depletion likely occurred earlier as indicated. All cultures were supplemented with 100 mg/L carbenicillin. Induction occurred at an OD between 0.3-0.4 adding 0.2 mg/L AHT. Growth was recorded by direct OD measurement.

Throughout the experiment samples were taken more frequently to monitor product formation and substrate consumption in detail (**Figure 12**). After induction (4 h) ectoine was constantly produced and excreted into the medium, reaching an extracellular concentration of 11.4 mM after 16 h. At this time point in the process the first batch of carbon source (glycerol) was depleted. After the additional 4.6 g/L glycerol were consumed (~ 26 h), an ectoine concentration of 15.3 mM was measured. To accurately evaluate and compare the two separate batch phases (0-16 h; 16-24 h), the substrate yield ($g_{ectoine}/g_{glycerol}$) as well as the specific production ($g_{ectoine}/g_{dcw}$) were calculated for the product ectoine. During consumption of the first 4.6 g/L of glycerol (0-16 h), 1.62 g/L of ectoine were produced with a substrate yield of 0.35 $g_{ectoine}/g_{glycerol}$. The specific production for this time period was approximately 1.8 $g_{ectoine}/g_{dcw}$, calculated from the sampled biomass (0.9 g_{dcw}/L) at time-point 16 h. During consumption of the second 4.6 g/L of glycerol (16-24 h), additional 0.55 g/L ectoine were produced with a substrate yield of 0.12 $g_{ectoine}/g_{glycerol}$. The specific production for this time period was approximately 0.32 $g_{ectoine}/g_{dcw}$ calculated from the sampled biomass (1.7 g_{dcw}/L) at time-point 24 h. Together, these results demonstrate that improved culture conditions of the base strain *E. coli* K12 DSM498 pASK_ectABC led to an increase in overall ectoine production to 15 mM (2.1 g/L) in shake flask culture, but a significant decrease in the later process was observed.

3.2. ^{13}C-Flux analysis

During base strain design it became apparent that product formation slows down after approximately 10 h post induction. This is reflected by a lower specific production (1.8 *vs* 0.32 $g_{ectoine}/g_{dcw}$) and lower substrate yield (0.35 *vs* 0.12 $g_{ectoine}/g_{glycerol}$) in the second production period (cf. Figure 12). To identify potential bottlenecks in the process that may limit ectoine production at later time points, stable isotope labelling was performed. Site specific ^{13}C-labelled substrates were fed into the process leading to incorporation of the isotopes into cell building blocks of the metabolic routes. With a theoretical metabolic network (cf. Figure 7), the information of labelling positions in ectoine can be translated into metabolic routes contributing to the product formation.

3.2.1. Stable Isotope Labelling with Glycerol

Stable isotope labelling experiments were established during this study using *E. coli* K12 pASK_ectABCD$_{mut}$. Therefore, all isotope labelling experiments were conducted using this strain. Due to the symmetry of the glycerol molecule, only two different isotope variants can be discriminated (1,3-^{13}C and 2-^{13}C) in labelling experiments. After feeding the isotopes into an ectoine overproduction experiment, the product's labelling pattern was analyzed in ^{13}C-NMR spectroscopy. Since acquisition of NMR data requires a high concentration of ectoine in the sample (> 5 mg/mL), glycerol labelling experiments were performed with buffer components reduced to a quarter (12.5 mM KH_2PO_4). This allowed for a direct concentration of ectoine by evaporation of the medium.

The shake flask experiments were performed using 0.05 L MM63 with 0% NaCl and 4,6 g/L glycerol. Cultures were supplemented with either 20% 1,3-^{13}C or 2-^{13}C glycerol (0.92 g/L labelled glycerol + 3.68 g/L normal glycerol = 4.6 g/L). Under all three culture conditions (1,3-^{13}C, 2-^{13}C or non-labelled glycerol), cells showed similar growth curves (**Figure 13**). Ectoine formation increased steadily after induction (4.9 h) to values between 4-5 mM, with glycerol being fully consumed at the end of the process. In all cultures more than 25 mg ectoine were produced, which was sufficient for ^{13}C-NMR analysis. A minimum of 5 mg of the produced ectoine were concentrated and resuspended in D_2O for ^{13}C-NMR analysis (**Figure 14A**). The different NMR signals could be clearly assigned to the carbon skeleton of ectoine (**Figure 14A-B**). Integrals of the signals were first corrected for the natural abundance of the ^{13}C isotope in the no labelling control and subsequently normalized to the 1,2-^{13}C acetate standard. C2, C3, C4 and C6 were normalized to the methyl group (23 ppm) while C1 and C5 were normalized to the acetyl group (181 ppm), to account for disproportionality of the signals. Using this setup, a relative labelling distribution for ectoine could be calculated (**Figure 14C**).

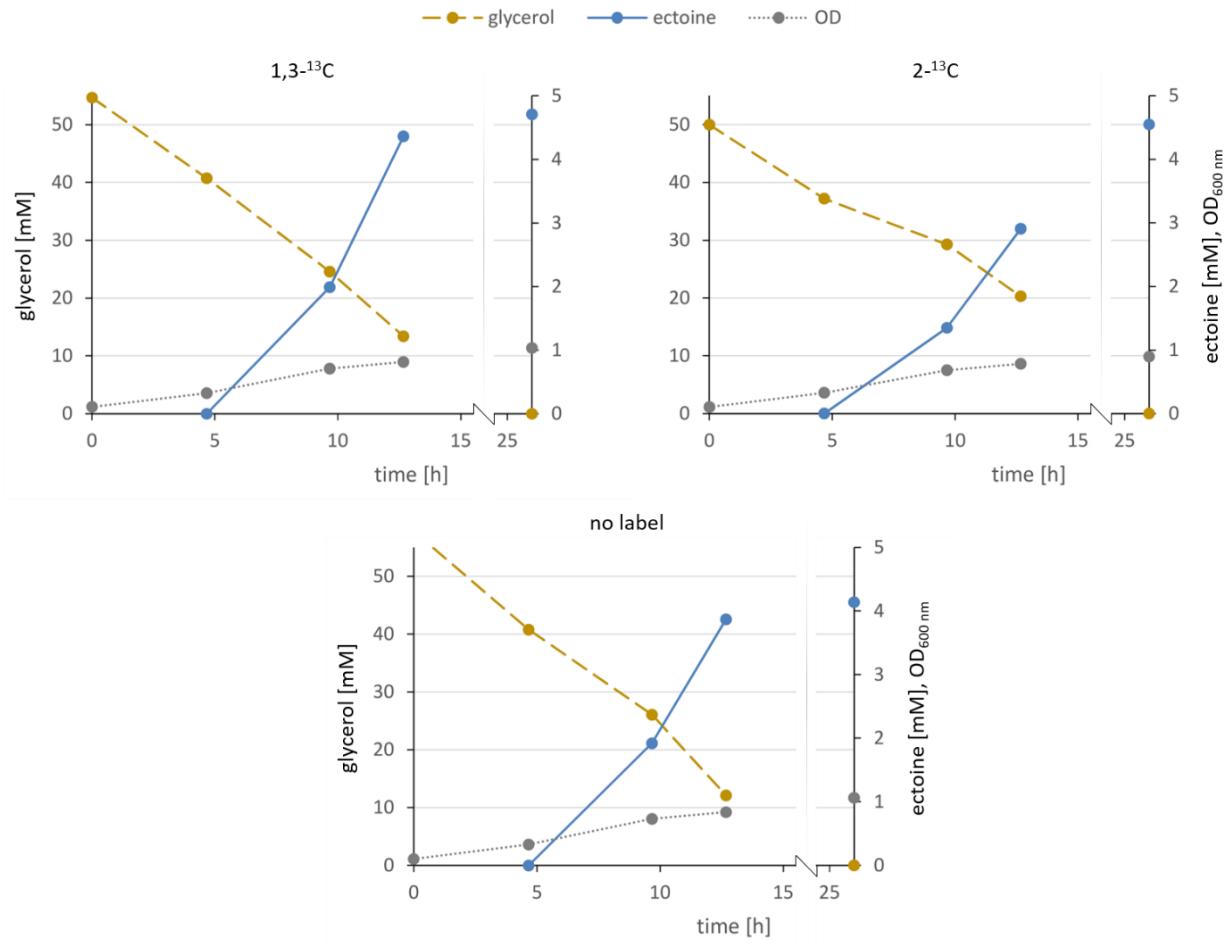

Figure 13 Ectoine formation [mM], glycerol consumption [mM] and growth curve [OD] seized during the glycerol labelling experiments. 20% 1,3-^{13}C and 2-^{13}C stable isotopes of glycerol were added to the MM63 medium with 0% NaCl and 4.6 g/L glycerol. All cultures were supplemented with 100 mg/L carbenicillin. Induction was executed at an OD between 0.3-0.4 (4.9 h) adding 0.2 mg/L AHT. Growth was recorded by direct OD measurement.

In accordance with the theoretical model of ectoine biosynthesis that was generated previously (cf. Figure 7), we observed an intense labelling in positions C5 and C6 (**Figure 14 C**). These strong signals originate from the acetylation via EctA and clearly reflect the labelling pattern of acetyl-CoA. Similarly, the labelling in position C1 and C4 are coherent with the theoretical model. Surprisingly, however, we observed a significant 2-^{13}C signal in positions C2 and C3, which could not be explained by the first theoretical model. Therefore, the theoretical network must be incomplete. Since the symmetry of the glycerol molecule limited the information (due to indistinguishable 1- and 3-^{13}C position), a new labelling strategy was designed. This new labelling strategy (pyruvate labelling) made use of distinguishable isotopes at the different positions.

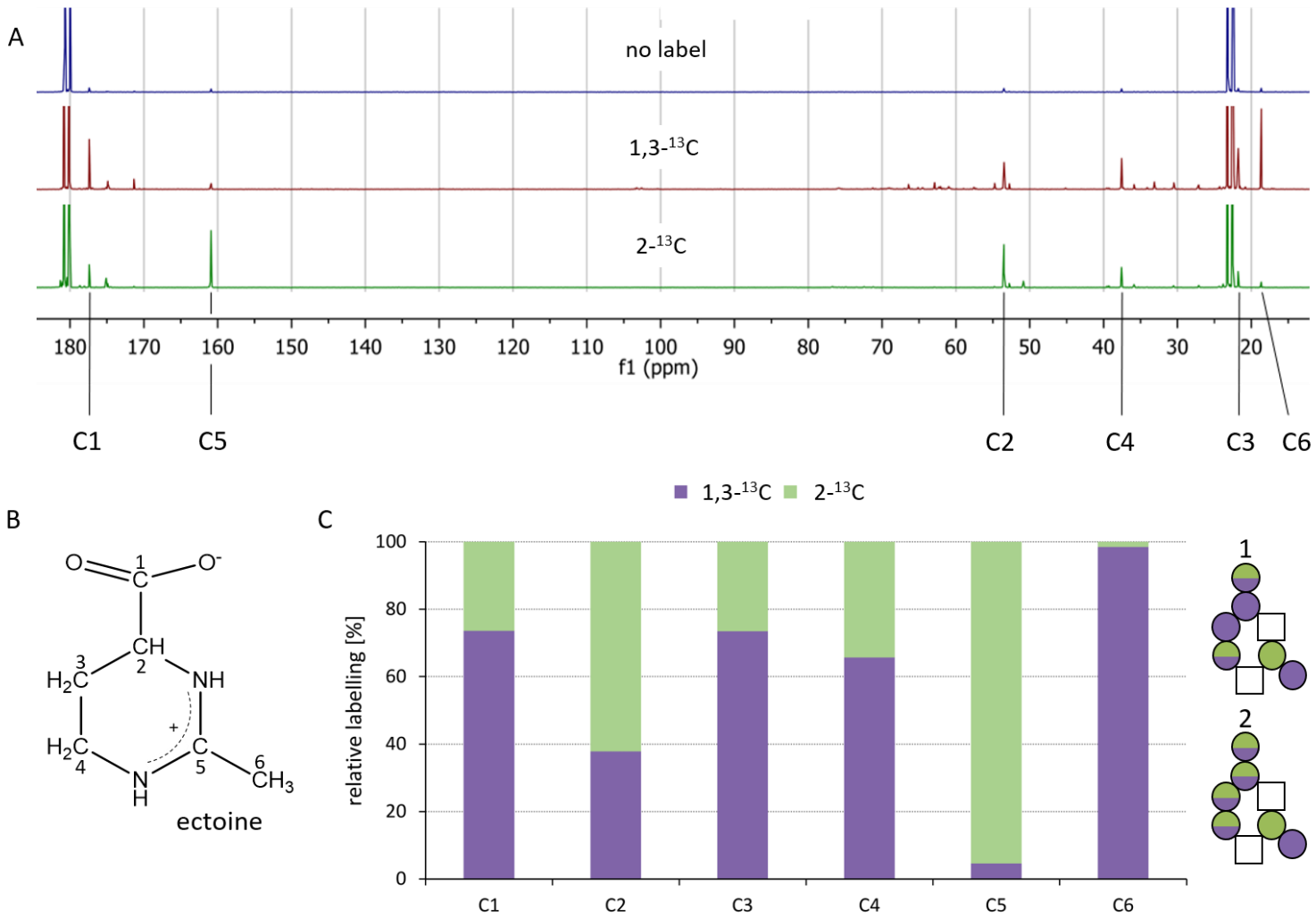

Figure 14 ^{13}C-NMR analysis process of the glycerol labelling experiments. NMR spectrogram of concentrated ectoine, produced during cultivation with no isotope (blue), 1,3-^{13}C glycerol (red) or 2-^{13}C glycerol (green) (**A**). The signals for the ectoine carbon atoms are labeled according to the scheme given in **B**. The remaining high signals at 23 ppm and 181 ppm belong to the standard 1,2-^{13}C acetate. After normalization of the integrals, a relative labelling distribution could be displayed for each carbon atom of ectoine (**C**). The measured labelling pattern (**2**) does not match the theoretical pattern (**1**) completely (cf. Figure 7).

3.2.2. Stable Isotope Labelling with Pyruvate

To increase the information output of the labelling experiment by additional distinct labelling positions, pyruvate was used as a substrate. Pyruvate offered three distinguishable isotope positions 1-^{13}C, 2-^{13}C and 3-^{13}C. The experiment was performed in MM63 with 0% NaCl and 5.5 g/L sodium pyruvate. Since metabolism of this carbon source leads to an alkalization of the medium, the phosphate buffer was substituted for a TRIS/HCl-buffer. In consequence, an additional ion-exchange chromatography had to be employed to separate the buffer components from ectoine in the culture supernatant, before concentrating the product for ^{13}C-NMR analysis.

Growth and ectoine production with pyruvate as carbon source were slightly slower than with glycerol. At the end of the process between 3.5 and 5.5 mM ectoine were quantified (data not shown), resulting in sufficient material for NMR analysis. Using the three distinguishable isotope variants, ^{13}C-NMR results under pyruvate labelling displayed a more distinctive picture of labelling distribution compared to glycerol labelling (**Figure 15**). Similar to the glycerol experiment we identified an intense labelling in positions C5 and C6 resulting from the labelling in acetyl-CoA, as well as a similar 2- and 3-^{13}C label appearing in C1 and C4. In addition, however, we could also observe 1-^{13}C isotopes in positions C1 and C4. These new 1-^{13}C labels as well as the 2-^{13}C isotope in positions C2 and C3 can not be explained with the first theoretical model (cf. Figure 7). To explain the labelling positions the theoretical model had to be edited.

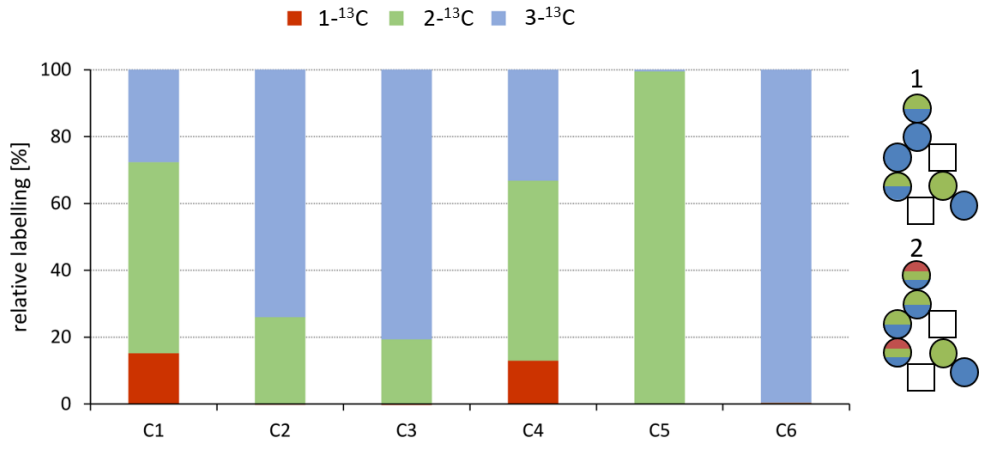

Figure 15 *^{13}C-NMR analysis of the pyruvate labelling experiment. Labelling intensities of ectoine, produced during cultivation with 1-^{13}C (red), 2-^{13}C (green) or 3-^{13}C (blue) pyruvate. With the empirical results of three distinct isotope positions (**2**) it becomes apparent that the real labelling in positions C1 to C4 is not covered fully by the first theoretical network (**1**).*

To find a solution for the unexpected 1-^{13}C label in positions C1 and C4, as well as the 2-^{13}C label in positions C2 and C3, different anaplerotic routes were added to the theoretical ectoine biosynthesis model (cf. Figure 7). This is justified because the large ectoine drain requires a supplementation of the TCA. For example, if the metabolic flux was redirected into the glyoxylate shunt, no new labelling would be generated in oxaloacetate (**Figure 16**). Thus, the addition of the glyoxylate shunt does not explain the measured labelling pattern. At most, it would increase the accumulation of the 2-^{13}C labelling in position C1 and especially C4 through an enlarged incorporation of acetyl-CoA and the conservation of carbon atoms.

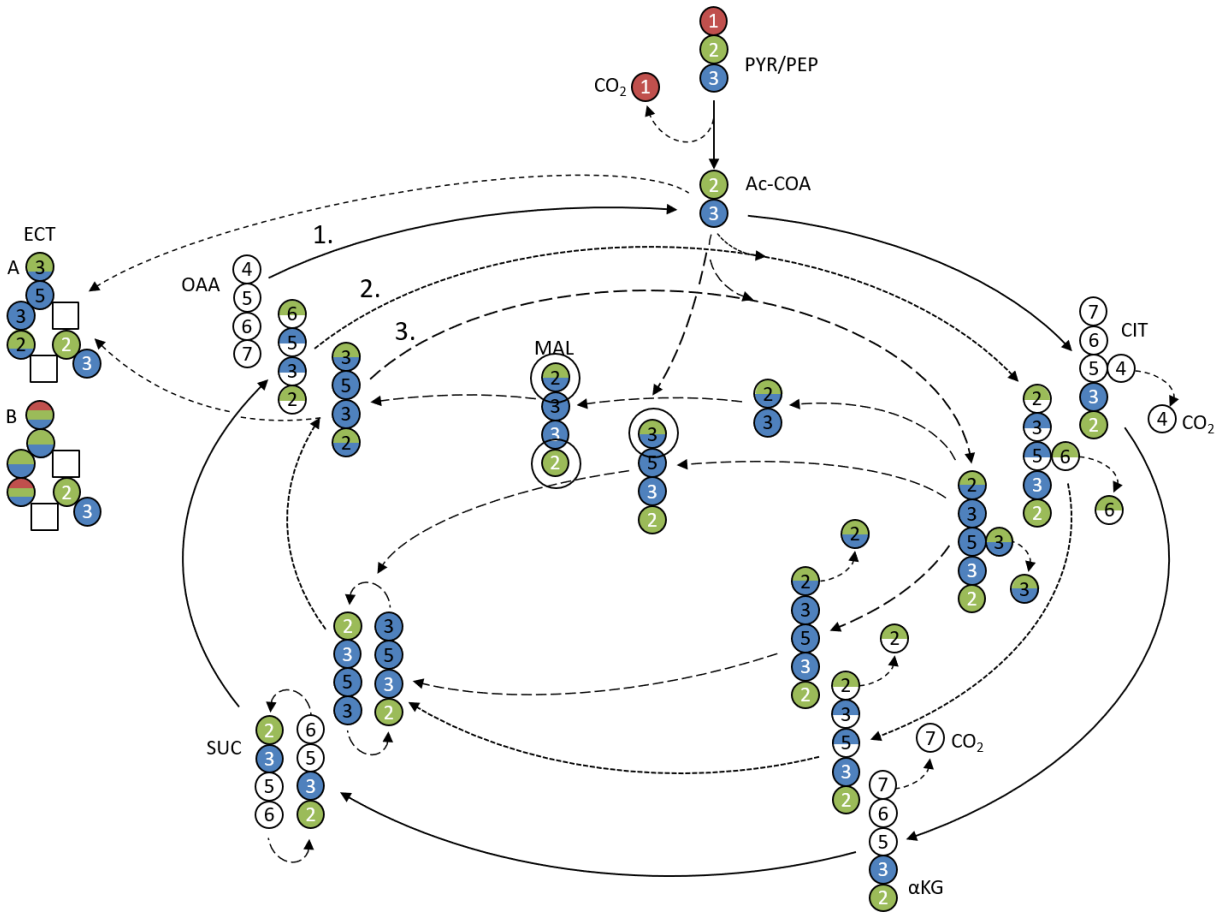

Figure 16 Theoretical labelling pattern for 1-^{13}C (red), 2-^{13}C (green) or 3-^{13}C (blue) pyruvate extended by the glyoxylate shunt. The overall labelling pattern is not affected (**A**) and therefore the glyoxylate shunt can not explain the real labelling pattern (**B**). The anaplerotic reaction would, however, lead to an increased incorporation of the 2-^{13}C label in positions C1 and C4, through the additional acetyl-CoA incorporation and conservation of carbon atoms (black circles).
PYR/PEP = pyruvate/phosphoenolpyruvate, Ac-COA = acetyl-CoA, CIT = citrate, αKG = α-ketoglutarate, SUC = succinate, OAA = oxaloacetate, ECT = ectoine

Interestingly, the measured labelling positions became explainable, once we expanded the network by the anaplerotic PEP-carboxylase (PPC) reaction. This reaction converts phosphoenolpyruvate to oxaloacetate by a carboxylation with CO_2 (**Figure 17**). This way, the 1-^{13}C label in position C1 and the 2-^{13}C label in position C2 are generated, when a direct conversion of the newly synthesized oxaloacetate into ectoine occurs. The 1-^{13}C labelling in position C4 can be similarly generated by a direct transition to ectoine, if the CO_2 utilized for carboxylation of PEP is 1-^{13}C labelled. The 2-^{13}C label in position C3 can occur by redirecting the anaplerotically generated oxaloacetate through the TCA. Additionally, channeling the flux after PEP carboxylation through the glyoxylate shunt would generate the measured labelling pattern. Together, these results demonstrate the importance of the anaplerotic PPC reaction refueling the oxaloacetate pool for ectoine production in our system.

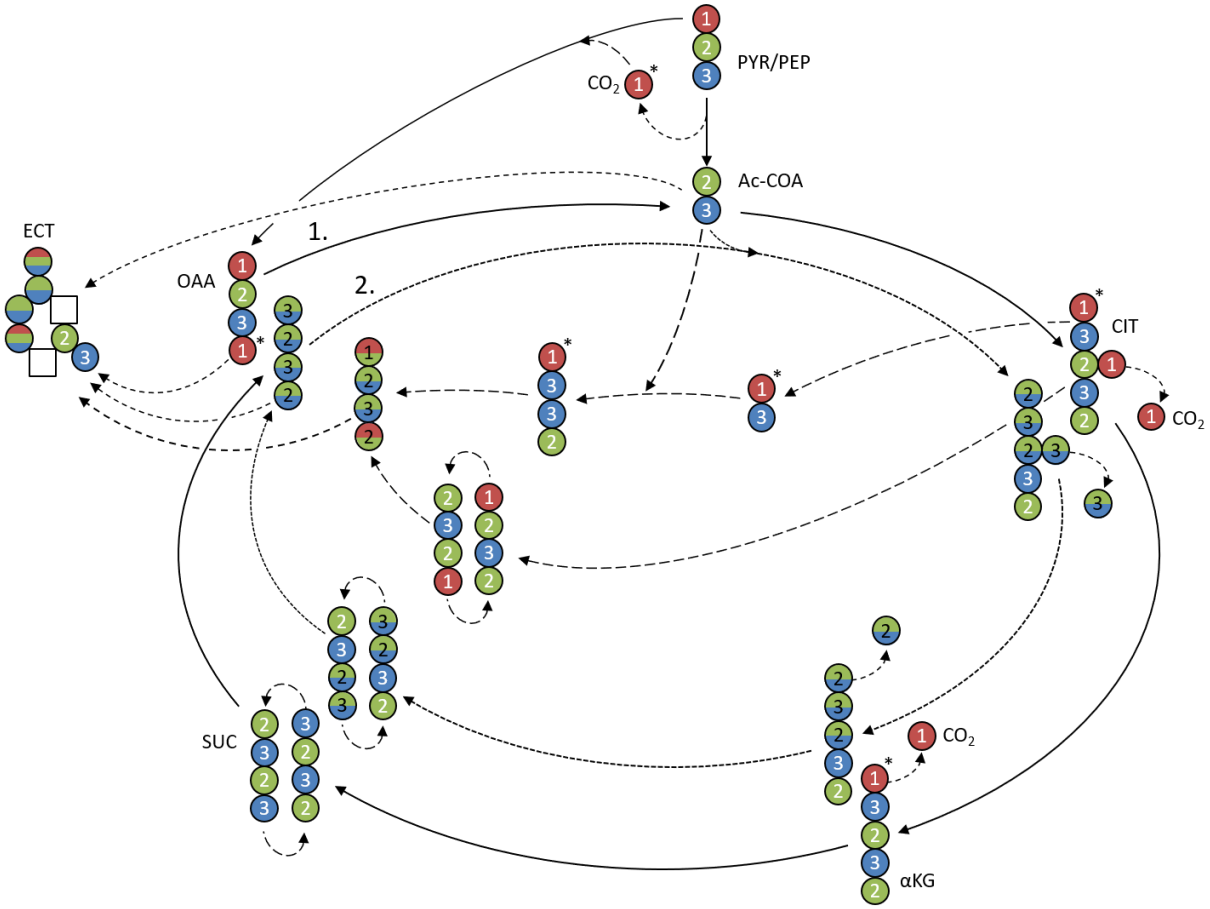

Figure 17 Theoretical labelling pattern for 1-^{13}C (red), 2-^{13}C (green) or 3-^{13}C (blue) pyruvate extended by the anaplerotic PEP-carboxylase reaction and the glyoxylate shunt. The theoretical labelling pattern now matches the measured pattern. The pattern can be generated without the glyoxylate shunt if a 1-^{13}C labelled CO_2 is incorporated into PEP to form oxaloacetate (*) plus redirecting a part of oxaloacetate into the TCA. Alternatively, it can be generated by the glyoxylate shunt. PYR/PEP = pyruvate/phosphoenolpyruvate, Ac-COA = acetyl-CoA, CIT = citrate, αKG = α-ketoglutarate, SUC = succinate, OAA = oxaloacetate, ECT = ectoine

Using these data, I was then able to analyze the difference in ectoine metabolic routes of our production strain (K12 pASK_ectABCD$_{mut}$) to the natural producer strain *H. elongata*. To do so, I made use of previously generated pyruvate labelling data for *H. elongata* generated by Voß (unpublished). To enforce ectoine production in the natural producer the organism was shocked from 3% to 10% NaCl. In order to find discrepancies between metabolic routes of both strains, the labelling intensities generated by the heterologous strain were subtracted from the natural producer strain's labelling intensities (**Figure 18**). This comparison revealed an increase in accumulation of the 1-^{13}C isotope in position C1 and C4, as well as of the 2-^{13}C isotope in position C2 for the natural producer strain. These are positions generated through the anaplerotic reaction, once more emphasizing its importance for ectoine biosynthesis.

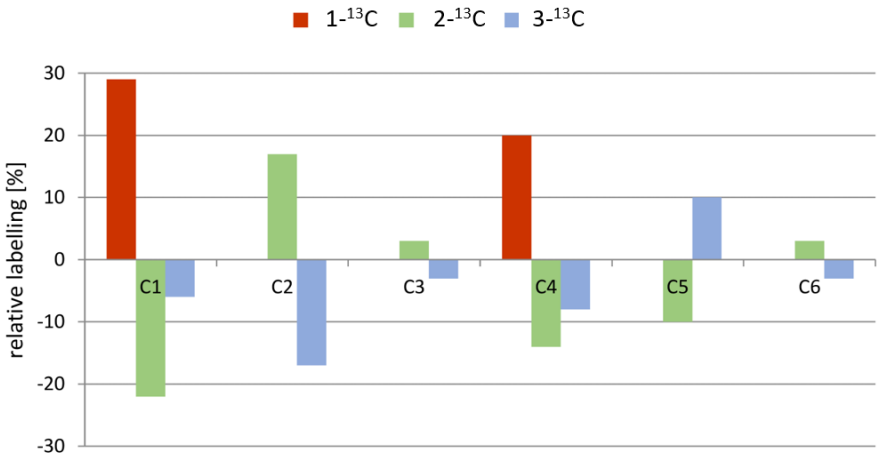

Figure 18 Comparison of ectoine labelling in the natural producer *H. elongata* and the heterologous producer strain *E. coli* K12 pASK_ectABCD$_{mut}$. Both labelling patterns were generated using 1-^{13}C (red), 2-^{13}C (green) and 3-^{13}C (blue) isotope variants of pyruvate. After ^{13}C-NMR analysis the labelling intensities of the heterologous producer strain were subtracted from the natural producer's labelling pattern. Ectoine labelling experiments in *H. elongata* were executed by Voß (unpublished).

3.2.3. *In-silico* Flux Analysis

By combining experimental data with theoretical design, I was already able to generate a metabolic network (cf. Figure 17) that predicts and explains the metabolic route of ectoine biosynthesis in *E. coli* K12. The manual tracing of labelling distributions, however, remains limited. In order to precisely fit the relative quantities of measured isotopes at specific positions to flux quantities, it was necessary to iterate pathway probabilities mathematically. Therefore, a flux software was

developed calculating the probabilities of metabolic routes that contribute to the isotope distribution in ectoine (Sümmermann, Bethlehem and Galinski, unpublished). Based on the ^{13}C-NMR experimental data, the software calculates probabilities of fluxes in a given network (cf. 2.4.6. Nuclear Magnetic Resonance Spectroscopy (NMR)). The probabilities can then be displayed in a flux-map, enabling a complete overview about the metabolic routes, which are active in the network.

Using this software, I found that in the production strain K12 pASK_ectABCD$_{mut}$ nearly one third of the carbon used for ectoine formation is being directed via the PPC (**Figure 19**). The flux observed for the anaplerotic route matches the flux towards ectoine, replenishing the precursor oxaloacetate. Consequently, one third of the flux from acetyl-CoA was incorporated into ectoine. The remaining flux is coordinated into the TCA, while nearly no flux is passing the glyoxylate-shunt utilizing glycerol as carbon source. This might be explained by the lack of acetyl-CoA, which is required for the glyoxylate-shunt and already heavily utilized for ectoine formation.

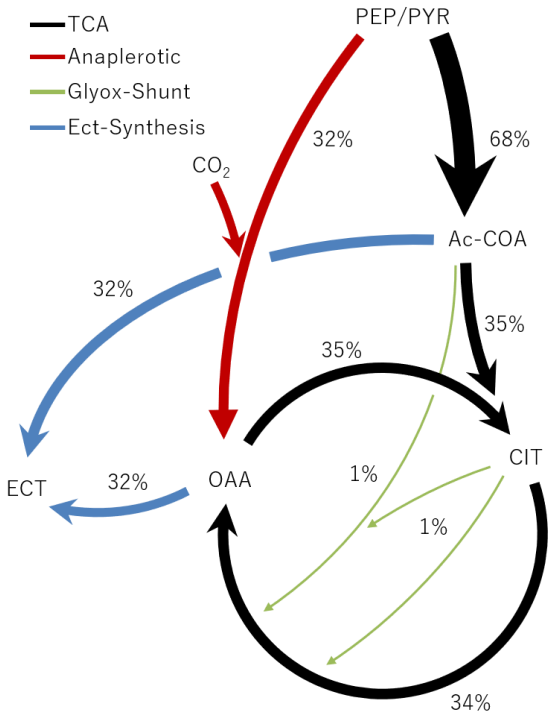

Figure 19 Flux-map for ectoine production with *E. coli* K12 pASK_ectABCD$_{mut}$ growing on glycerol. The probabilities of metabolic routes were calculated *in-silico* on the basis of the labelling pattern in the product ectoine, acquired through ^{13}C-NMR. Absolute values are displayed starting from PEP/PYR (100%). The software was developed in collaboration with Moritz L. Sümmermann (Sümmermann, Bethlehem and Galinski, unpublished). PYR = pyruvate, PEP = phosphoenolpyruvate, Ac-COA = acetyl-CoA, CO_2 = carbon dioxide, CIT = citrate, OAA = oxaloacetate, ECT = ectoine, TCA = tricarboxylic acid cycle

Using flux-maps, one has an eloquent tool to compare and to study the ectoine fluxes under different conditions, like alternating carbon sources or different producing organisms (**Figure 20**). For example, I initially predicted that the anaplerotic reaction was a predominant route of ectoine biosynthesis in the K12 pASK_ectABCD$_{mut}$ strain (c.f Figure 17). Now, subtracting the fluxes in pyruvate from the glycerol fluxes in this new model, I again found that the anaplerotic flux is highly relevant for efficient ectoine biosynthesis in *E. coli* K12 (**Figure 20A**). Consuming glycerol instead of pyruvate during ectoine formation, leads to a higher anaplerotic flux and reduced fluxes into the TCA and glyoxylate shunt. When growing on pyruvate as the only carbon source *E. coli* has to convert pyruvate to PEP first, consuming one ATP, before performing the anaplerotic reaction to oxaloacetate. This leads to a reduced anaplerotic flux and an increased flux into the TCA and glyoxylate shunt on pyruvate, which explains the increased ectoine production consuming glycerol compared to pyruvate in *E. coli*.

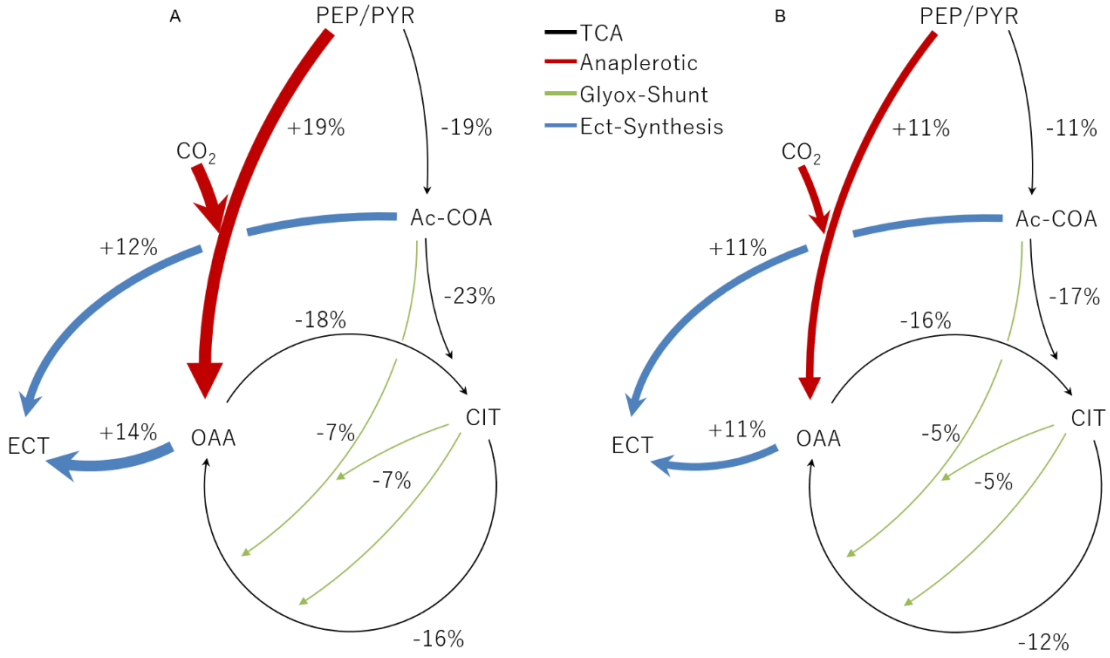

Figure 20 Flux-maps for ectoine production comparing different substrates and producer strains. The probabilities of metabolic routes were calculated *in-silico* on the basis of the labelling pattern for ectoine, acquired through ^{13}C-NMR. Differences of K12 pASK_ectABCD$_{mut}$ producing ectoine utilizing glycerol over pyruvate as a carbon source (**A**). Differences in fluxes towards ectoine generated by the natural producer *H. elongata* over the heterologous producer strain *E. coli* K12 pASK_ectABCD$_{mut}$ growing on pyruvate (**B**). PYR = pyruvate, PEP = phosphoenolpyruvate, Ac-COA = acetyl-CoA, CO_2 = carbon dioxide, CIT = citrate, OAA = oxaloacetate, ECT = ectoine, TCA = tricarboxylic acid cycle

Alternatively, comparing the ectoine flux between K12 pASK_ectABCD$_{mut}$ and *H. elongata* under pyruvate consumption in the new model reveals a similar pattern as already described in Figure 18. Once more, an increase in the anaplerotic flux towards ectoine seems to be a key mechanism in ectoine production (**Figure 20B**). When growing on pyruvate as the only carbon source, the flux in in the natural strain is more efficiently channeled towards ectoine. The ectoine in *H. elongata* was, however, generated under stress conditions by shifting the NaCl concentration from 3 to 10%. This could explain the drastic regulation towards ectoine production. Furthermore, *H. elongata* is capable to reverse the reaction of the malic enzyme and therefore convert pyruvate directly to malate and thereby refueling the TCA more efficiently while growing on pyruvate compared to *E. coli*. These findings give valuable insights into the relevant routes for ectoine production in our heterologous strain and provide targets for metabolic engineering (anaplerotic reactions).

3.3. Metabolic engineering

Making use of the information obtained by stable isotope labelling, I designed new strategies for metabolic engineering of the ectoine overproduction base strain *E. coli* K12 pASK_ectABC. Flux maps revealed that the anaplerotic flux via the PPC is highly important for efficient ectoine production in the heterologous strain. Hence, the replenishment of oxaloacetate represents a crucial factor in ectoine biosynthesis in *E. coli* K12 pASK_ectABC. The only enzyme, however, fulfilling this task directly is the PPC. To increase anaplerotic fluxes in our overproduction strain, I therefore introduced the pyruvate-carboxylase (PYC) enzyme originating from *C. glutamicum*. This enzyme is capable of converting pyruvate to oxaloacetate and thereby adding another pathway for the generation of the ectoine biosynthesis precursor. For this, PYC was cloned into the pBBR1_MCS vector for simultaneous expression with pASK_ectABC.

As a second strategy to improve ectoine production, I implemented the feedback resistant aspartate kinase LysC from *C. glutamicum* encoded on the pAKect1 vector in our system. This vector was generated by Bestvater *et al.* (2008) and carries the LysC controlled by the *tac* promotor, next to the ectoine biosynthesis gene cluster of *Marinococcus halophilus* under control of its natural promotor (*promA*). This system was initially used for optimized salt-induced ectoine biosynthesis

in *E. coli* and since *promA* is salt dependent pAKect1 does not produce any ectoine under the conditions employed for heterologous overproduction in this study (0% NaCl) (Wienberg, 2017). Instead, this system was exploited to implement an IPTG inducible LysC expression. The metabolic conversion of L-aspartate to L-aspartyl-4-phosphate catalyzed by the *E. coli* aspartate kinase is strongly feedback inhibited by the products of the aspartate amino acid family and has been demonstrated to limit ectoine production in *E. coli* (Bestvater *et al.*, 2008).

The plasmids pBBR1_pyc and pAKect1 were each cloned into individual stains of *E. coli* K12 pASK_ectABC. For the stable maintenance of the secondary plasmids (pBBR1_pyc or pAKect1), cells were additionally to carbenicillin cultured in presence of chloramphenicol. The resulting performance of ectoine production was compared to the base strain K12 pASK_ectABC under best conditions. For this, cells were cultured in 0.05 L MM63 with 0% NaCl, 4.6 g/L glycerol and 3.96 g/L ammonium sulfate. Glycerol was additionally fed after 15-16 h.

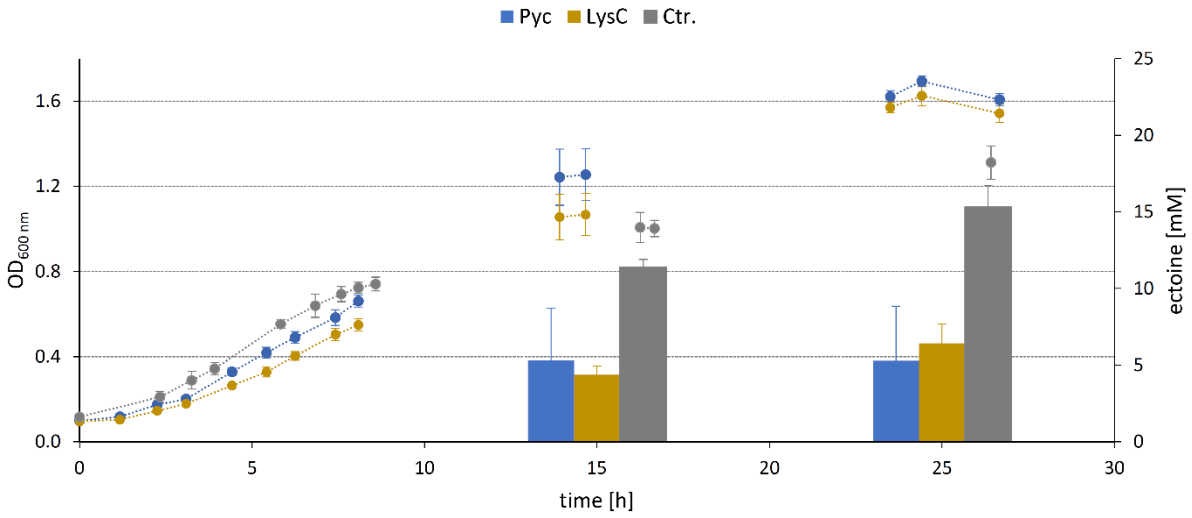

Figure 21 Ectoine overproduction [mM] with the metabolic engineered strains *E. coli* K12 pASK_ectABC + pBBR1_pyc (PYC), pASK_ectABC + pAKect1 (LysC) and the control strain without a secondary plasmid. Cultivation was performed in 0.05 L MM63 with 0% NaCl and 4.6 g/L glycerol. The carbon source (4.6 g/L) was fed again after depletion (15-16 h). The cultures with a second plasmid were supplemented with 50 mg/L carbenicillin and 25 mg/L chloramphenicol, while the control strain was supplemented with 100 mg/L carbenicillin only. Induction occurred at an OD between 0.3-0.4 (4-5 h) adding 0.2 mg/L AHT and additional 120 mg/L IPTG in the case of pAKect1. Growth was recorded by direct OD measurement.

The growth of the engineered strains (pASK_ectABC + pBBR1_pyc, pASK_ectABC + pAKect1) was slower in the first 9 h of cultivation, compared to growth of the control strain (pASK_ectABC) (**Figure 21**). After 15-16 h however, when the first batch of glycerol was consumed (data not shown), the control strain exhibited a slightly lower OD than the engineered strains. The ectoine concentration at this time point was 11.4 mM for the control strain, but only ~ 5 mM for the engineered strains. After feeding additional 4.6 g/L glycerol the engineered strains grew substantially, while growth of the control strain was only minor. However, within this second growth phase nearly no additional ectoine was produced by the engineered strains. The final ectoine concentrations of 5.3 mM for the PYC-strain and 6.4 mM for LysC-strain were considerably lower compared to 15.3 mM ectoine produced by the control strain. The introduction of the new plasmids proofed detrimental for ectoine production with *E. coli* K12 pASK_ectABC. This might be not directly connected to the introduced enzymes but to the burden of the additional chloramphenicol exposure. Later it could be shown that the acetylation of chloramphenicol by the chloramphenicol acetylase (CAT), significantly decreases ectoine production.

3.4. Medium Composition

The here implemented metabolic engineering strategies did not increase ectoine production in the base strain *E. coli* K12 pASK_ectABC. Instead, they resulted in a decrease in ectoine production. Even though the detrimental effect might not have been caused by the introduced enzymes, I figured that there was a more essential problem (next to the described enzymatic bottlenecks) present in the heterologous strain that interfered heavily with the ectoine production process and could not be solved by metabolic engineering. As a next step I, therefore, aimed to investigate the influence of the growth medium composition on ectoine biosynthesis in our system. At first, individual supplementation experiments were performed to investigate negative effects of nutrient or co-factor deficiencies. Neither the supplementation of the co-factor iron (5.5 mg/L) or the co-enzyme PLP (24.7 mg/L), nor the addition of complex media components (FP-S490, 0.4%) had positive effects on ectoine production (Suppl. Figure 5).

To completely exclude medium composition as a major cause for the inhibition of ectoine production, a parallel batch experiment was performed: At the point of production breakdown, a

second production process was started with the biomass of the first batch in fresh minimal medium. If the inhibition of ectoine production would still persist under these conditions, nutrient deficiency could be excluded as the cause for the stop in ectoine production. For this experiment, the ectoine overproduction was performed under optimal conditions in 0.05 L MM63 with 0% NaCl, 4.6 g/L glycerol, 3.96 g/L ammonium sulfate and 100 mg/L carbenicillin. Glycerol was again supplemented after 12 h of cultivation in each batch. After 12 h of the first batch, part of the biomass was centrifuged and washed to inoculate the second production culture.

The first batch grew to an OD of 0.7 and produced 5.5 mM ectoine, while consuming the first 4.6 g/L of glycerol (12 h) (**Figure 22**). At this time point, the first batch was again fed with glycerol (4.6 g/L), while growth of the second batch was initiated in fresh medium. Following the parallel cultivation of the two batches (time point 12-26 h), another 3 mM ectoine were produced in the first batch, while only 1.6 mM ectoine were produced in the second batch. The second batch, however, showed a slight growth advantage compared to the first batch with an OD of 1.2 (compared to only 0.7 in the first batch after 12 h). Since at this time point glycerol was depleted in the second batch, glycerol (4.6 g/L) was again fed into the system.

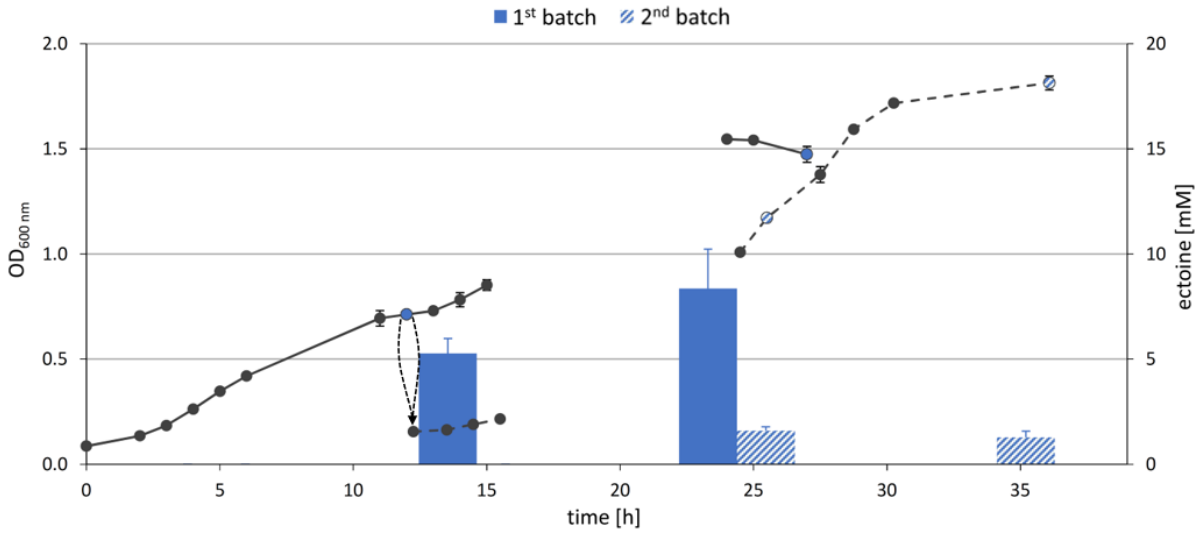

Figure 22 Ectoine overproduction [mM] in a parallel batch experiment with the base strain *E. coli* K12 pASK_ectABC. Sampling is indicated by the colored circles, as well as the transfer of biomass (1st batch) to start the 2nd batch (dotted arrow). Cultivation under optimal conditions in MM63 with 0% NaCl and 4.6 g/L glycerol. The carbon source (4.6 g/L) was fed again after depletion (12 h 1st batch, 26 h 2nd batch). All cultures were supplemented with 100 mg/L carbenicillin. Induction was executed at an OD between 0.3-0.4 (4 h 1st batch, 16 h 2nd batch) adding 0.2 mg/L AHT. Growth was recorded by direct OD measurement.

Interestingly, no additional ectoine was produced in the second batch after feeding additional carbon source. Thus, the first batch measured a final ectoine concentration of 8.5 mM, while the second batch measured only 1.3 mM ectoine. Together, this demonstrates that the media composition itself is not the limiting factor, which diminishes ectoine production in K12 pASK_ectABC at later time points.

3.5. Ectoine Overproduction in Bioreactors

Since all so far implemented modifications were unable to resolve the inhibition of ectoine production over time, cultures were transferred from shake flask experiments to bioreactor experiments. Bioreactor experiments allow for a more controlled environment throughout the process, such as controlled pH, temperature and oxygen supply. Additionally, more elaborate sampling and feeding strategies can be applied. The first fermentation was performed in a 1 L bioreactor with 0.8 L MM63, 0% NaCl, 2.8 g/L glycerol (30 mM), 1 g/L ammonium sulfate (7.6 mM), 1 mL/L trace element solution (TES) and 100 mg/L carbenicillin. Heterologous gene expression was induced with 0.2 mg/L AHT at an OD between 0.3-0.4 (5.5 h) and again after 12 h, due to higher metabolic activity in bioreactor experiments. Antifoam was added regularly, since the foam produced in bioreactors can inhibit growth and product formation. The first batch of carbon and nitrogen were calculated to be sufficient to reach the time point of induction, from where on a continuous fed-batch process was carried out. Feeding occurred at a flowrate of 1.5 mL/h supplementing 0.45 g/h glycerol and 0.2 g/h ammonium sulfate.

The growth of *E. coli* K12 pASK_ectABC during the initial batch phase in the first bioreactor experiment resembled the one in shake-flask experiments, reaching the point of induction after 5.5 h (**Figure 23**). At this time point the fed-batch phase was started and ectoine accumulated in the medium to a concentration of 5.4 mM within the first 12 h of the process. To aid ectoine production, a second induction was performed and the O_2 supply was increased. Ectoine concentration increased continuously for three more hours and stagnated at 8.8 mM, while cell growth was maintained until the end of the process (final OD = 5.7). As soon as ectoine production came to a halt (15 h), the fermentation side products acetate and formate were detected. During the remaining 10 h of the process, acetate accumulated to a concentration of 43 mM and formate

to 31 mM in the medium. During this time period the growth rate of *E. coli* K12 pASK_ectABC was reduced substantially from 0.32 h^{-1} in the beginning to ~ 0.13 h^{-1} in the second fermentation phase.

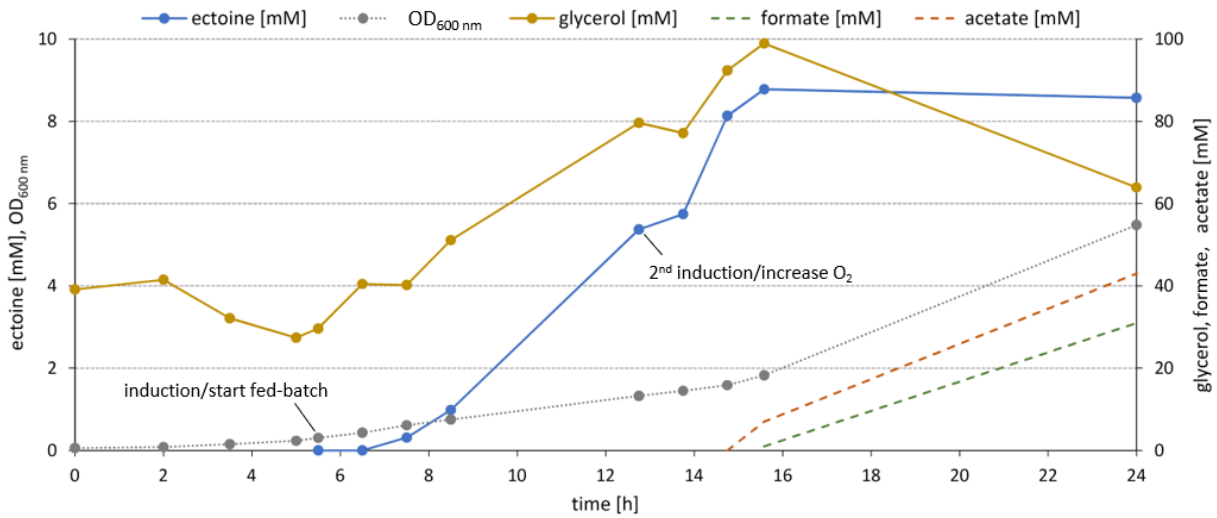

Figure 23 Ectoine overproduction [mM] in the 1 L bioreactor with *E. coli* K12 pASK_ectABC utilizing 0.8 L MM63 with 0% NaCl, 2.8 g/L glycerol, 1 g/L ammonium sulfate, 100 mg/L carbenicillin and 1 mL/L TES. Fermentation was performed in fed-batch mode (1.5 mL/h) after induction, feeding glycerol (0.45 g/h) and ammonium sulfate (0.2 g/h). Induction with 0.2 mg/L AHT occurred after 5.5 and 12 h. OD values represent diluted real measurements.

The accumulation of the fermentation side products acetate and formate, together with an overall low final OD of 5.7, indicate a deficiency of O_2 supply in bioreactor experiments. The observed drastic shift in the acetate metabolism could as well explain the simultaneous break-down in ectoine production. To solve this problem, a setup with improved stirring capacities was used to increase oxygen input. Further, the dissolved oxygen (DO) content in the medium was monitored throughout the entire process. The fermentation in the 5 L bioreactor was performed in 4 L MM63 with 0% NaCl, 9.2 g/L glycerol (100 mM), 6 g/L ammonium sulfate (45 mM), 1 mL/L TES and 100 mg/L carbenicillin. To simplify the process and due to unknown growth rates, it was performed as a discontinuous fed-batch. At timepoint 14 h 9.2 g/L glycerol and 6 g/L ammonium sulfate were supplemented. Heterologous gene expression was induced with 0.2 mg/L AHT at an OD between 0.3-0.4 (3 h), and additionally after 14 h. Antifoam was added frequently due to strong foaming.

The time point of induction was already reached after 3 h, due to the accelerated growth during this optimized fermentation process (**Figure 24**). Growth occurred until the end of cultivation (21 h) up to a final OD of 12. The oxygen supply was adjusted if necessary by increasing the stirrer speed manually, often accompanied by antifoam addition due to foaming. Under these conditions, ectoine production was maintained until 12 h post induction with a final concentration of ~ 8 mM. Interestingly, the growth rate dropped during the ectoine production phase (~ 0.3 to 0.16 h^{-1}) until its stop and increased again for the rest of the process (~ 0.36 h^{-1}). Also, 1 h before the observed halt in ectoine production the direct ectoine precursor N-γ-acetyl-diaminobutyric acid (ADABA) started accumulating in the medium, reaching a concentration of 5.5 mM after 19 h. Compared to previous bioreactor experiments, however, only low concentrations of acetate (< 10 mM at 19 h) and no formate were measured. This showed that an increase in oxygen supply can not prevent the stop in ectoine formation and rather decreases the final ectoine concentration, while supporting the biomass formation of *E. coli* K12 pASK_ectABC.

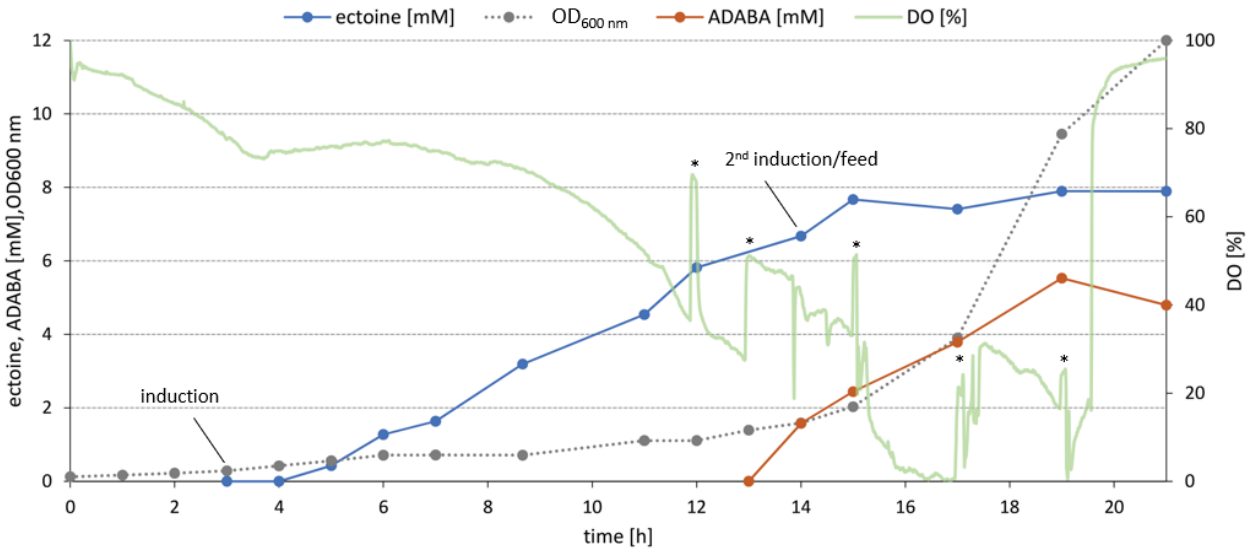

Figure 24 Ectoine overproduction [mM] in the 5 L bioreactor with *E. coli* K12 pASK_ectABC cultivated in 4 L MM63 with 0% NaCl, 9.2 g/L glycerol, 6 g/L ammonium sulfate, 100 mg/L carbenicillin and 1 mL/L TES. Fermentation was performed in a discontinuous fed-batch mode, feeding 9.2 g/L glycerol and 6 g/L ammonium sulfate after 14 h. Induction with 0.2 mg/L AHT occurred after 3 and 14 h. Oxygen supply was adjusted by increasing stirrer speed manually (*). OD values represent diluted real measurements.

3.5.1. Analysis and Maintenance of Heterologous Protein Levels

Increasing the oxygen supply in the fermentation process did decrease side product formation, but did not prevent the halt in ectoine production. Product formation stopped after 12 h post induction, when concentrations of the direct precursor molecule ADABA increased. Previous experiments indicated, but did not proof a plasmid-instability (Suppl. Figure 4). Plasmid instability can be caused by a decrease in selective pressure, due to antibiotic degradation. This is especially the case for β-lactam antibiotics, since the β-lactamase enzyme, which is encoded on the plasmid remains active even when excreted into the cultivation medium (Kemp and Britz, 1987).

To slow down antibiotic degradation (and hence delay a loss in selective pressure), bioreactor experiments were performed at a lower cultivation temperature. For this, a smaller fermentation system was implemented, with a cooling bath to maintain a constant temperature of 28 °C. Cultivation was performed in 0.2 L MM63 medium with 0% NaCl, 9.2 g/L glycerol, 3.4 g/L ammonium chloride, 1 mL/L TES and 100 mg/L carbenicillin. Fermentation was again performed in discontinuous fed-batch mode, resupplying 9.2 g/L glycerol and 3.4 g/L ammonium chloride after 14, 21 and 34 h. Heterologous gene expression was induced with 0.2 mg/L AHT at an OD between 1.5-2 (4 h) and after 21 h. Antifoam was added frequently due to strong foaming. The conditions for the small-scale ectoine fermentation system were established by Grujičić (2019). The system allows for parallel small-scale (0.2 L) bioreactor processes under controlled conditions. Grujičić could show for the first time that ectoine overproduction with K12 pASK_ectABC was possible starting the bioreactor cultivation with a higher inoculum (OD 1-2). This was enabled by the lower process temperature. Furthermore, ammonium sulfate was substituted by ammonium chloride, to ease solubility of medium components during medium preparation.

Growth was significantly reduced under lower temperature, with a growth rate of 0.15 h^{-1} at 28°C compared to > 0.3 h^{-1} at 37 °C (**Figure 25**). The ectoine gene cluster was induced after 4 h at an OD of 2. Subsequently, ectoine production occurred in a linear fashion until ~17 h post induction. Oxygen saturation decreased slowly until the measured values for DO dropped rapidly to 0% (8 h), when antifoam was added. The DO increased only upon the depletion of carbon source (14 h) and after strong foaming (30 h). Overall, a decrease in the cultivation temperature from 37 °C to 28 °C led to a prolonged ectoine production phase of 17 h, resulting in a drastically

increased final product concentration of 20 mM (compared to 8-9 mM at 37 °C). However, again the ectoine production came to a halt shortly after an accumulation of the precursor ADABA was detected. Similar to ectoine formation, the precursor generation was prolonged and reached a final concentration of over 30 mM. After 48 h the experiment was terminated when no further product formation or growth were detected.

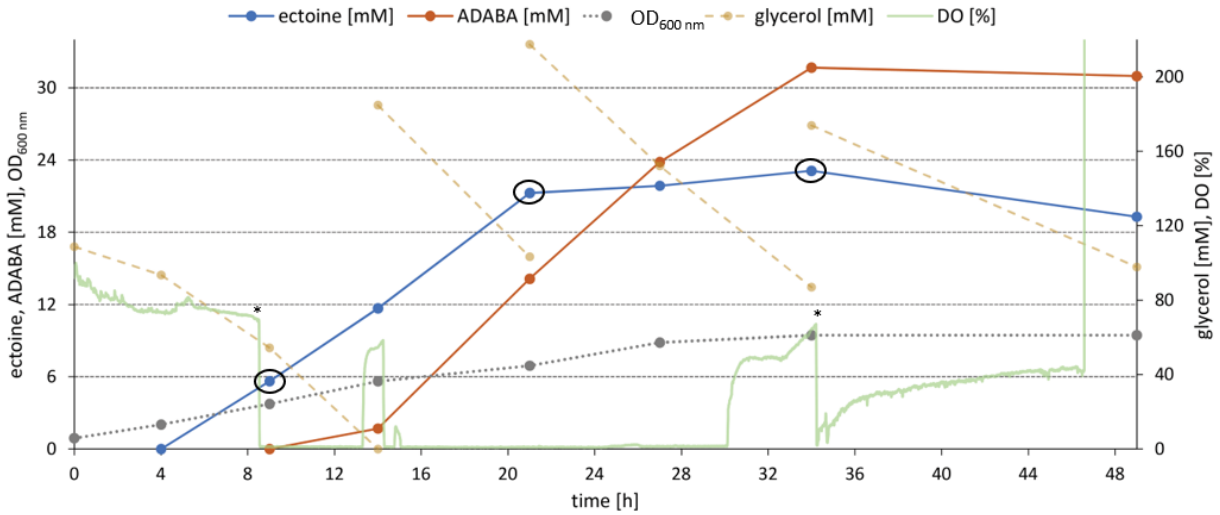

Figure 25 Ectoine overproduction [mM] at lower temperature in the 0.2 L bioreactor process. Cultivation of *E. coli* K12 pASK_ectABC in 0.2 L MM63 with 0% NaCl, 9.2 g/L glycerol, 3.4 g/L ammonium chloride, 100 mg/L carbenicillin and 1 mL/L TES. Fermentation was performed in discontinuous fed-batch mode, feeding 9.2 g/L glycerol and 3.4 g/L ammonium chloride after 14, 21 and 34 h. Induction with 0.2 mg/L AHT occurred after 4 and 21 h. Drops in DO occurred due to the addition of antifoam (*). Adjustment of stirring speed or air influx was not possible. Black circles represent the time-points for protein sampling. OD values represent diluted real measurements.

Overall, lowering the cultivation temperature drastically increased the final ectoine titer from ~ 1.2 g/L to 3 g/L (> 20 mM) with a specific production of 0.7 $g_{ectoine}/g_{dcw}$ at the end of the process. This suggests that lowering the temperature prolonged plasmid and protein stability. However, ectoine production still came to a halt 17 h post induction. If the reason for this arrest in ectoine biosynthesis was plasmid instability, one would expect a successive loss of transcript and protein levels of ectoine biosynthesis enzymes EctA, EctB and EctC over time. To confirm this hypothesis, protein samples were isolated at 5, 17 and 30 h post induction and analyzed for EctA, EctB and EctC protein levels by mass-spectrometry and e*ctB* and *ectC* transcript levels by qPCR. Of note, transcript levels of *ectA* could not successfully be determined, due to a lack of primer specificity for this coding sequence. 5 h past induction EctB was highly expressed in the production strain,

while the expression of EctA and EctC was about four times lower (**Figure 26A**). At 17 h post induction EctA and EctB were expressed at similar levels compared to 5 h post induction, however EctC expression was already drastically reduced. In line with the protein data, *ectB* transcript expression was only reduced by half at 17 h post induction (from 140 at 5 h to 73 at 17 h), while *ectC* expression was reduced more than 10-fold (from 1.3 at 5 h to 0.09 at 17 h) (**Figure 26B**). Interestingly, at this time point the halt in ectoine biosynthesis and the increase in ADABA levels were observed in the bioreactor process (cf. Figure 25). At 30 h post induction protein abundance of EctB was reduced by half (compared to 5 h time point), while EctC expression was nearly absent. These results were similarly reflected on RNA level (**Figure 26B**).

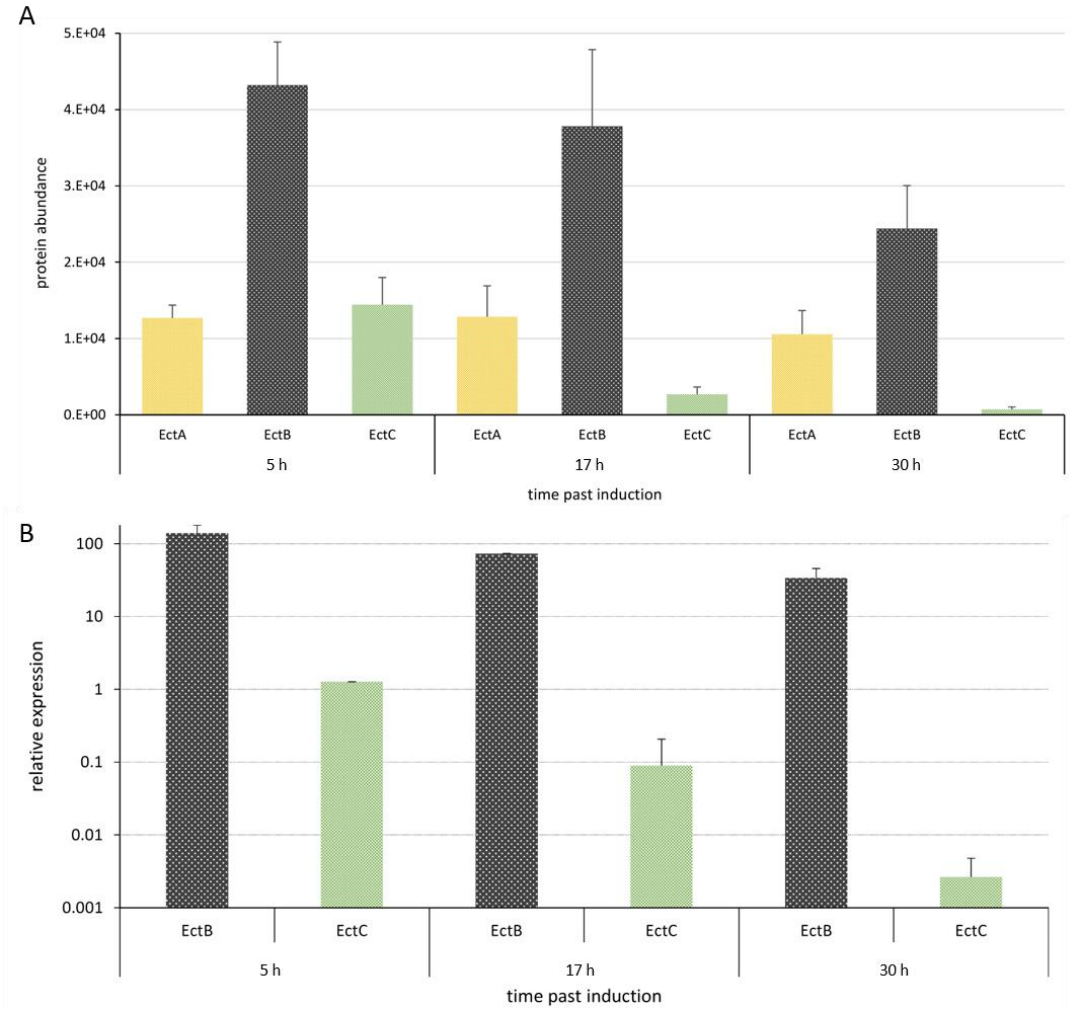

Figure 26 Relative abundance of the heterologous proteins EctA, B and C, during ectoine overproduction in the small-scale bioreactor (**A**). Protein abundance was acquired by mass spectrometry, performed by the mass-spectrometry core facility (University of Bonn). The transcript abundances of *ectB* and *ectC*, generated by qPCR, are displayed on a logarithmic scale relative to the house keeping gene *hcaT* (**B**). Samples correspond to time-points 5, 17 and 30 h post induction (cf. Figure 25).

At this time point also in the bioreactor processes no ectoine and ADABA were produced anymore. Throughout the entire experiment only the expression of EctA remained stable, as shown by relative protein abundance. These results indicate that a loss of EctB and EctC transcript and protein levels limits ectoine production at late time points. Ultimately, this shows that lowering the cultivation temperature was able to reduce, but not completely resolve process instability.

As a strategy to fully prevent plasmid loss, therefore the beta-lactamase inhibitor clavulanic acid was added into the overproduction medium. Clavulanic acid can prevent a decline in selective pressure by inhibiting the β-lactamases, which would otherwise degrade the antibiotic in the cultivation medium over time. In order to see whether clavulanic acid may increase plasmid stability (and therefore ectoine production), the bioreactor process was performed as described, but with addition of 10 mg/L clavulanic acid at 0 h, 21 h and 34 h (**Figure 27**).

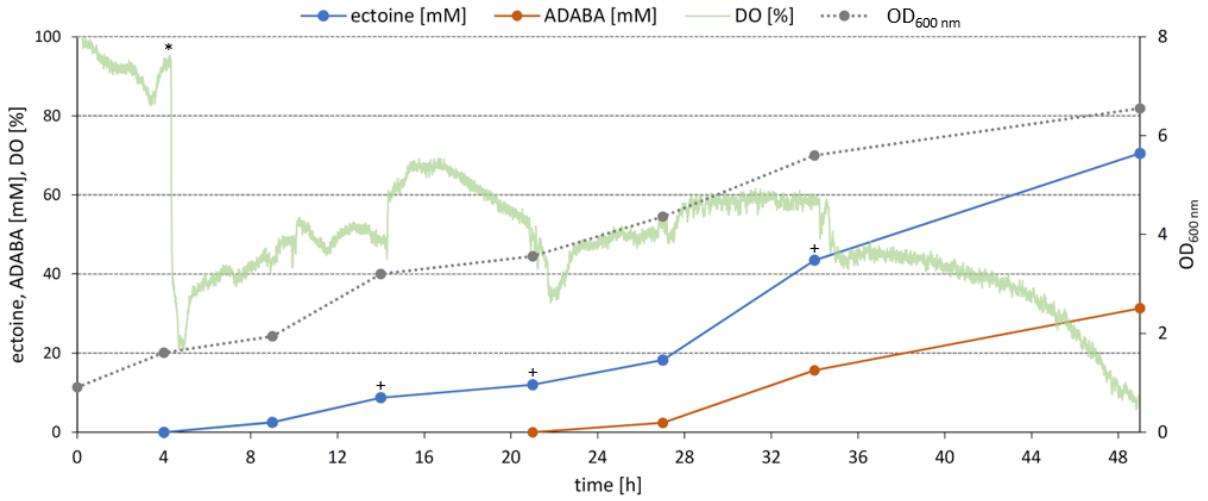

Figure 27 Ectoine overproduction [mM] with the addition of clavulanic acid at lower temperature in a small-scale bioreactor process. Cultivation of *E. coli* K12 pASK_ectABC in 0.2 L MM63 with 0% NaCl, 9.2 g/L glycerol, 3.4 g/L ammonium chloride, 100 mg/L carbenicillin, 1 mL/L TES and 10 mg/L clavulanic acid. Fermentation was performed in discontinuous fed-batch mode, feeding 9.2 g/L glycerol and 3.4 g/L ammonium chloride after 14, 21 and 34 h (+). Induction with 0.2 mg/L AHT occurred after 4 and 21 h. A drop in DO occurred due to the addition of antifoam (*). Adjustment of stirring speed or air influx was not possible. OD values represent diluted real measurements.

Under addition of clavulanic acid, the growth rate of the ectoine production strain *E. coli* K12 pASK_ectABC declined to about 0.08 h^{-1} (compared to 0.15 h^{-1} without clavulanic acid), leading to a final OD of 6.5 (compared to 9.5 without clavulanic acid). The oxygen supply dropped after addition of antifoam (4 h), but was above 20% until the end of the process. Remarkably, ectoine

was constantly produced throughout the entire process of 48 hours, achieving very high extracellular concentrations of more than 70 mM. Strikingly, also the precursor ADABA was not detected before 27 h in the process (compared to 9 h without clavulanic acid). These results clearly demonstrate that supplementation of clavulanic acid is a valid strategy to prolong ectoine biosynthesis in the production strain, possibly by extending plasmid stability. Overall, under these conditions a maximal ectoine product titer of 10 g/L could be achieved, with a specific production of 3 $g_{ectoine}/g_{dcw}$. Although precursor excretion could not entirely be prevented (4.8 g/L ADABA), the here presented bioreactor process is the most efficient way to produce ectoine that was described so far. Comparing the production and growth with and without clavulanic acid, a shift in microbial cell-population from fast growing and non-producing (without clavulanic acid) to slower growing but producing cells becomes apparent (**Figure 28**). This problem of population heterogeneity in the production strain is evoked by the loose selective pressure of β-lactam antibiotics in combination with the metabolic burden of the extraordinary high specific ectoine production in *E. coli* K12 pASK_ectABC.

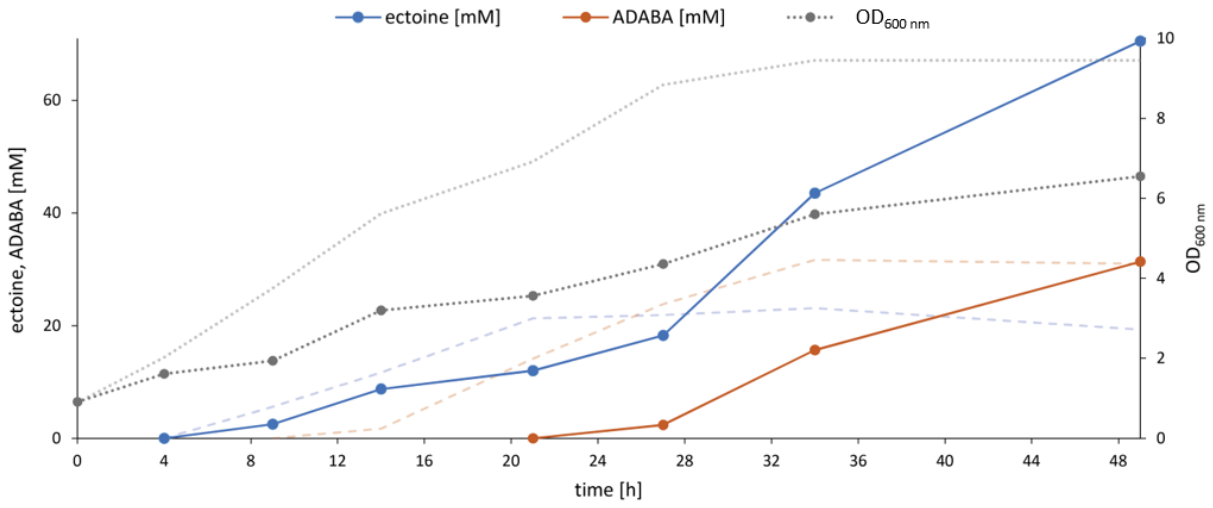

Figure 28 Comparison of product formation [mM] and OD during ectoine overproduction in the two small-scale bioreactor processes with (solid lines) and without (transparent lines) the addition of 10 mg/L clavulanic acid. Both fermentations were performed at 28 °C with 0.2 L MM63 and 0% NaCl, 9.2 g/L glycerol, 3.4 g/L ammonium chloride, 100 mg/L carbenicillin and 1 mL/L TES (cf. Figure 25, Figure 27).

So far only very few attempts of hydroxyectoine overproduction have been documented, with rather minor success (Becker *et al.*, 2013; Czech *et al.*, 2018). Hydroxyectoine overproduction with the biosynthesis gene cluster of *A. cryptum* has shown to be promising, generating 1.6 g/L of product with an extraordinary high specific production of 2.2 g/g_{dcw} (Moritz, 2018). More stable hydroxyectoine production was tested under the optimized conditions in a bioreactor process.

Performing hydroxyectoine overproduction with the strain K12 pASK_ectABCDask under the same conditions resulted in an accumulation of 20 mM hydroxyectoine (3.2 g/L) and 10 mM ectoine (1.4 g/L) (Suppl. Figure 6). Despite the addition of clavulanic acid, the production could not be stabilized and it stopped after 19 h post induction. The production of the precursor ectoine stopped simultaneously, while only traces of ADABA (< 1 mM) could be detected in the medium. The growth was not significantly influenced by the addition of the β-lactamase inhibitor and was comparable to the growth of K12 pASK_ectABC without clavulanic acid. The higher heterologous enzyme load by *ectD* and *ask* may explain the increased instability of the hydroxyectoine production. In lack of time, the process could not be further optimized or repeated. Since the product titer could be increased compared to previous studies, the hydroxyectoine production in *E. coli* with the gene cluster of *A. cryptum* is still a very promising approach, which needs to be further optimized.

4. Discussion

4.1. Base Strain Design

The implementation of the hydroxyectoine biosynthesis gene cluster from *A. cryptum* into *E. coli* DH5α already generated a potent ectoine overproduction strain (Bethlehem, 2015). After optimizing the cultivation conditions in shake flask experiments (4.6 g/L glycerol and 0.5% NaCl in minimal medium) the strain was capable of producing up to 12 mM ectoine (2.9 $g_{ectoine}/g_{dcw}$) (Moritz, 2018). Still, the strain was quite remote from performances of industrial strains, concerning product titer and process stability. The first key in improving the process of ectoine overproduction with the non-halophilic gene cluster from *A. cryptum* was the base strain optimization. Initially, *E. coli* DH5α was utilized as a base strain in this project. This strain is commonly employed for DNA conservation, but is rarely utilized in production processes. This is due to the diverse mutations in the strain's genome affecting metabolism and cell growth (Casali, 2003). Furthermore, in minimal medium (MM63) maximal growth rates of this strain generally do not exceed 0.3 h^{-1} and growth is dependent on additional, very costly additives, limiting the revenue in industrial processes substantially.

Due to the common use of *E. coli* in science and industry for more than a century, there are countless variations of strains to choose from as an alternative to *E. coli* DH5α. For biotechnological processes BL21 is one of the preferred *E. coli* strains, due to its benefits like faster growth rates in minimal medium with reduced acetate production and increased recombinant protein yield. This is mainly caused by differences in pathway regulation, deficiencies in proteases and increased porin permeability (Herrera *et al.*, 2002; Yoon *et al.*, 2012). Performing ectoine overproduction with pASK_ectABCD$_{mut}$ in BL21, however, resulted in significantly lower extracellular concentrations of ectoine, compared to ectoine production in *E. coli* DH5α pASK_ectABCD$_{mut}$. The B-strain accumulated about 1 mM ectoine in glucose and glycerol medium, while DH5α generated about 6 and 7.9 mM, respectively. In turn, BL21 showed accelerated growth rates for glucose (0.35 h^{-1}) and glycerol (0.33 h^{-1}), as well as an increased final OD compared to DH5α. The reason for the inferior performance in ectoine production of *E. coli* BL21 could not be determined, but is probably connected to the plasmid instability described for the ectoine overproduction with the vector pASK_ectABC.

In this work it was shown that in the process of ectoine overproduction with *E. coli* K12 pASK_ectABC an imbalance of slow-growing ectoine-producing and fast-growing non-producing cells is generated. The reason for this imbalance was connected to plasmid instability (due to degradation of carbenicillin), leading to the loss of heterologous protein expression in the fast-growing population. The faster growth of BL21 on minimal medium compared to DH5α suggests that plasmid instability during ectoine overproduction might also be elevated in BL21. The correct segregation of plasmids is impaired at high growth rates, due to the diluting effect (Mairhofer *et al.*, 2013; Sieben *et al.*, 2016). Furthermore, the degree in population shift usually correlates with the growth rate difference of the two populations (de Taxis du Poët *et al.*, 1987). Additionally, the selective pressure of carbenicillin could deteriorate quicker when *E. coli* BL21 is employed, due to an increased secretion of β-lactamases through the larger pore protein OmpF and an increased stability of β-lactamases through the missing proteases OmpT and Lon in BL21. These features are exclusives to B-strains and therefore could explain the much poorer performance of *E. coli* BL21 compared to *E. coli* DH5α. In support of this theory, different studies have demonstrated that a complete loss of heterologous plasmids is only observed in BL21, but not in *E. coli* K-strains (Marisch *et al.*, 2013; Sieben *et al.*, 2016). Yet another explanation for the poorer performance of *E. coli* BL21 compared to *E. coli* DH5α is the difference in cell metabolism: BL21 exhibits a higher activity of the glyoxylate shunt than *E. coli* DH5α (Phue *et al.*, 2005). This might negatively affect ectoine overproduction as this pathway seems to play no pronounced role for ectoine overproduction in *E. coli* (cf. Figure 19). An increased carbon flow in the glyoxylate shunt might, in fact, even decrease ectoine production by draining the acetyl-CoA pool.

The second strain tested in this study was *E. coli* K12. This is a non-pathogenic wildtype strain, which is routinely employed as a reference strain in water quality analysis (Edberg *et al.*, 2000). So far, the use of this strain in industrial processes for the overproduction of pharmaceuticals or proteins is not described. During ectoine overproduction with pASK_ectABCD$_{mut}$ in shake flask experiments (4.6 g/L glycerol, 0.5% NaCl), however, the strain performed exceptionally well. Similar to DH5α, *E. coli* K12 accumulated up to 7.9 mM ectoine, but grew substantially faster (0.35 h^{-1}). Since no studies have been carried out so far characterizing this K12 strain as an industrial host, the cause for its fitness in this application remains unclear. The fact that other closely related *E. coli* K-strains (MG1655 and W3110) exhibited a significantly weaker ectoine production under the same conditions complicates the interpretation even more. A detailed analysis

of the genomic background, transcriptional profile and the metabolism of *E. coli* K12 DSM498 would be needed to elucidate and clarify this question. Nonetheless, due to its good performance during ectoine overproduction and its wildtype genomic background, K12 DSM498 was chosen as the base strain for further strain development in this thesis.

Comparing the carbon sources glucose and glycerol during base strain design revealed a generally higher ectoine production utilizing glycerol. The increase in performance might be connected to an elevated anaplerotic reaction of the PPC under glycerol. The importance to replenish the precursor molecule oxaloacetate by this reaction was demonstrated by ^{13}C-Flux analysis (cf. 3.2. ^{13}C-Flux analysis). Glycerol passes the membrane of *E. coli* by facilitated diffusion supported by the glycerol uptake facilitator protein GlpF, followed by phosphorylation via the glycerol kinase (GlpK) utilizing ATP as a phosphoryl donor (Sanno *et al.*, 1968). The uptake of glucose in contrast, is mediated by the phosphotransferase system (PTS) utilizing PEP as a phosphoryl donor. This reaction leads to comparably high pyruvate and low PEP levels on glucose (Kundig *et al.*, 1964; Mori and Shiio, 1985). In contrast to PEP, pyruvate can not be directly introduced into an anaplerotic reaction to replenish the TCA in *E. coli*. The reversal of the malic enzyme's reaction, interchanging malate into pyruvate for gluconeogenesis, is not physiologically feasible in *E.* coli. The anaplerotic feed of pyruvate into the TCA is only possible through conversion into PEP, which demands the expense of ATP. This restriction of *E. coli* to efficiently perform anaplerotic reactions with pyruvate might evoke the lower production of ectoine on glucose. Additionally, the accelerated growth on the carbon source glucose compared to glycerol (demonstrated for all strains) could contribute to the issue of losing the heterologous proteins during the ectoine production process.

4.2. Establishing reference conditions

One of the main goals in optimizing the process of ectoine overproduction was to reduce the high NaCl concentration that is needed for ectoine production in the natural producer strain *H. elongata*. Thus, the ectoine biosynthesis gene cluster of *A. cryptum* was selected, due to its high enzyme activities at low salt concentrations. The capacity of the non-halophilic proteins at low salt concentrations was demonstrated by Moritz *et al.* (2015). The ectoine synthase showed

the highest activity (4 U/mg) *in vitro* at 0% NaCl, while the corresponding enzyme of *H. elongata* showed an optimum (8 U/mg) at 3% NaCl, and a drastic drop (1.5 U/mg) at 0% NaCl. When using *E. coli* K12 pASK_ectABC as a producer strain, the NaCl content could successfully be reduced to 0% (excluding 13.6 g/L KH_2PO_4 and 4.21 g/L KOH). Ectoine production under these low salt conditions extremely facilitates downstream processes increasing product yield and reduces costs of equipment maintenance and waste water treatment. To optimize the newly developed ectoine overproduction system further, the redundant *ectD* gene was removed from the vector pASK_ectABCD$_{mut}$. The unfunctional ectoine hydroxylase gene in the vector pASK_ectABCD$_{mut}$ (Bethlehem, 2015) inherits a point mutation close to the ligand binding site in position 118, by exchange of leucine for proline (Moritz, 2018). The ectoine biosynthesis gene cluster (*ectABC*) was cloned into pASK-IBA3, generating the plasmid pASK_ectABC. Expression of the heterologous proteins could not be verified with certainty by SDS-PAGE analysis (Suppl. Figure 3), but was later confirmed through mass spectrometry (cf. Figure 26). The low expression level of EctABC, however, was intentional to avoid an overload of the host's metabolism (Gießelmann *et al.*, 2019). The *E. coli* K12 strain with the new plasmid performed slightly better compared to the old plasmid (7.9 *vs* 11.4 mM consuming 4.6 g/L glycerol). The increase most probably is related to the increased nitrogen content employed in the cultivation with *E. coli* K12 pASK_ectABC.

The production of ectoine demands high levels of nitrogen due to the high nitrogen abundance in ectoine. 10 mM ectoine (1.42 g/L) require approximately 0.28 g nitrogen (~ 20% N / g ectoine). This is already about 70% of the nitrogen available in standard MM63 (1.96 g $(NH_4)_2SO_4$ = 0.42 g nitrogen). With the remaining 0.14 g nitrogen only about 1 g biomass can be generated (~ 12% N per g biomass). This demonstrates that with the standard formulation of MM63 (1.96 g $(NH_4)_2SO_4$) a nitrogen limitation occurs easily for the highly efficient ectoine production described in this thesis. Thus, an increase in nitrogen source was necessary to sustain the nitrogen demanding ectoine overproduction. To extend the ectoine production period over the entire cultivation time of 24 h, the $(NH_4)_2SO_4$ content was doubled and a second 4.6 g/L glycerol was fed after the first was depleted. Notably, only 3.9 mM ectoine were generated in the second production period, compared to 11.4 mM in the first. The optimizations performed resulted in an overall ectoine concentration of 15.3 mM (2.2 g/L), which is an increase by 29% compared to previous studies (Moritz, 2018).

4.3. Stable Isotope Labelling

After concluding the base strain design and setting the reference conditions, stable isotope labelling was conducted to analyze ectoine formation in *E. coli* K12. By the identification of the main metabolic routes contributing to product generation, bottlenecks could be successfully revealed as targets for metabolic engineering. Furthermore, it was achieved to create a convincing *in-silico* solution to analyze stable isotope results efficiently (in cooperation with Moritz L. Sümmermann, Institute for Mathematical Didactics, University Cologne).

To analyze ^{13}C-labelling patterns a theoretical pathway network has to be established on existing data, to retrace the metabolic routes contributing to the product formation (cf. Figure 7). The network was generated by the implementation of data from EcoCyc.org (Keseler *et al.*, 2017). First an experiment with stable isotope variants of glycerol was performed, since this carbon source led to the most efficient ectoine production in *E. coli* K12 pASK_ectABC. The lower ectoine concentration in this experiment was possibly caused by a faster decrease in pH during shake flask experiments, as buffer capacity had been lowered. The results of the labelling experiment are still valid, since the formation of the product should not be influenced by the amount of product generated.

Interestingly, the labelling distribution was not entirely coherent with the theoretical network. The symmetry of the glycerol molecule, however, prevented a precise attribution of the measured labelling distribution to pathways in the glycerol labelling experiment. The indistinguishable ^{13}C-isotopes in the positions 1 and 3 of the molecule, led to an uncertainty in the information output. Therefore, a stable isotope experiment with pyruvate was performed enabling three distinct labelling positions. This led to an unmistakable labelling pattern in ectoine for all three substrate isotopes. Again, the theoretical labelling pattern did not correspond with the real labelling distribution determined in the ^{13}C-pyruvate experiments. After extending the theoretical network by the anaplerotic PPC reaction, the labelling positions in ectoine could precisely be traced back to important reactions contributing to ectoine formation in *E. coli* K12. The intense 1-^{13}C label in position C1 revealed a significant influence of the anaplerotic reaction via the PPC, replenishing the precursor molecule oxaloacetate in the TCA. Similarly, the strong appearance of 2-^{13}C in position C2 and 3-^{13}C in position C3 can be attributed to the PPC reaction. The asymmetry in the labelling pattern in the positions C2 and C3 reflects the direct incorporation of oxaloacetate into

ectoine, that was generated by the anaplerotic reaction. The other reactions should generate a symmetric labelling pattern in these positions. The degree of asymmetry can therefore be attributed to the pool size of oxaloacetate generated by the PPC reaction. Next, the weaker 1-^{13}C labelling in position C4 is derived from either incorporation of labelled CO_2 or from the glyoxylate shunt. Since a significant amount of 1-^{13}C labelled CO_2 is produced to fuel the formation of ectoine with acetyl-CoA, a direct incorporation of the 1-^{13}C labelling from CO_2 seems comprehensible. In contrast, the glyoxylate shunt is only upregulated in the excess of acetyl-CoA and downregulated when growing on pyruvate and other substrates with more than two carbon atoms (Walsh and Koshland, 1984). In the case of ectoine production the acetyl-CoA pool is, however, additionally reduced by the incorporation into the compatible solute. Since the heterologous strain was grown on pyruvate and was producing ectoine in great amounts, a prominent influence of the glyoxylate shunt seems rather unlikely. At last, the 2-^{13}C label in position C3 can be explained by the anaplerotically generated oxaloacetate being reintroduced into the TCA and / or additionally into the glyoxylate shunt.

Comparison of the pyruvate labelling results of *E. coli* K12 pASK_ectABCD$_{mut}$ to the natural ectoine producer *H. elongata* again revealed the importance to effectively regenerate the precursor oxaloacetate. In contrast to *E.* coli, *H. elongata* is capable of effectively upregulating the malic enzyme to form malate from pyruvate for ectoine production (Kindzierski *et al.*, 2017). This explains the more efficient ectoine production of the natural producer when grown on pyruvate. Additionally, the stable isotope experiment with *H. elongata* was performed after shocking the organism from 3% to 10% NaCl in the medium. Under these stress conditions the organism is forced to regulate its metabolism in a way to channel the flux very directly to the compatible solute. In contrast, the heterologous *E. coli* in this study has no actual demand in producing ectoine and exhibits no natural regulatory switches to enforce the production.

By the design of a powerful *in-silico* software, the metabolic routes could be analyzed in more detail and more efficiently. The *in-silico* flux software enabled the generation of quantitative pathway maps on the basis of the ^{13}C-labelling patterns. The tool calculates probabilities of fluxes towards the product ectoine in a given network. In contrast to the manually generated networks, the software can consider the labelling intensity in the different carbon positions, by cycling through the possible routes until the measured quantities are matched. For ectoine production on

glycerol, the flux-map revealed that a third of the flux from PEP was channeled into oxaloacetate, replenishing the outflow of the precursor towards ectoine (cf. Figure 19). Accordingly, a third of the carbon source was directed from acetyl-CoA towards the compatible solute. The remaining flux towards ectoine was channeled into the TCA. These results are coherent with a previously determined carbon balance for the producer strain *E. coli* DH5α pASK_ectABCD$_{mut}$ (Moritz, 2018), where three glycerol molecules were described to be necessary to produce one molecule of ectoine.

Notably, also the calculation of the flux-software determined only a minor role of the glyoxylate shunt in ectoine formation on glycerol. This would fit the assumption that the glyoxylate shunt is not active in *E. coli* during ectoine production when grown on glycerol. When in contrast pyruvate is used as carbon source in the heterologous production strain, flux maps reveal a less effective metabolism towards ectoine. The flow towards the precursor oxaloacetate can not be replenished as efficient as on glycerol, leading to an increased flux into the TCA. Also, the flux of the glyoxylate shunt is slightly increased on pyruvate. This might be a regulation to keep the TCA running as efficiently as possible, despite the outflow of oxaloacetate. Altogether, *in-silico* flux comparison of glycerol and pyruvate can depict nicely why *E. coli* K12 pASK_ectABC produces ectoine more efficiently on glycerol. In contrast, flux analysis in *H. elongata* now precisely demonstrated a more efficient way to produce ectoine when growing on pyruvate. *H. elongata* exhibits a more efficient carbon flux from pyruvate towards oxaloacetate via the reverse reaction of the malic enzyme generating malate from pyruvate. This demonstrates how organisms that naturally produce ectoine are more versatile in adapting to the demand of the compatible solute production. In total, this acquired knowledge can be exploited to construct a more efficient heterologous ectoine production strain. To realize this objective the effective replenishment of the precursor oxaloacetate should be a central target to fuel the ectoine production in *E. coli* and at the same time allow the TCA to function correctly. This could be achieved by introducing additional anaplerotic routes or by improving existing routes.

In a more general context, the developed flux software is a powerful tool for the analysis of stable isotope experiments with respect to the analyzed product's labelling pattern. As such, it can be implemented effectively in strain optimization processes, quickly identifying relevant pathways for product formation. This is of pronounced importance, since a more frequent application of

metabolic flux analysis in science is impeded by the complicated and tiresome software solutions available. Besides the accessibility of the software, the practical execution and analysis of the labelling experiments are streamlined in this protocol. To generate a precise picture of the metabolic flux towards a compound, only the product itself needs to be isolated and analyzed for isotope incorporation, making elaborate purification and analysis of intermediates superfluous.

4.4. Metabolic Engineering

With the insights gained from stable isotope labelling, strategies for metabolic engineering of the ectoine overproduction strain K12 pASK_ectABC were developed. The metabolic flux analysis enabled a systemic and rational design approach, which is superior in many aspects to traditional random mutagenesis approaches. While random mutagenesis is time consuming (screening), limited to the host genome and can lead to unwanted alterations, a rational design enables fully defined adjustments to be implemented effectively. Additionally, the broad knowledge on microbial strains and an in-depth understanding of pathways and their regulations from systems biology facilitate this process (Li *et al.*, 2017).

By introducing the PYC from *C. glutamicum*, an increase in the supply of the precursor oxaloacetate was intended. The major impact of the precursor regeneration in ectoine overproduction with *E. coli* has been shown in the labelling experiments. An increase in succinate formation by the overexpression of the PYC from *C. glutamicum* has been demonstrated by Yang *et al.* (2014). The enzyme allows for an additional pathway to regenerate oxaloacetate via pyruvate, besides the existing anaplerotic reaction via PEP in *E. coli*. In contrast to PPC the PYC from *C. glutamicum* is not feedback-inhibited by malate and only slightly inhibited by aspartate. Interestingly, however, the new strain carrying pASK_ectABC and the additional plasmid pBBR1_pyc accumulated substantially less product (~ 5 mM) than the base strain under optimal conditions (~ 15 mM). An excess overexpression of the enzyme, often leading to detrimental effects, can be excluded since an overexpression of PYC was not detectable by SDS-PAGE analysis. Only on pyruvate the strain (K12 pASK_ectABC/pBBR1_pyc) displayed a clearly improved growth, hence an active pyruvate bypass seems likely (data not shown).

One of the main reasons for the bad performance in ectoine production of K12 pASK_ectABC/pBBR1_pyc might be the chloramphenicol resistance cassette, which is encoded on the secondary plasmid (Imperial, Lin and Posarac, 2005). The chloramphenicol acetyltransferase (CAT) covalently attaches acetyl from acetyl-CoA to the antibiotic, preventing it from binding the ribosomes (Shaw *et al.*, 1979). The availability of acetyl-CoA, however, is of prime importance for the ectoine production. This theory is supported by further experiments where the ectoine biosynthesis gene cluster was cloned into the vector pASK-IBA2C, which includes a chloramphenicol instead of an ampicillin resistance. Regardless of the fact that the plasmid was identical otherwise to pASK_ectABC, no ectoine production could be detected with the plasmid pASK2C_ectABC. Only a faint production of < 1 mM was achieved when the chloramphenicol concentration was reduced from 50 to 25 mg/L (data not shown). This indicates that the ectoine overproduction strain is highly susceptible to interference at the acetyl-CoA-knot. Additionally, the decrease in carbenicillin concentration (from 100 mg/L to 50 mg/L) might have contributed to the loss of ectoine biosynthesis proteins. A decrease of the antibiotics concentration when using two antibiotics is usually done to still enable normal growth under these harsh conditions. In the case of *E. coli* K12 pASK_ectABC it might, however, have caused a quicker loss of the heterologous plasmid for ectoine production due to a lower selective pressure by carbenicillin. Altogether, these data show that introduction of PYC on pBBR1 does not result in the desired increase of ectoine product titers. This, however, was probably caused by the secondary plasmid and not by the new protein. In future optimizations chloramphenicol should be avoided. Alternatively, PYC could be encoded on the same plasmid as EctABC, or integrated on the genome. Another way to increase the anaplerotic flux towards oxaloacetate would be an increase in expression of PPC. By enhancing the PPC promotor on the genome of *E. coli*, Lee *et al.* (2007) achieved a 27.7% increase in threonine production.

Another strategy of metabolic engineering involved the optimization of ectoine production by the addition of the feedback-resistant LysC from *C. glutamicum* MH20-22B. The aspartate kinase has been described as an important bottleneck in the generation of products from the aspartate amino acid family (Menkel *et al.*, 1989; Cremer, Eggeling and Sahm, 1991). The enzyme is a negative regulatory switch, activated by the accumulation of the end products threonine, methionine and lysine. This regulation can inhibit the production and accumulation of a desired product branching from this pathway. The implementation of LysC in the heterologous ectoine production strain

E. coli DH5α pAKect1 resulted in a three-fold increase in intracellular product formation (Bestvater, Louis and Galinski, 2008). The plasmid pAKect1 should in this study, however, not produce ectoine, but only express LysC. When *E. coli* pASK_ectABC/pAKect1 is cultivated at 0% NaCl, no additional ectoine is produced by the pAKect1 plasmid, but the LysC can still be expressed upon addition of IPTG (Wienberg, 2017). Performing ectoine production with K12 pASK_ectABC/pAKect1 under optimal conditions resulted in significantly less product formation (~ 6 mM) compared to the base strain (15.3 mM). Interestingly, similar to pBBR1_pyc also pAKect1 carries a chloramphenicol resistance cassette.

The very similar outcome evoked by the different secondary plasmids, supports the hypothesis of the CAT being responsible for the low ectoine production in the metabolically engineered strains. Therefore, an actual positive effect by enhancing the anaplerotic flux towards oxaloacetate (PYC), or by the incorporation of a feedback resistant aspartate kinase (LysC) should not be excluded. The impact of these metabolic engineering strategies should be investigated in the future, by designing alternative ways of expression. The sensitivity of the ectoine production to changes in the acetyl-CoA pool, on the other hand, is a valuable information on the demands for efficient ectoine production in *E. coli* K12 pASK_ectABC.

4.5. Medium Composition

As metabolic engineering could not resolve the halt in ectoine production with *E. coli* K12 pASK_ectABC, medium component deficiencies were tested. A deficiency can likely occur in minimal medium at later time points in the process, which would explain the decrease in product formation. In the beginning, the addition of single or complex medium components was tested. Since iron concentrations are low in MM63, iron was supplemented in higher concentrations, as it is needed as a co-factor of ectoine synthase (Widderich *et al.*, 2016). Further, addition of PLP was tested, since it is a potential co-factor for the transaminase EctB (Ma *et al.*, 2015). Additionally, ectoine production was tested in presence of complex medium components. However, none of the additives led to a significant increase in ectoine production (Suppl. Figure 5).

To finally exclude any medium component deficiencies the source of the ectoine formation breakdown in *E. coli* K12 pASK_ectABC, a parallel batch experiment was performed. In this

experiment it was tested if the stop in ectoine production was persistent in fresh medium by comparing the production after the breakdown in fresh and original medium. If a nutrient deficiency in the medium composition was responsible for the halt in ectoine production, a boost in performance should be detectable in fresh medium. However, after transferring part of the producing biomass into fresh MM63 with fresh antibiotic and re-inducing with AHT, the exact opposite was observed. The transferred cells production only 1.6 mM ectoine in the first 13 h and after an additional glycerol feed no more ectoine production was observed. In comparison, the original batch of *E. coli* K12 pASK_ectABC produced about 5.5 mM ectoine in the first 12 h and another 3 mM after feeding glycerol. Together, this demonstrates that the halt in ectoine production is not caused by media deficiencies. Instead, the fresh medium rather showed a positive effect on growth than on ectoine production. Interestingly, this would imply that the reduced plasmid carrying cell population is capable of ensuring fast growth in the fresh antibiotic supplemented medium (Yurtsev *et al.*, 2013). This could in future be tested by correlating plasmid carrying cells to the degradation of carbenicillin in the medium.

4.6. Ectoine Overproduction in Bioreactors

To study the ectoine overproduction with the base strain *E. coli* K12 pASK_ectABC in more detail and under controlled conditions, cultivation in bioreactors was performed. In contrast to shake flask experiments, the production in bioreactors allowed to control and analyze the experiment fully throughout the production process and to perform feeding strategies more precisely. A fed-batch process for example can be beneficial in production processes, since it prevents overflow metabolism and substrate inhibition through a controlled feed rate (Ljunggren and Häggström, 1992). In this process a feed rate of 0.45 $g_{glycerol}/L*h^{-1}$ was utilized. The feed rate was set higher than the consumption in shake flask experiments, since a higher growth rate was anticipated for bioreactor experiments. In shake flask experiments 4.6 g/L glycerol were consumed in under 15 h, resulting in a consumption of > 0.35 $g_{glycerol}/L*h^{-1}$. However, the carbon source accumulated throughout the fed-batch fermentation until side product formation started after 16 h. This was due to the fact that the growth rate in the first 12 h was already lower than expected (0.32 h^{-1}) and even dropped substantially to 0.13 h^{-1} in the second period of the fermentation. This decrease in growth and the significant accumulation of fermentation side products suggests an

anaerobic or microaerobic growth under glycerol (Murarka *et al.*, 2008). Since these phenomena begin parallel to the halt in ectoine product formation, a connection was assumed. Especially, since a crucial sensitivity to interferences in the acetyl-CoA pool has already been demonstrated and the accumulation of acetate would mean a drain of acetyl-CoA. The fed-batch strategy was abandoned for the following bioreactor experiments, since data were missing on the exact growth performance in an optimized bioreactor process. Furthermore, the equipment for contemporary precise feeding processes was not available.

In a fermenter with improved stirring capacities the overproduction of ectoine was repeated with increased oxygen supply. The content of DO was monitored throughout the process and kept above 20% for most of the fermentation, by manually adjusting the stirrer speed. By this, the accumulation of fermentation side products could be significantly reduced, measuring acetate concentrations below 10 mM at the end of the process, while no formate was detected. Additionally, of course the lowered substrate (glycerol) availability compared to the first fermentation could have contributed to the lower side product accumulation. To prevent acetate formation entirely, a more modern fermentation system with an automated and more efficient stirrer and feed-rate control would be needed. In the optimized conditions, a final OD twice as high could be reached (OD 12), compared to the first bioreactor experiment. Together with the prevention of the accumulation of fermentation side products, this demonstrates the more efficient O_2 supply.

Interestingly the growth rate decreased significantly during ectoine production, from 0.3 h^{-1} in the first 6 h to 0.16 h^{-1} during ectoine production. With the stop in ectoine production, however, the growth rate increased again to 0.36 h^{-1}, until the end of the process. A similar effect of decreased growth rates during induction of plasmid-based systems in *E. coli* was described by Mairhofer *et al.* (2013). The reduction in growth is connected to a high dosage of heterologous protein expression or similar stress caused by the plasmid preservation and metabolic interruptions. In the case of *E. coli* pASK_ectABC the fundamental impact of the ectoine biosynthesis on main metabolic routes of the organism (maximal 3 $g_{ectoine}/g_{dcw}$) definitely explains a slower growth of ectoine producing cells. This consequently results in a negative selection of this population compared to non-ectoine producing cells. Additionally, at later time points it was observed that ectoine production was substituted for production of its direct precursor ADABA. This might

indicate a successive loss of ectoine biosynthesis proteins over time. Altogether, these results suggested a negative selection of producing cells as the major cause for the halt in ectoine production, which can not be balanced by the pressure of carbenicillin.

4.7. Analysis and Maintenance of Heterologous Protein Levels

To slow down the suggested process of protein degradation, fermentation was performed at reduced temperature. A reduction in temperature can lead to a decrease in protein degradation and an increase in protein solubility (Baldwin, 1986; Koopaei *et al.*, 2018). Furthermore, it should reduce the degradation of carbenicillin, as well as the growth rate of the heterologous production strain, both contributing to process stability. With a specialized low temperature fermentation system, ectoine production could be achieved at 28 °C (Grujičić, 2019). Interestingly, at lowered temperatures ectoine production was even efficient when starting with a higher inoculum (OD 1). In comparison, starting with higher inoculum at 37 °C led to no ectoine formation in *E. coli* K12 pASK_ectABC (data not shown). Performing ectoine overproduction at reduced temperature indeed prolonged the production phase of ectoine by about seven hours, leading to an increase in final ectoine concentration of more than 100% (> 20 mM) compared to previous bioreactor experiments (8-9 mM). The halt in ectoine production and the formation of its precursor ADABA, however, were only delayed. In the end, the generation of ADABA was similar to the ectoine production prolonged, accumulating more than 30 mM of the precursor (compared to 5.5 mM). Nonetheless, a decrease in temperature positively affected the process stability and greatly increased ectoine titers (3 g/L compared to 1.3 g/L), thus supporting the hypothesis that a successive loss in heterologous proteins is the reason for the halt in ectoine production at later time points.

To accurately determine the loss of heterologous proteins during the production process, mass spectrometry was performed. The abundance of EctA, B and C was monitored during critical time points in the production process. Interestingly, the halt in product and precursor formation was directly correlated with the decrease in protein abundance of EctC and EctB. The decrease in protein abundance could be further connected to reduced transcript levels of *ectC* and *ectB* during the process, as determined by qPCR. Since the induction of protein expression with AHT was

repeated during the process, a deficiency in induction could be excluded as cause for the weaker protein expression. A more likely explanation was the reduction of plasmid-carrying cells over time, which was shown to be problematic in a plate-counting experiment (Suppl. Figure 4). A loss in plasmid-carrying cells during cultivation with β-lactam antibiotics, can occur due to overexpression of the *bla* gene. The *bla* gene encodes for the β-lactamase, which subsequently can be secreted into the medium, leading to a quick degradation of the antibiotic and to a relief in selective pressure. Consequently, non-resistant cells can prosper at the reduced antibiotic concentration, under the protection of a small proportion of β-lactamase secreting cells (Yurtsev *et al.*, 2013). The proportion of plasmid-bearing cells can be increased by the addition of β-lactamase inhibitors (Kim *et al.*, 1998). The inhibitor blocks the hydrolysis of antibiotics in the culture medium, maintaining the selective pressure.

By addition of the β-lactamase inhibitor clavulanic acid to the fermentation process (at 28 °C) a further increase in ectoine formation by 350% was achieved (> 70 mM compared to 20 mM). Although ADABA formation was further delayed it was not prevented. Interestingly, the precursor again accumulated to a concentration of 30 mM. Nonetheless, ectoine product formation under these conditions did not stop until the end of the process (48 h), clearly demonstrating the potential of the β-lactamase inhibitor for stabilizing the process of ectoine production with *E. coli* K12 pASK_ectABC.

When comparing ectoine formation and growth characteristics of the fermentation at 28 °C with and without clavulanic acid, a decrease in biomass formation and growth rate becomes apparent for the supplemented bioreactor (cf. Figure 28). The lower biomass in the second fermentation suggests that the cell population under these conditions is mainly constituted of ectoine-producing cells, which in turn grow slower due to the metabolic burden of ectoine production (3 $g_{ectoine}/g_{dcw}$). The higher biomass of the fermentation at 28 °C without clavulanic acid instead consisted at the end mainly of a cell population that had lost or reduced the number of pASK_ectABC plasmids. These cells were therefore not producing ectoine anymore, but growing faster due to the relief in metabolic burden (0.7 $g_{ectoine}/g_{dcw}$). In microbial communities, there is a substantial population heterogeneity present, even if descending from a single colony (Ackermann, 2015). Unfortunately, the heterogeneity in the here-used overproduction strain could not be analyzed or tracked during production in more detail. To do so, an ectoine biosensor was tested, which would have allowed

for an in-depth study of this phenomenon by GFP-assisted identification of ectoine producing cells. The biosensor, however, did not respond efficiently to the presence of ectoine (Wienberg, 2017).

In conclusion, the problem of the ectoine production stop could successfully be prevented by the addition of clavulanic acid. This led to an increase in product titer by more than 350% (10 g/L) compared to already improved conditions in this study (2.8 g/L) and of over 500% compared to previous studies (2 g/L) (Moritz, 2018). Remarkably, the specific production could be kept high (3 $g_{ectoine}/g_{dcw}$) by stabilizing the production plasmid and despite the drastically increased product titer. The persisting precursor accumulation, however, demonstrates that further improvement is possible. With the information gained, the expression system should be modified for the final industrial application. The new system should not be depending on antibiotics to circumvent a relief in selective pressure and to reduce the process costs (direct costs by antibiotics and purification costs). This can be achieved by an alternative plasmid addiction system or by genomic integration. Whereby, the transfer to a new plasmid-based expression system would be easier, since the genomic integration would greatly influence the expression pattern by the reduced copy number. An auxotrophy that is complimented by the expression plasmid is an eloquent way to stabilize plasmids and is not dependent on external additives and should be stable throughout the process (Velur Selvamani *et al.*, 2014). Additionally, one should consider to test codon-optimization by synonymous substitution to reduce the GC-content of the heterologous genes (65-71%). This could prevent secondary mRNA structures and thereby increase translation levels (Boël *et al.*, 2016).

4.8. Comparison to Literature

Until today the commercial production of ectoine is still performed with the natural producer strain *H. elongata*. The limitations of the bacterial milking process have been eliminated by now, with the implementation of super-leaky mutants (Sauer and Galinski, 1998; Kunte, Lentzen and Galinski, 2014). Still, the use of the moderate halophilic organism at elevated salt concentrations limits the industrial production efficiency, due to elaborate down-stream processes and deterioration of the fermentation equipment. Consequently, there have been concerted efforts over the last 20 years to design a superior heterologous ectoine overproduction system. To meet this

goal, diverse ectoine biosynthesis gene clusters have been incorporated into industrially relevant microbial producer strains.

The strain *E. coli* pASK-*ectABC*, with the ectoine biosynthesis gene cluster of *Chromohalobacter salexigens*, was the first described heterologous strain accumulating ectoine in the medium supernatant (**Schubert** *et al.*, 2007). This strain yielded a moderate ectoine titer of 6 g/L, but exhibited only a poor productivity over time, with a fed-batch process running over 160 h. The reason for the very inefficient and time-consuming process might be connected to the employed gene cluster. Interestingly, the basic strain design (with the exception of the moderate halophilic donor strain for the ectoine gene cluster) was very comparable to this study. In contrast to this study, however, no stop in ectoine production was documented. One reason why there was no halt in ectoine production for more than 160 h, might have been the significantly reduced metabolic burden by very slow ectoine formation.

A different study of **He** *et al.* (2015) described the only whole-cell biocatalysis attempt for ectoine production, employing the ectoine biosynthesis gene cluster of *H. elongata* in *E. coli* BW25113. In fed-batch fermentation they achieved a high cell density, which subsequently converted the precursor aspartate in combination with glycerol to ectoine. With a titer of 25.1 g/L and high productivities, the process was very efficient. However, due to a higher price for the substrate L-aspartate than for the product ectoine, this biocatalysis process failed to generate a profitable industrial process.

In 2016, **Ning** *et al.* documented a new efficient ectoine overproduction system, with the biosynthesis gene cluster of *H. elongata* 1A01717 in *E. coli* W33110. Through extensive metabolic engineering they could achieve an increase in product titers from 4.88 g/L (0.16 g/g_{dcw}) to 13.6 g/L (1.7 g/g_{dcw}) in shake flask experiments. The pool of the central precursor L-aspartate-β-semialdehyde was increased by deleting *thrA* and introducing the feedback resistant aspartate kinase *lysC* from *C. glutamicum*. To fuel the increased fluxes towards ectoine, the oxaloacetate supply was improved by greater flux through the glyoxylate shunt (Δ*iclR*) and a reinforced anaplerotic reaction by overexpression of PPC. In a fed-batch fermentation the optimized strain was capable of producing 25.1 g/L ectoine, with a rather low specific production of 0.8 g/g_{dcw}.

In 2018, **Czech** *et al.* demonstrated an elevated ectoine production with the biosynthesis gene cluster of *P. stutzeri* A1505 and its inherit promotor in *E. coli*. After modification of the promotor region, the strain produced 1.5 g/L ectoine, with a specific production of 1.1 g/g_{dcw}. Due to the

halophilic nature of this promotor, however, optimal ectoine production was dependend on addition of 2.3% NaCl. Consequently, it became necessary to delete the ectoine uptake systems ProU and ProP, as well as the trehalose biosynthesis gene cluster.

Interestingly, **Becker** *et al.* (2013) were the first to utilize *C. glutamicum*, the preferred strain for industrial L-lysine production, for heterologous ectoine formation. With the ectoine biosynthesis gene cluster of *P. stutzeri* A1505 a titer of 4.5 g/L with a very low specific production of 0.3 g/g_{dcw} could be achieved in fed-batch fermentation. Despite metabolic engineering, however, the ectoine production remained moderate. A possible reason might have been an unbalanced heterologous gene expression.

As recently shown by **Gießelmann** *et al.* (2019), ectoine titers could substantially be increased to 65 g/L in fed-batch fermentation using the same ectoine biosynthesis gene cluster as Becker *et al.* (2013). By performing only basic metabolic engineering (LysC, ΔLysE), Gießelmann *et al.* (2019) proved the importance of heterologous expression balance. This way, the product titer could be increased 5-fold, by generating a large library with differentially expression patterns for EctA, B and C. Only, the low specific production of 0.65 g/g_{dcw} is a substantial flaw in the industrial application of this process.

Pérez-García *et al.* (2017) followed a different strategy, by changing to the gene cluster of *C. salexigens.* In fed-batch experiments they achieved an ectoine production in *C. glutamicum* of 22 g/L ectoine. Additionally, the strain was optimized by feedback resistant LysC and a reinforced pyruvate carboxylase, assuring increased precursor supply. Substantial byproduct formation of lysine, however, could not successfully be overcome in this study. Also, ectoine titers did not reach similar levels as proven by Gießelmann *et al.* (2019).

In this study, an *E. coli* K12 ectoine overproduction strain was designed, employing the unique biosynthesis gene cluster of the non-halophilic *A. cryptum*. The process could be optimized, by generating the expression plasmid pASK_ectABC, integrated into the non-auxotrophic K12 DSM498. The resulting strain enables efficient overproduction at 0 % NaCl, which leads to a natural accumulation of ectoine in the cultivation medium and reduces down-stream process costs.

The strain demonstrates its competitiveness to other heterologous ectoine producers by an unparalleled specific production (3 $g_{ectoine}/g_{dcw}$) and production rate (0.28 $g/(g_{dcw} \times h)$). With this productivity, theoretically product-titers above 100 g/L are reasonable in industrial high cell density fermentation. An additional benefit of this strain is its highly efficient carbon yield (0.33 $g_{ectoine}/g_{glycerol}$), reducing substrate costs for the already cheap carbon source glycerol. As a downside of the hitherto unparalleled specific production, which channels the vast majority of the carbon source available into ectoine and thus causing a high metabolic burden, we identified the instability of the heterologous expression system. We could prove and solve this issue by the addition of the β-lactamase inhibitor clavulanic acid, stabilizing the production by keeping the selective pressure for the heterologous expression plasmid high. In conclusion, I could successfully prove the great potential of the hydroxyectoine gene cluster from the non-halophilic *A. cryptum* for ectoine overproduction in *E. coli*.

Table 18 Comparison of the most relevant heterologous ectoine overproduction strains, accounting for strains accumulating ectoine extracellularly under low salt conditions (0-0.5% NaCl) (with the exception of Czech et al. (2018), 2.3% NaCl). Values with a tilde (~) were determined based on the production data given in the references. Adopted from Moritz & Bethlehem (unpublished). α-KG: α-ketoglutarate, Ac: acetate, dcw: dry cell weight, Glu: glutamate, Lys: lysine, ND: not determinable, Spec.: specific.

Production strain	Donor strain	Procedure	Titer [g/L]	Spec. production [g/g dcw]	Production rate[a] [mg/(g dcw x h)]	Yield[b] [g/g]	Side products[c]	Reference
E. coli pASK_ectABC	*A. cryptum*	Fed-batch (flask)	2.2	1.3	194	0.24	None	This study
		Fed-batch	10	3	280	0.33[d]	32% ADABA	
E. coli pASK_ectABCD$_{mut}$	*A. cryptum*	Batch (flask)	1.7	2.9	345	0.36	None	Moritz & Bethlehem (unpublished)
E. coli SK51 pLC75	*P. stutzeri*	Batch (flask)[e]	1.5	1.1	ND	~ 0.18[f]	None	Czech *et al.*, 2018
E. coli ECT05	*H. elongata*	Fed-batch (flask)	13.6	1.7	~ 160	~ 0.38[g]	None	Ning *et al.*, 2016
		Fed-batch	25.1	0.8	~ 125	~ 0.11[g]	< 7% Ac, 4% α-KG	
E. coli pBAD-ectABC	*H. elongata*	Whole-cell biocatalysis	25.1[h]	4.1[h]	~ 250[h]	ND	None	He *et al.*, 2015
E. coli pASK-*ectABC*	*C. salexigens*	Fed-batch	6.0	0.3	~ 5	~ 0.02	None	Schubert *et al.*, 2007
C. glutamicum ectABC^{opt}	*P. stutzeri*	Fed-batch	65	0.65	~12	0.19	5% trehalose	Gießelmann *et al.*, 2019
C. glutamicum Ecto5	*C. salexigens*	Fed-batch	22.0	~ 1.8	~ 120	0.16	21% Lys, 4% Glu	Pérez-García *et al.*, 2017
C. glutamicum ECT-2[i]	*P. stutzeri*	Fed-batch	4.5	~ 0.3	~ 30	ND	6% hydroxyectoine	Becker *et al.*, 2013

[a] Maximum specific production rate; corresponds to the highest increase in extracellular solute concentration relative to the time difference and mean dcw

[b] Yield of extracellular ectoine per g carbon source

[c] Side products accumulated in the medium in addition to ectoine; the percentage refers to the extracellular total solute content

[d] Assumption that the entire carbon source was depleted (36.8 g/L); glycerol could not be determined

[e] NaCl content 2.3%

[f] Yield was estimated from the amount of glucose (5 g/L) and aspartate (25 mM = 3.3 g/L) used

[g] Yield refers only to the consumed glucose; the medium additionally contained 2 g/L yeast extract and 4 g/L tryptone

[h] Formation of the biomass used in whole-cell biocatalysis is not included in the data

[i] *ect* genes were codon-optimized and integrated into the genome, while the other heterologous systems are based on a plasmid

The industrial production of hydroxyectoine is even more complicated and cost inefficient than the original ectoine production. The continuous fermentation process with the natural producer *H. elongata* is performed with > 10% NaCl and at a temperature of 40 °C, producing a 50% mixture of hydroxyectoine and ectoine (Meffert, 2011). The complicated purification of hydroxyectoine from ectoine is the reason why commercialization of hydroxyectoine is prevented. The generation of an efficient hydroxyectoine production strain would allow for entirely new applications.

Eilert *et al.* (2013) could achieve the production of 2.8 g/L, with only 2% of ectoine present. The utilization of the yeast *Hansenula polymorpha* resulted, however, in a low specific production of 0.1 $g_{product}/g_{dcw}$. Analogous to ectoine, **Czech** *et al.* (2018) designed a hydroxyectoine overproducing strain, sharing the same features. Consequently, production is dependent on the addition of > 2% NaCl to run efficiently. The strain is capable of generating 1.3 g/L hydroxyectoine with a specific production of 1.2 g/g_{dcw}. Unfortunately, the strain produces about 32% of ectoine alongside hydroxyectoine, making chromatographic purification necessary.

The hydroxyectoine strain K12 pASK_ectABCDask, generated in this study, is the only strain capable of producing hydroxyectoine at 0 % NaCl. Compared to Moritz (2018) the product titer could be more than doubled (3.4 g/L), while keeping a good specific production (1 $g_{product}/g_{dcw}$). In contrast to ectoine production with *E. coli* pASK_ectABC, the production of hydroxyectoine could not be substantially stabilized by the addition of clavulanic acid. The reason for this might be the increased expression burden generated by the additional enzymes EctD and Ask. The critically low protein abundance observed for EctA, EctB and EctC during ectoine production, might be even lower in the hydroxyectoine production strain. Similar to pASK_ectABC, further improvement of the expression system is needed to overcome this issue. Additionally, the impact of the Ask protein on production should be clarified. In conclusion, the process presented here still is far from optimal, but could already demonstrate the potential of the *ectABCDask* gene cluster from *A. cryptum* for hydroxyectoine production.

5. Outlook

The strength of heterologous ectoine overproduction with the hydroxyectoine biosynthesis gene cluster of *A. cryptum* could be demonstrated in this study. The here described system resulted in high product titers (10 g/L) and an exceptionally high specific production (3 $g_{ectoine}/g_{dcw}$). After showing the potential of the here used non-halophilic enzymes for ectoine overproduction at low salt concentrations, an optimized expression system should be generated.

The expression of the heterologous ectoine biosynthesis proteins should be further stabilized, either by a different plasmid addiction system or by genomic integration. To avoid any costly additives for plasmid addiction, the generation of an auxotrophic strain with a complementary plasmid should be considered. Genomic integration on the other hand would maintain EctA, B, C stability efficiently, but could substantially interfere with expression strength, due to a lack of high copy numbers. Since Gießelmann *et al.* (2019) could demonstrate, however, that a rather low level of EctA, EctB and EctC expression is beneficial for ectoine production, genomic integration seems to be a feasible strategy. Further, they could demonstrate that a very similar expression-strength pattern of EctA, B and C as described in this study is substantial for effective ectoine overproduction. A rather low, but stable expression of the ectoine biosynthesis proteins should therefore be targeted for future designs, while preserving their relative expression ratios.

After the generation of a stable ectoine base strain, metabolic engineering should again be performed with the knowledge gained by ^{13}C-flux analysis. With the final strain, optimizations in the fermentation process should be pursued, within a contemporary high cell density fed-batch production. Due to the facilitated and less cost-intense production conditions of ectoine within this system, a patent claim should be considered for the future. Additionally, a stable process for hydroxyectoine overproduction may be designed, to allow for the first effective hydroxyectoine production. Due to the lack of current hydroxyectoine overproduction strains, this strategy may hold great promise for future studies and is very relevant for industrial applications.

6. Appendix

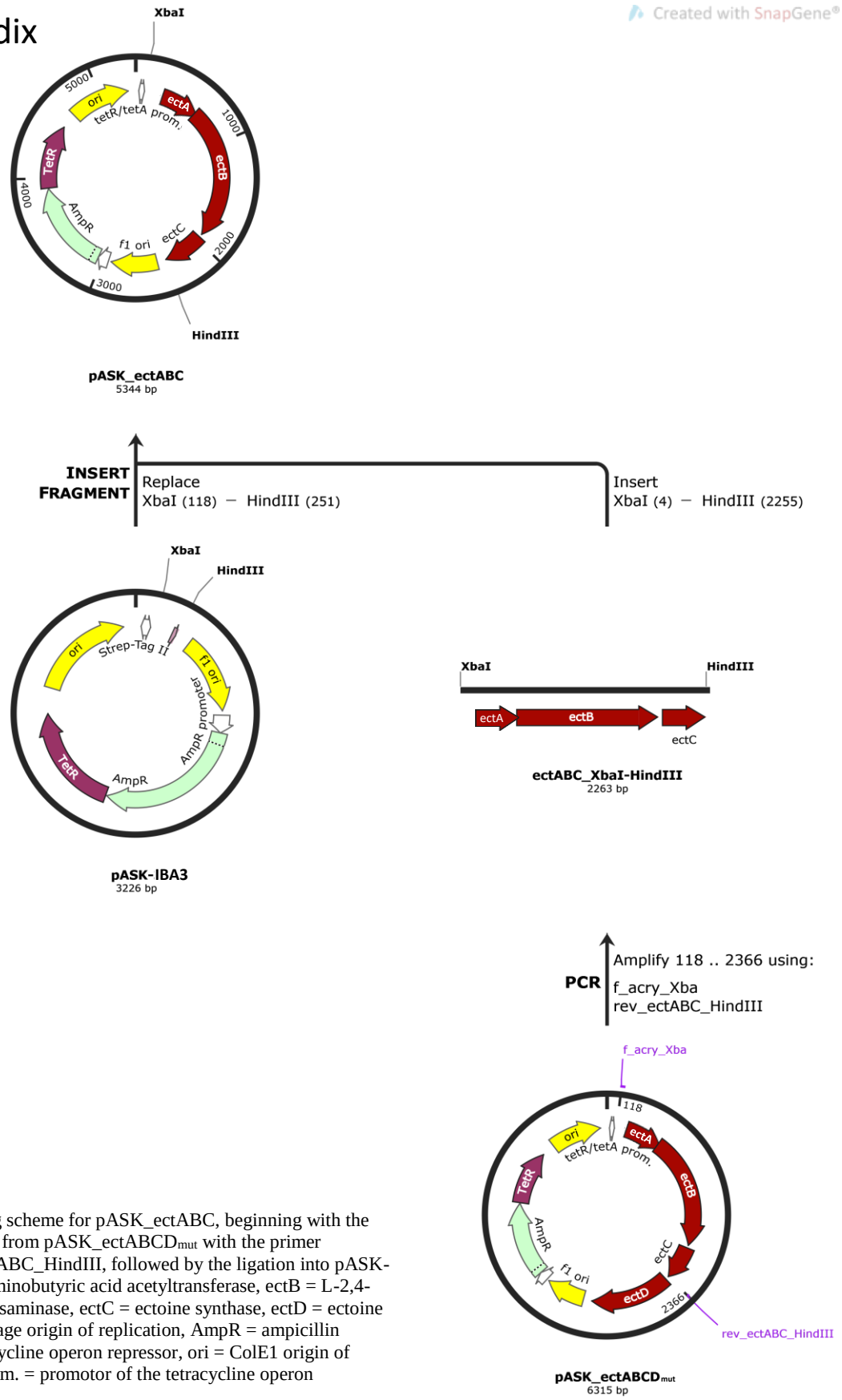

Suppl. Figure 1 Cloning scheme for pASK_ectABC, beginning with the amplification of *ectABC* from pASK_ectABCD$_{mut}$ with the primer f_acry_Xba and rev_ectABC_HindIII, followed by the ligation into pASK-IBA3. ectA = L-2,4-diaminobutyric acid acetyltransferase, ectB = L-2,4-diaminobutyric acid transaminase, ectC = ectoine synthase, ectD = ectoine hydroxylase, f1 ori = phage origin of replication, AmpR = ampicillin resistance, TetR = tetracycline operon repressor, ori = ColE1 origin of replication, *tetR/tetA* prom. = promotor of the tetracycline operon

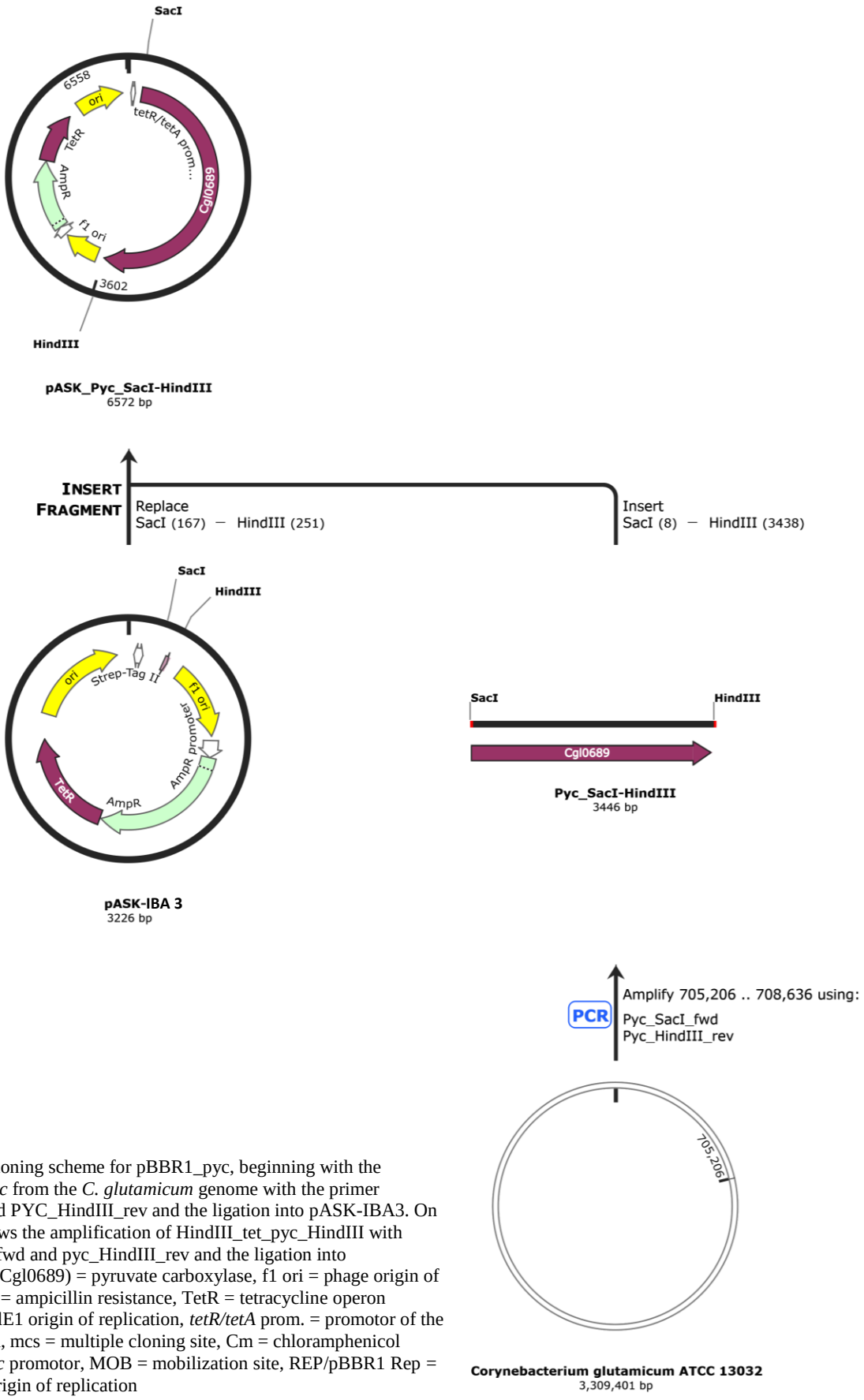

Suppl. Figure 2 Cloning scheme for pBBR1_pyc, beginning with the amplification of *pyc* from the *C. glutamicum* genome with the primer PYC_SacI_fwd and PYC_HindIII_rev and the ligation into pASK-IBA3. On the next page follows the amplification of HindIII_tet_pyc_HindIII with PYC_tet_HindIII_fwd and pyc_HindIII_rev and the ligation into pBBR1MCS. pyc (Cgl0689) = pyruvate carboxylase, f1 ori = phage origin of replication, AmpR = ampicillin resistance, TetR = tetracycline operon repressor, ori = ColE1 origin of replication, *tetR/tetA* prom. = promotor of the tetracycline operon, mcs = multiple cloning site, Cm = chloramphenicol resistance, lac = *lac* promotor, MOB = mobilization site, REP/pBBR1 Rep = broad host range origin of replication

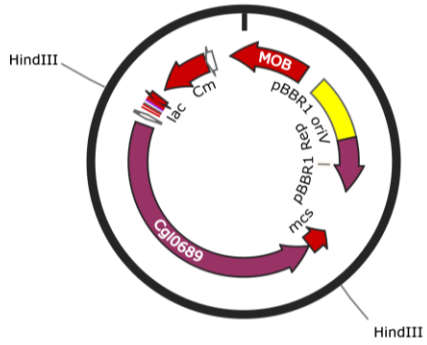

pBBR1_pyc
8324 bp

INSERT FRAGMENT
Insert at HindIII (3281)
Flip and insert HindIII (4) – HindIII (3621)

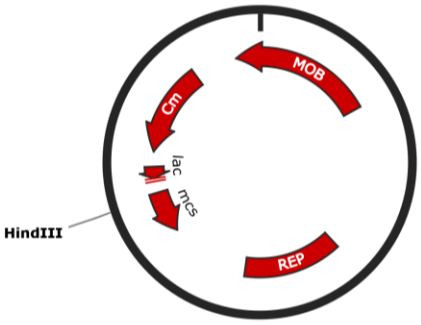

pBBR1MCS
4707 bp

PCR-HindIII_tet_pyc_HindIII
3629 bp

PCR
Amplify 6558 .. 3602 using:
Pyc_tet_HindIII_fwd
Pyc_HindIII_rev

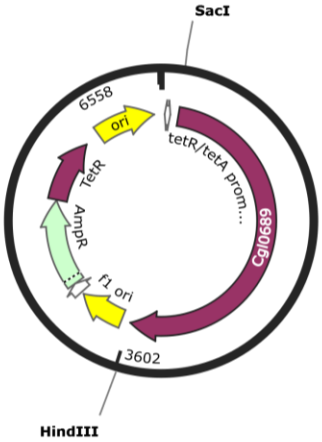

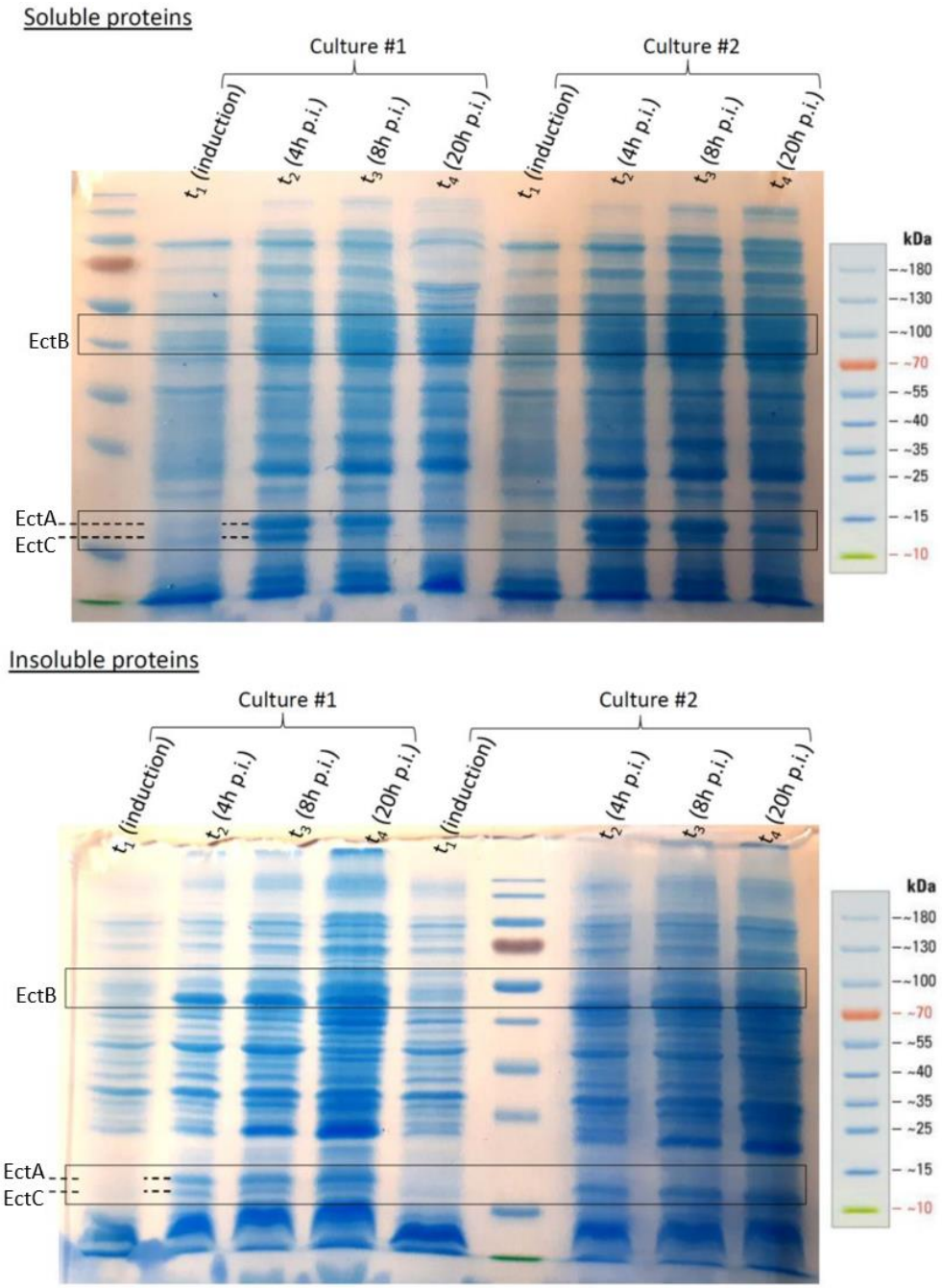

Suppl. Figure 3 SDS-PAGE analysis of the heterologous ectoine biosynthesis proteins. The entire proteins from *E. coli* K12 pASK_ectABC were extracted from cell-pellets (cf. 2.4.2. Protein Extraction) generated in the ectoine overproduction performed in the small-scale fermentation system. Cultivation was performed at 28 °C and with 0.2 L MM63, 0% NaCl, 9.2 g/L glycerol, 3.4 g/L ammonium chloride, 100 mg/L carbenicillin and 1 mL/L TES. The process was performed in discontinuous fed-batch mode, feeding 9.2 g/L glycerol and 3.4 g/L ammonium chloride after 14, 21 and 34 h (cf. Figure 25). EctA (18 kDA) and EctC (15 kDa) can be identified with high probability in the soluble protein fraction after induction, while EctB (46.5 kDa) is hard to distinguish from the background. In the insoluble fraction EctB seems to be most prominent.

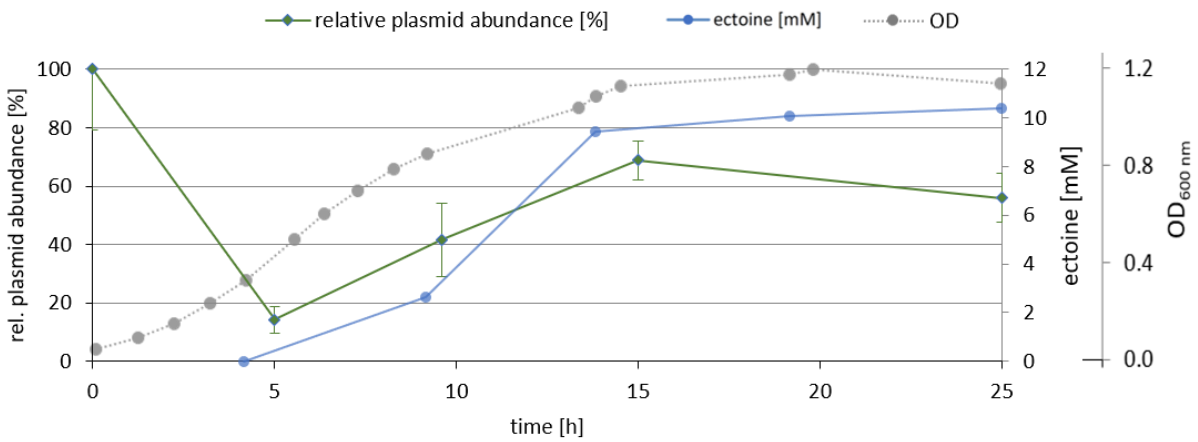

Suppl. Figure 4 Test for plasmid stability during ectoine overproduction. Plasmid abundance was discriminated by determining plasmid carrying CFU on plates with antibiotics (100 mg/L carbenicillin) against CFU on plates without antibiotic. The experiment was performed in triplicates and plating the cells in at least three different dilutions, to enable precise counting. The experiment was performed in shake flasks with MM63, 0% NaCl and 4.6 g/L glycerol.

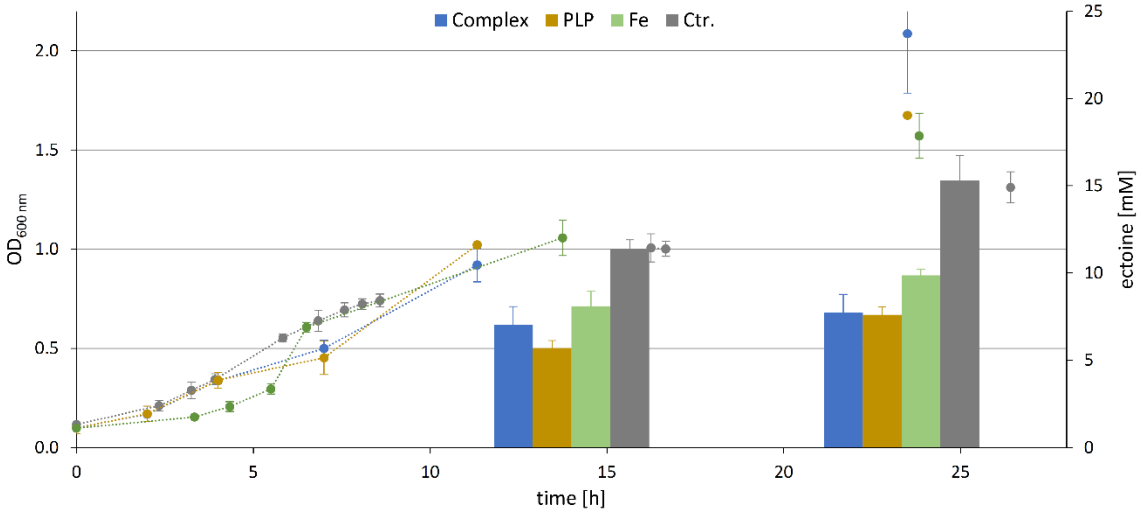

Suppl. Figure 5 Comparison of ectoine production with the supplementation of medium components to reference conditions. Ectoine overproduction at reference conditions with MM63 at 0% NaCl and 4.6 g/L glycerol, which was fed again after 14-15 h. All cultures were supplemented with 100 mg/L carbenicillin. Induction was executed at an OD between 0.3-0.4 adding 0.2 mg/L AHT. Supplementation includes 0.4% fish peptone (Complex), 24.7 mg/L PLP and 5.5 mg/L iron sulfate (Fe).
Ctr. = control without supplementation

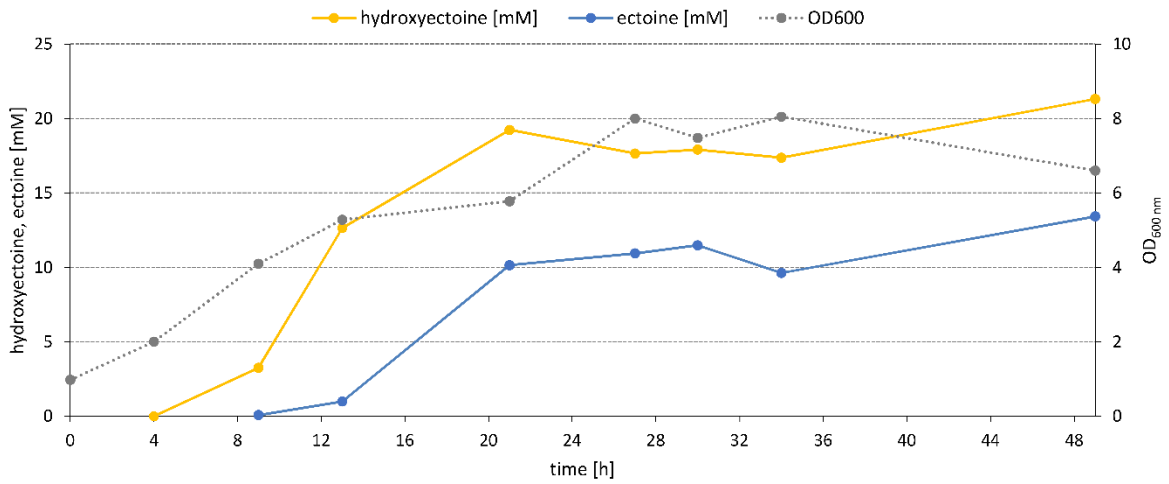

Suppl. Figure 6 Hydroxyectoine overproduction [mM] with the addition of clavulanic acid at lower temperature in a small-scale bioreactor process. Cultivation of *E. coli* K12 pASK_ectABCDask in 0.2 L MM63 with 0% NaCl, 9.2 g/L glycerol, 3.4 g/L ammonium chloride, 100 mg/L carbenicillin, 1 mL/L TES and 10 mg/L clavulanic acid. Fermentation was performed in discontinuous fed-batch mode, feeding 9.2 g/L glycerol and 3.4 g/L ammonium chloride after 13, 21 and 34 h. Induction with 0.2 mg/L AHT occurred after 4 and 21 h. Adjustment of stirring speed or air influx was not possible. OD values represent diluted real measurements.

7. References

Abdel-Aziz, H. *et al.* (2015) 'Bacteria-Derived Compatible Solutes Ectoine and Hydroxyectoine act as Intestinal Barrier Stabilizers to Ameliorate Experimental Inflammatory Bowel Disease', *Journal of Natural Products*. 78(6), pp. 1309–1315.

Ackermann, M. (2015) 'A functional perspective on phenotypic heterogeneity in microorganisms', *Nature Reviews Microbiology*. 13(8), pp. 497–508.

Arakawa, T. and Timasheff, S. N. (1985) 'THE STABILIZATION OF PROTEINS BY OSMOLYTES', *Biophysical* Journal. 47(March), pp. 411–414.

Baldwin, R. L. (1986) 'Temperature dependence of the hydrophobic interaction in protein folding (hydrocarbon model)', *Proc. Natl. Acad. Sci*, 83(November), pp. 8069–8072.

Becker, J. *et al.* (2011) 'From zero to hero—Design-based systems metabolic engineering of *Corynebacterium glutamicum* for l-lysine production', *Metabolic Engineering*, 13(2), pp. 159–168.

Becker, J. *et al.* (2013) 'Systems metabolic engineering of *Corynebacterium glutamicum* for production of the chemical chaperone ectoine', *Microbial Cell Factories*, 12(1).

Bentley, W. E. and Kompala, D. S. (1990) 'Stability in continuous cultures of recombinant bacteria: A metabolic approach', *Biotechnology Letters*, 12(5), pp. 329–334.

Bertani, G. (1951) 'Studies on lysogenesis. I. The mode of phage liberation by lysogenic Escherichia coli.', *Journal of bacteriology*, 62(3), pp. 293–300.

Bestvater, T., Louis, P. and Galinski, E. A. (2008) 'Heterologous ectoine production in Escherichia coli: By-passing the metabolic bottle-neck', *Saline Systems*, 4(1), pp. 1–14.

Bethlehem, L. (2015) 'Production of ectoines in Escherichia coli utilizing the hydroxyectoine gene cluster from the non-halophilic *Acidiphilium cryptum*', Master-thesis, Rheinische Friedrich-Wilhelms-Universität Bonn.

Boël, G. *et al.* (2016) 'Codon influence on protein expression in *E. coli* correlates with mRNA levels', *Nature*, 529(7586), pp.358-363

Borges, N., Ramos, A., Raven, N. D., Sharp, R. J.&Santos, H. (2002) 'Comparative study of the thermostabilizing properties of mannosylglycerate and other compatible solutes on model enzymes.', *Extremophiles : life under extreme conditions*, 6(3), pp. 209-16.

Botta, C. *et al.* (2008) 'Genotoxicity of visible light (400–800nm) and photoprotection assessment of ectoin, l-ergothioneine and mannitol and four sunscreens', *Journal of Photochemistry and Photobiology B: Biology*, 91(1), pp. 24–34.

Brown, A. D. (1976) 'Microbial water stress.', *Microbiological reviews*, 40(4), pp. 803-46.

Bursy, J. *et al.* (2007) 'Osmotically induced synthesis of the compatible solute hydroxyectoine is mediated by an evolutionarily conserved ectoine hydroxylase', *Journal of Biological Chemistry*, 282(43), pp. 31147–31155.

Casale, M. *et al.* (2019) 'Topical Ectoine : A Promising Molecule in the Upper Airways Inflammation — A Systematic Review', *BioMed research international*.

Casali, N. (2003) '*Escherichia coli* host strains.', *Methods in molecular biology (Clifton, N.J.)*, 235(4), pp. 27–48.

Castro, K. F. *et al.* (2019) 'Homoectoine Protects Against Colitis by Preventing a Claudin Switch in Epithelial Tight Junctions', *Digestive Diseases and Sciences*. Springer US, 64(2), pp. 409–420.

Chien, A., Edgar, D. B. and Trela, J. M. (1976) 'Deoxyribonucleic acid polymerase from the extreme thermophile Deoxyribonucleic Acid Polymerase from the Extreme Thermophile Thermus aquaticus', *Journal of Bacteriology*, 127(3), pp. 1550-7.

Chung, C. T., Niemela, S. L. and Miller, R. H. (1989) 'One-step preparation of competent *Escherichia coli*: transformation and storage of bacterial cells in the same solution.', *Proceedings of the National Academy of Sciences of the United States of America*, 86(7), pp. 2172–2175.

Cremer, J., Eggeling, L. and Sahm, H. (1991) 'Control of the lysine biosynthesis sequence in *Corynebacterium glutamicum* as analyzed by overexpression of the individual corresponding genes', *Applied and Environmental Microbiology*, 57(6), pp. 1746–1752.

Cummings, D. E. *et al.* (2007) 'Reduction of Cr(VI) under acidic conditions by the facultative Fe(lll)-reducing bacterium *Acidiphilium cryptum*.', *Environmental science & technology*, 41(1), pp. 146–152.

Czech, L. *et al.* (2018) 'Tinkering with osmotically controlled transcription allows enhanced production and excretion of ectoine and hydroxyectoine from a microbial cell factory', *Applied and Environmental Microbiology*, 84(2), pp. 1–29.

Czech, L., Stöveken, N. and Bremer, E. (2016) 'EctD-mediated biotransformation of the chemical chaperone ectoine into hydroxyectoine and its mechanosensitive channel-independent excretion', *Microbial Cell Factories*, 15(1), pp. 1–16.

Daegelen, P. *et al.* (2009) 'Tracing Ancestors and Relatives of *Escherichia coli* B, and the Derivation of B Strains REL606 and BL21(DE3)', *Journal of Molecular Biology*, 394(4), pp. 634–643.

Delbruck, M. (1946) 'BACTERIAL VIRUSES OR BACTERIOPHAGES', *Biological Reviews*, 21(1), pp. 30–40.

Edberg, S. C. *et al.* (2000) '*Escherichia coli*: the best biological drinking water indicator for public health protection', *Journal of Applied Microbiology*, 88(S1), pp. 106S-116S.

Eilert, E. *et al.* (2013) 'Synthesis and release of the bacterial compatible solute 5-hydroxyectoine in *Hansenula polymorpha*.', *Journal of biotechnology*, 167(2), pp. 85–93.

Fedorec, A. J. H. *et al.* (2019) 'Two New Plasmid Post-segregational Killing Mechanisms for the Implementation of Synthetic Gene Networks in *Escherichia coli*', *iScience*. Elsevier Inc., 14, pp. 323–334.

Fischer, J. *et al.* (2002) 'Inducible aluminum resistance of *Acidiphilium cryptum* and aluminum tolerance of other acidophilic bacteria.', *Archives of microbiology*, 178(6), pp. 554–558.

Friehs, K. (2004) 'Plasmid copy number and plasmid stability.', *Advances in biochemical engineering/biotechnology*, 86, pp. 47–82.

Galinski, E. A. (1985) 'A novel cyclic amino acid from halophilic phototrophic bacteria of the genus', *European Journal of Biochemistry*,139, pp. 135–139.

Galinski, E. A. (1995) 'Osmoadaptation in bacteria.', *Advances in microbial physiology*, 37, pp. 272–328.

Galinski, E. A. and Trüper, H. G. (1994) 'Microbial behaviour in salt-stressed ecosystems', *FEMS Microbiology Reviews*, 15(2), pp. 95–108.

Gießelmann, G. *et al.* (2019) 'Metabolic Engineering of *Corynebacterium glutamicum* for High - Level Ectoine Production : Design, Combinatorial Assembly, and Implementation of a Transcriptionally Balanced Heterologous Ectoine Pathway', *Biotechnology Journal*, 14(9), pp. 1–10.

Goeller, K. & Galinski, E. A. (1999) 'Protection of a model enzyme (lactate dehydrogenase) against heat, urea and freeze-thaw treatment by compatible solute additives.', *Journal of Molecular Catalysis*, 7(1-4), pp. 37-45.

Grammann, K., Volke, A. and Kunte, H. J. (2002) 'New Type of Osmoregulated Solute Transporter Identified in Halophilic Members of the Bacteria Domain : TRAP Transporter TeaABC Mediates Uptake of Ectoine and Hydroxyectoine in *Halomonas elongata* DSM 2581 T', 184(11), pp. 3078–3085.

Grujičić, G. V. (2019) 'Bioreactor process optimization for the heterologous production of ectoine in *Escherichia coli*', Industrial-practical, Rheinische Friedrich-Wilhelms-Universität Bonn.

Guell, D. C. and Brenner, H. (1996) 'Physical Mechanism of Membrane Osmotic Phenomena', Industrial & Engineering Chemistry Research, 35(9), pp. 3004–3014.

Guyer, M. S. *et al.* (1981) 'Identification of a sex-factor-affinity site in *E. coli* as gamma delta.', *Cold Spring Harbor symposia on quantitative biology*, 45 Pt 1, pp. 135–140.

Hanahan, D. (1983) 'Studies on Transformation of *Escherichia coli* with Plasmids Department of Biochemistry and Molecular Biology', *Journal of Molecular Biochemistry*, 166(4), pp. 557–580.

Harishchandra, R. K. *et al.* (2010) 'The effect of compatible solute ectoines on the structural organization of lipid monolayer and bilayer membranes.', *Biophysical chemistry*, 150(1–3), pp. 37–46.

Harrison, A. P., Jarvis, B. W. and Johnson, J. L. (1980) 'Heterotrophic bacteria from cultures of autotrophic *Thiobacillus ferrooxidans*: Relationships as studied by means of deoxyribonucleic acid homology', *Journal of Bacteriology*, 143(1), pp. 448–454.

He, Y.Z. *et al.* (2015) 'High production of ectoine from aspartate and glycerol by use of whole-cell biocatalysis in recombinant *Escherichia coli*', *Microbial Cell Factories*, 14(1), pp. 1–10.

Herrera, G, Martinez, A, Blanco, M, O'Connor, J. E. (2002) 'Assessment of *Escherichia coli* B With Enhanced Permeability to Fluorochromes for Flow Cytometric Assays of Bacterial Cell Function', *Clinical Cytometry*, 50(5), pp. 239–242.

Hill, C. W. and Harnish, B. W. (1981) 'Inversions between ribosomal RNA genes of *Escherichia coli*', *Proceedings of the National Academy of Sciences of the United States of America*, 78(11), pp. 7069–7072.

Holms, H. (1996) 'Flux analysis and control of the central metabolic pathways in *Escherichia coli*.', *FEMS microbiology reviews*, 19(2), pp. 85–116.

Huang, C. J., Lin, H. and Yang, X. (2012) 'Industrial production of recombinant therapeutics in *Escherichia coli* and its recent advancements', *Journal of Industrial Microbiology and Biotechnology*, 39(3), pp. 383–399.

Imhoff, J. F. and Trüper, H. G. (1977) '*Ectothiorhodospira halochloris* sp. nov., a new extremely halophilic phototrophic bacterium containing bacteriochlorophyll b', *Archives of Microbiology*, 114(2), pp. 115–121.

Imperial, S., Lin, T. and Posarac, V. (2005) 'Intracellular acetyl-CoA depletion by the cat gene is responsible for growth inhibition of *Escherichia coli* C584 on M9 minimal media', *Journal of Experimental Microbiology and Immunology*, 7(April), pp. 49–56.

Inbar, L. and Lapidot, A. (1988) 'The Structure and Biosynthesis of New Tetrahydropyrimidine Derivatives in Actinomycin D Producer *Streptomyces parvulus*', *The Journal of Biological* Chemistry, 263(31), pp. 16014–16022.

Joyce, A. R. and Palsson, B. O. (2006) 'The model organism as a system: integrating "omics" data sets.', *Nature reviews. Molecular cell biology*, 7(3), pp. 198–210.

Kempf, B. and Bremer, E. (1998) 'Uptake and synthesis of compatible solutes as microbial stress responses to high-osmolality environments', *Archives of Microbiology*, 170(5), pp. 319–330.

Kemp, G. W. and Britz, M. L. (1987) 'Removal of beta-lactam antibiotics during growth of *Escherichia coli* strains hosting pUR and pEX vectors', Biotechnology Techniques, 1(3), pp. 157–162.

Kent, W. J. *et al.* (2002) 'The human genome browser at UCSC.', *Genome research*, 12(6), pp. 996–1006.

Keseler, I. M. *et al.* (2017) 'The EcoCyc database: Reflecting new knowledge about *Escherichia coli K-12*', *Nucleic Acids Research*, 45(D1), pp. D543–D550.

Kim, C. H. *et al.* (1998) 'Fermentation strategy to enhance plasmid stability during the cultivation of *Escherichia coli* for the production of recombinant levansucrase', *Journal of Fermentation and Bioengineering*, 86(4), pp. 391–394.

Kim, H. U., Kim, T. Y. and Lee, S. Y. (2008) 'Metabolic flux analysis and metabolic engineering of microorganisms', *Molecular BioSystems*, 4(2), pp. 113–120.

Kindzierski, V. *et al.* (2017) 'Osmoregulation in the Halophilic Bacterium *Halomonas elongata*: A Case Study for Integrative Systems Biology', *PLoS ONE*, 12(1), pp. 1–22.

Kishimoto, N. and Tano, T. (1987) 'ACIDOPHILIC HETEROTROPHIC BACTERIA ISOLATED FROM ACIDIC MINE DRAINAGE, SEWAGE, AND SOILS', *The Journal of General and Applied Microbiology*, 33(1), pp. 11–25.

Koopaei, N. N. *et al.* (2018) 'Optimization of rPDT fusion protein expression by Escherichia coli in pilot scale fermentation: a statistical experimental design approach', *AMB Express*, 8(1), pp. 135.

Kundig, W., Ghosh, S. and Roseman, S. (1964) 'Phosphate Bound To Histidine in a Protein as an Intermediate in a Novel Phospho-Transferase System', *Proceedings of the National Academy of Sciences of the United States of America*, 52(4), pp. 1067–1074.

Kunte, H. J., Lentzen, G. and Galinski, E. A. (2014) 'Industrial Production of the Cell Protectant Ectoine : Protection Mechanisms , Processes and Products', *Current Biotechnology*, 3(1), pp. 10–25.

Laemmli, U. K. (1970) 'Cleavage of Structural Proteins during the Assembly of the Head of Bacteriophage T4', *Nature*, 227(5259), pp. 680–685.

Larsen, P. I. *et al.* (1987) 'Osmoregulation in *Escherichia coli* by accumulation of organic osmolytes: betaines, glutamic acid, and trehalose', *Archives of Microbiology*, 147(1), pp. 1–7.

Lee, K. H. *et al.* (2007) 'Systems metabolic engineering of *Escherichia coli* for L-threonine production', *Molecular Systems Biology*, 3(149).

Levy, Y. & Onuchic, J. N. (2004) 'Water and proteins : A love – hate relationship', *Proceedings of the National Academy of Sciences of the United States of America*, 101(10), pp. 3325–3326.

Li, Y. *et al.* (2017) 'Current status on metabolic engineering for the production of L-aspartate family amino acids and derivatives', *Bioresource Technology*, 245(29), pp. 1588–1602.

Lippert, K. and Galinski, E. (1992) 'Enzyme stabilization be ectoine-type compatible solutes: protection against heating, freezing and drying', *Applied Microbiology and Biotechnology*, 37(1), pp. 61–65.

Ljunggren, J. and Häggström, L. (1992) 'Glutamine limited fed-batch culture reduces the overflow metabolism of amino acids in myeloma cells', *Cytotechnology*, 8(1), pp. 45–56.

Louis, P., Trüper, H. G. and Galinski, E. A. (1994) 'Survival of *Escherichia coli* during drying and storage in the presence of compatible solutes', *Applied Microbiology and Biotechnology*, 41(6), pp. 684–688.

Ma, W. *et al.* (2015) 'Engineering a pyridoxal 5 ' -phosphate supply for cadaverine production by using *Escherichia coli* whole-cell biocatalysis', *Nature Publishing Group*, (July), pp. 1–10.

MacElroy, R. D. (1974) 'Some comments on the evolution of extremophiles.', *Biosystems*, 6(1), pp. 74–75.

Mahr, R. *et al.* (2014) 'Application of a Genetically Encoded Biosensor for Live Cell Imaging of L-Valine Production in Pyruvate Dehydrogenase Complex-Deficient *Corynebacterium glutamicum* Strains', *PLoS ONE*, 17, 9(1).

Mairhofer, J. *et al.* (2013) 'Comparative Transcription Profiling and In-Depth Characterization of Plasmid-Based and Plasmid-Free *Escherichia coli* Expression Systems under Production Conditions', 79(12), pp. 3802–3812.

Manzanera, M., Vilchez, S. and Tunnacliffe, A. (2004) 'High survival and stability rates of *Escherichia coli* dried in hydroxyectoine', FEMS Microbiology Letters, 233(2), pp. 347–352.

Marisch, K. *et al.* (2013) 'Evaluation of three industrial *Escherichia coli* strains in fed-batch cultivations during high-level SOD protein production', *Microbial Cell Factories*, 12 (58), pp. 1–11.

Martínez-Gómez, K. *et al.* (2012) 'New insights into *Escherichia coli* metabolism: Carbon scavenging, acetate metabolism and carbon recycling responses during growth on glycerol', *Microbial Cell Factories*, 11, pp. 1–21.

Meffert, A. (2011) 'Die Hydroxylierung von Ectoin und Derivaten durch die Hydroxylase EctD aus *Halomonas elongata*, Dissertation, Rheinische Friedrich-Wilhelms-Universität Bonn.

Menkel, E. *et al.* (1989) 'Influence of increased aspartate availability on lysine formation by a recombinant strain of *Corynebacterium glutamicum* and utilization of fumarate', *Applied and Environmental Microbiology*, 55(3), pp. 684–688.

Mori, M. and Shiio, I. (1985), Purification and Some Properties of Phosphoenolpyruvate Carboxylase from *Brevibacterium flavum* and Its Aspartate-Overproducing Mutant, *The Journal of Biochemistry*, 97(4).

Moritz, K. D. (2012) 'Untersuchungen zum Hydroxyectoin-Biosynthesegencluster aus *Acidiphilium cryptum* JF-5', Diploma-thesis, Rheinische Friedrich-Wilhelms-Universität Bonn.

Moritz, K. D. *et al.* (2015) 'The hydroxyectoine gene cluster of the non-halophilic acidophile *Acidiphilium cryptum*', *Extremophiles*, 19(1), pp. 87–99.

Moritz, K. D. (2018) '*Escherichia coli* und *Synechocystis sp.* als heterologe Produktionssysteme für Ectoin und Hydroxyectoin', Dissertation, Rheinische Friedrich-Wilhelms-Universität Bonn.

Moritz, K. D. and Bethlehem, L. (no date) 'Efficient hydroxyectoine and ectoine production in *Escherichia coli* using a non-halophilic gene cluster under low salt conditions', unpublished.

Murarka, A. *et al.* (2008) 'Fermentative utilization of glycerol by *Escherichia coli* and its implications for the production of fuels and chemicals', *Applied and Environmental Microbiology*, 74(4), pp. 1124–1135.

Myers, J. A., Curtis, B. S. and Curtis, W. R. (2013) 'Improving accuracy of cell and chromophore concentration measurements using optical density', *BMC Biophysics*, 6(1), p. 4.

Nichols, D. *et al.* (1999) 'Developments with Antarctic microorganisms: culture collections, bioactivity screening, taxonomy, PUFA production and cold-adapted enzymes', *Current Opinion in Biotechnology*, 10(3), pp. 240–246.

Ning, Y. *et al.* (2016) 'Pathway construction and metabolic engineering for fermentative production of ectoine in *Escherichia coli*', *Metabolic Engineering*, 36, pp. 10–18.

Oh, M.-K. and Liao, J. C. (2000) 'Gene Expression Profiling by DNA Microarrays and Metabolic Fluxes in *Escherichia coli*', *Biotechnology Progress*, 16(2), pp. 278–286.

Ollivier, B. *et al.* (1994) 'Anaerobic bacteria from hypersaline environments.', Microbiological reviews, 58(1), pp. 27–38.

Oren, A. (1999) 'Bioenergetic aspects of halophilism.', *Microbiology and molecular biology reviews*, 63(2), pp. 334–348.

Orth, J. D. *et al.* (2011) 'A comprehensive genome-scale reconstruction of *Escherichia coli* metabolism (2011)', *Molecular systems biology*, 7, pp. 535.

Palsson, B. (2004) 'Two-dimensional annotation of genomes.', *Nature biotechnology*, 22(10), pp. 1218–1219.

Pastor, J. M. *et al.* (2010) 'Ectoines in cell stress protection: Uses and biotechnological production', *Biotechnology Advances*, 28(6), pp. 782–801.

Pérez-García, F. *et al.* (2017) 'Improved fermentative production of the compatible solute ectoine by *Corynebacterium glutamicum* from glucose and alternative carbon sources', *Journal of Biotechnology*, 258, pp. 59–68.

Phue, J. N. *et al.* (2005) 'Glucose metabolism at high density growth of *E. coli* B and *E. coli* K: Differences in metabolic pathways are responsible for efficient glucose utilization in *E. coli* B as determined by microarrays and Northern blot analyses', *Biotechnology and Bioengineering*, 90(7), pp. 805–820.

Rieckmann, T. *et al.* (2019) 'The inflammation-reducing compatible solute ectoine does not impair the cytotoxic effect of ionizing radiation on head and neck cancer cells', *Scientific Reports*, 9(1), pp. 1–8.

Rippka, R. *et al.* (1979) 'Generic Assignments, Strain Histories and Properties of Pure Cultures of Cyanobacteria', *Microbiology*, 111(1), pp. 1–61.

Rothschild, L. J. and Mancinelli, R. L. (2001) 'Life in extreme environments', *Nature*, 409(6823), pp. 1092–1101.

Rozen, S. and Skaletsky, H. (2000) 'Primer3 on the WWW for general users and for biologist programmers', *Methods in molecular biology*, 132, pp. 365–386.

Sambrook, J. (1989) 'Molecular Cloning: A Laboratory Manual' *Cold Spring Harbor Protocols*, 4th Edition.

Sanno, Y., Wilson, T. H. and Lin, E. C. C. (1968) 'Control of permeation to glycerol in cells of *Escherichia coli*', *Biochemical and Biophysical Research Communications*, 32(2), pp. 344–349.

Satyanarayana, T., Raghukumar, C. and Shivaji, S. (2005) 'Extremophilic microbes: Diversity and perspectives', *Current Science*, 89(1), pp. 78–90.

Sauer, T and Galinski, E. (1998) 'Bacterial milking: A novel bioprocess for production of compatible solutes', *Biotechnology and bioengineering*, 59(1), p. 128.

Schubert, T. *et al.* (2007) 'Continuous synthesis and excretion of the compatible solute ectoine by a transgenic, nonhalophilic bacterium.', *Applied and environmental microbiology*, 73(10), pp. 3343–7.

Seip, B., Galinski, E. A. and Kurz, M. (2011) 'Natural and engineered hydroxyectoine production based on the *Pseudomonas stutzeri* ectABCD-ask gene cluster.', *Applied and environmental microbiology*, 77(4), pp. 1368–74.

Shaw, W. V. *et al.* (1979) 'Primary structure of a chloramphenicol acetyltransferase specified by R plasmids', *Nature*, 282(5741), pp. 870–872.

Sieben, M. *et al.* (2016) 'Testing Plasmid Stability of *Escherichia coli* Using the Continuously Operated Shaken BIOreactor System', *Biotechnology Progress*, pp. 1–8.

Smith, P. K. *et al.* (1985) 'Measurement of protein using bicinchoninic acid', *Analytical Biochemistry*, 150(1), pp. 76–85.

Studier, F. W. and Moffatt, B. A. (1986) 'Use of bacteriophage T7 RNA polymerase to direct selective high-level expression of cloned genes', *Journal of Molecular Biology*, 189(1), pp. 113–130.

Sümmermann, M., Bethlehem, L. and Galinski, E. A. (no date) 'Computation of metabolic flux ratios from ^{13}C NMR data', unpublished.

Tanne, C. *et al.* (2014) 'Glass-forming property of hydroxyectoine is the cause of its superior function as a desiccation protectant', 5(April), pp. 1–13.

de Taxis du Poët, P. *et al.* (1987) 'Plasmid stability in immobilized and free recombinant *Escherichia coli* JM105(pKK223-200): importance of oxygen diffusion, growth rate, and plasmid copy number.', *Applied and environmental microbiology*, 53(7), pp. 1548–1555.

Tran, B. *et al.* (2019) 'Ectoine-Containing Inhalation Solution versus Saline Inhalation Solution in the Treatment of Acute Bronchitis and Acute Respiratory Infections : A Prospective , Controlled , Observational Study', (2019), *BioMed Research International*, p. 8.

Tryfona, T. and Bustard, M. T. (2005) 'Fermentative production of lysine by *Corynebacterium glutamicum*: transmembrane transport and metabolic flux analysis', *Process Biochemistry*, 40(2), pp. 499–508.

Velur, R. *et al.* (2014) 'Antibiotic-free segregational plasmid stabilization in *Escherichia coli* owing to the knockout of triosephosphate isomerase (tpiA)', *Microbial Cell Factories*, 13(1), pp. 1-13.

Voß, P. (unpublished), Westfälische Wilhelms-Universität Münster.

Walsh, K. and Koshland, D. E. J. (1984) 'Determination of flux through the branch point of two metabolic cycles. The tricarboxylic acid cycle and the glyoxylate shunt.', The Journal of biological chemistry, 259(15), pp. 9646–9654.

Widderich, N. *et al.* (2014) 'Biochemical Properties of Ectoine Hydroxylases from Extremophiles and their wider Taxonomic Distribution among Microorganisms', *PLoS ONE*, 9(4).

Widderich, N. *et al.* (2016) 'Biochemistry and Crystal Structure of Ectoine Synthase : A Metal-Containing Member of the Cupin Superfamily', *PLoS ONE*, pp. 1–26.

Wienberg, F. (2017) 'Charakterisierung heterologer Ectoinproduktion in *Escherichia coli* mittels eines Biosensors, Bachelor-thesis, Rheinische Friedrich-Wilhelms-Universität Bonn.

Yang, J. *et al.* (2014) 'Metabolic engineering of *Escherichia coli* and in silico comparing of carboxylation pathways for high succinate productivity under aerobic conditions', *Microbiological Research*, 169(5–6), pp. 432–440.

Yoon, S. H. *et al.* (2009) 'Genomics, Biological Features, and Biotechnological Applications of *Escherichia coli* B: ``Is B for better?!''', in Lee, S. Y. (ed.) *Systems Biology and Biotechnology of Escherichia coli*. Dordrecht: Springer Netherlands, pp. 1–17.

Yoon, S. H. *et al.* (2012) 'Comparative multi-omics systems analysis of *Escherichia coli* strains B and K-12', *Genome Biology*, 13(5), p. 37.

Yurtsev, E. A. *et al.* (2013) 'Bacterial cheating drives the population dynamics of cooperative antibiotic resistance plasmids', *Molecular Systems Biology*, 9(683), pp. 1–7.

Zaccai, G. *et al.* (2016) 'Neutrons describe ectoine effects on water H-bonding and hydration around a soluble protein and a cell membrane', *Nature Publishing Group*, (July), pp. 1–12.

Zeikus, J. G., Vieille, C. and Savchenko, A. (1998) 'Thermozymes: biotechnology and structure-function relationships', *Extremophiles*, 2(3), pp. 179–183. doi: 10.1007/s007920050058.

Zhou, K. *et al.* (2011) 'Novel reference genes for quantifying transcriptional responses of *Escherichia coli* to protein overexpression by quantitative PCR', *BMC molecular biology*, 12, p. 18.